8-2018

Performance of Finned Heat Exchangers After Air-side Fouling and Cleaning

Harshad V. Inamdar
Purdue University

PERFORMANCE OF FINNED HEAT EXCHANGERS AFTER AIR-SIDE FOULINGAND CLEANING

by

Harshad V. Inamdar

A Dissertation

Submitted to the Faculty of Purdue University

In Partial Fulfillment of the Requirements for the degree of

Doctor of Philosophy

School of Mechanical Engineering

West Lafayette, Indiana

August 2018

THE PURDUE UNIVERSITY GRADUATE SCHOOL
STATEMENT OF COMMITTEE APPROVAL

Dr. Eckhard A. Groll, Co-chair
School of Mechanical Engineering
Dr. Suresh V. Garimella, Co-chair
School of Mechanical Engineering
Dr. James E. Braun
School of Mechanical Engineering
Dr. William T. Horton
Lyles School of Civil Engineering

Approved by:
Dr. Jay P. Gore
Head of the Graduate Program

TABLE OF CONTENTS

LIST OF TABLES

LIST OF FIGURES

NOMENCLATURE

A	area, m^2
CE	circle equivalent, dimensionless
C_D	coefficient of drag, dimensionless
C_S	thermal slip coefficient, dimensionless
C_t	thermal exchange factor, dimensionless
c	molar concentration, $kmol/m^3$
	mass concentration, kg/m^3
corf	correction factor for wavy fins, dimensionless
D	momentum diffusion coefficient of air, m^2/s
D_{bro}	deposition fraction attributed to Brownian motion, dimensionless
$D_{cumulative}$	cumulative deposition fraction at the end of a complete test run, dimensionless
D_{fin}	deposition fraction attributed to inertial impaction on fins, dimensionless
$D_{ent,i}$	deposition fraction attributed to random bursts of turbulence along direction *i*, dimensionless
D_{gra}	net deposition due to gravitational settling in wavy-finned-tube heat exchangers, dimensionless
$D_{gra,corr}$	deposition fraction attributed to gravitational settling in fin corrugations, dimensionless
$D_{gra,open}$	deposition fraction attributed to gravitational settling in open flow areas in the heat exchanger core, dimensionless
$D_{gra,plain\text{-}fins}$	deposition fraction attributed to gravitational settling in plain–finned tube heat exchangers
D_t	tube diameter, m
D'_t	tube diameter corrected for deposition buildup, m
D_{tube}	deposition due to inertial impaction on tubes, dimensionless
$D_{tur,i}$	deposition due to turbophoresis along direction *i*, dimensionless
D_{turb}	net deposition due to turbulence-related mechanisms, dimensionless
$D_{wv,air}$	mass diffusion coefficient of water vapor in air, m^2/s
d_p	particle diameter, m

$dist_i$	distance to nearest heat exchanger surface along direction *i*, m
F_{diff}	diffusiophoretic force acting on a particle, N
F_{ther}	thermophoretic force acting on a particle, N
g	gravitational acceleration, m/s^2
H_w	height (crest to trough distance) of one 'wave' in a wavy fin structure, m
h	height, m
$h_{a,in}$	enthalpy of moist air entering the heat exchanger, J/kg
$h_{a,out}$	enthalpy of moist air leaving the heat exchanger, J/kg
i	counter for fouling or steady state periods during a single test run, dimensionless
$J_{fl,i}$	Lagrangian (or integral) diffusion scale of times along direction *i*, s
Kn	Knudsen number of particle flow, dimensionless
k_{air}	thermal conductivity of air, W/m-K
k_p	thermal conductivity of particle, W/m-K
L_f	thickness of deposition layer, m
M_{air}	molecular mass of air, kg/kmol
M_{wv}	molecular mass of water, kg/kmol
$m_{d,dep}$	mass of dust deposited on heat exchanger, kg
$m_{d,down}$	mass of dust deposited on duct floor downstream of the heat exchanger, kg
$m_{d,inc}$	mass of dust incident on front face of heat exchanger, kg
$m_{d,up}$	mass of dust deposited on duct floor upstream of the heat exchanger, kg
m_p	mass of particle, kg
$\dot{m}_a$	mass flow rate of air, kg/s
$\dot{m}_w$	mass flow rate of water, kg/s
N_A	Avogadro constant, 1/kmol
N_t	number of transverse tube rows, dimensionless
P	probability, dimensionless
P_l	longitudinal tube pitch, m
P_t	transverse tube pitch, m
P_w	pitch (trough to trough distance) of one 'wave' in a wavy fin structure, m
$p_{a,in}$	total pressure of air entering the heat exchanger, Pa
$p_{a,out}$	total pressure of air leaving the heat exchanger, Pa

$p_{p,wv}$	partial pressure of water vapor in air, Pa
p_w	total pressure of water, Pa
$\dot{Q}_{act}$	actual rate of heat transfer through heat exchanger, W
$\dot{Q}_{air}$	air-side rate of heat transfer through heat exchanger, W
$\dot{Q}_{max}$	maximum possible rate of heat transfer through heat exchanger, W
S_{fin}	fin pitch, m
St_{fin}	Stokes number for flow over fins, dimensionless
St_{tube}	Stokes number for flow over tubes, dimensionless
T_{air}	temperature of free stream of air, K
$T_{a,in}$	temperature of air entering the heat exchanger, K
$T_{a,out}$	temperature of air at leaving the heat exchanger, K
$T_{w,in}$	temperature of water entering the heat exchanger, K
$T_{w,out}$	temperature of water leaving the heat exchanger, K
t_{fin}	fin thickness, m
t'_{fin}	fin thickness adjusted for deposition buildup, m
U_{duct}	primary (streamwise) air velocity approaching front face of heat exchanger, m/s
U_{hx}	primary (streamwise) air velocity inside heat exchanger core corrected for change in flow area, m/s
u_i	instantaneous airflow velocity along direction *i* (sum of mean and fluctuation velocities), m/s
$u_{p,i}$	instantaneous particle velocity along direction *i* (sum of mean and fluctuation velocities), m/s
$\bar{u}_i$	mean airflow or particle velocity along direction *i*, m/s
u'_i	instantaneous turbulent fluctuation airflow velocity along direction *i*, m/s
$u'_{p,i}$	instantaneous turbulent fluctuation particle velocity along direction *i*, m/s
$u'_{rms,i}$	RMS turbulent fluctuation airflow velocity along direction *i*, m/s
$u'_{p,rms,i}$	RMS turbulent fluctuation particle velocity along direction *i*, m/s
$u_{pho,i}$	turbophoretic deposition velocity along direction *i*, m/s
u_s	settling velocity of particle under gravity, m/s
$\overline{u'_i u'_j}$	Reynolds stress in *ij* plane due to turbulent airflow, N/m^2
$V_{a,in}$	velocity of air entering the heat exchanger, m/s

$v_{ther+diff}$	net particle velocity under thermophoretic and diffusiophoretic forces towards tubes, m/s
$w_{ther+diff}$	net particle velocity under thermophoretic and diffusiophoretic forces towards fins, m/s
x	spatial location, m
x_{air}	mole fraction of air, dimensionless
x_{wv}	mole fraction of water vapor in air, dimensionless
γ	mole fraction, dimensionless
Δm_{fil}	change in measured mass of filter, kg
Δp_{HX}	pressure drop in air across heat exchanger, Pa
$\Delta p_{HX,clean}$	pressure drop in air across clean heat exchanger, Pa
$\Delta p_{HX,fouled}$	pressure drop in air across fouled heat exchanger, Pa
Δp_{Pitot}	pressure drop in air across Pitot tube, Pa
Δp_{total}	combined pressure drop in air across heat exchanger and filter, Pa
ε	heat exchanger effectiveness, dimensionless
λ	molecular mean free path, m
μ_{air}	dynamic viscosity of humid air, kg/m-s
v_{air}	kinematic viscosity or momentum diffusivity of humid air, m^2/s
ρ_p	particle density, kg/m^3
$\tau_{imp,ent,i}$	time needed for particle to collide with heat exchanger due to entrainment in random velocity bursts, s
$\tau_{imp,tur,i}$	time needed for particle to collide with heat exchanger due to turbophoresis, s
$\tau_{p,i}$	relaxation time of particle for motion along direction i, s
ϕ	correction factor, dimensionless
$\phi_{a,in}$	relative humidity of air entering the heat exchanger, dimensionless
ψ	flow parameter used in analysis of deposition due to Brownian motion, dimensionless
$\omega_{a,in}$	humidity ratio of air entering the heat exchanger, kg water vapor/kg dry air
$\omega_{a,out}$	humidity ratio of air leaving the heat exchanger, kg water vapor/kg dry air

∇n_{wv}	gradient of molar concentration of water vapor in air, kmol/m^4
∇p_{wv}	gradient of vapor pressure of water between air stream and heat exchanger surface, Pa/m
∇T_{air}	gradient of temperature between air stream and heat exchanger surface, K/m
$\cup$	logical OR operation

ABSTRACT

Author: Inamdar, Harshad V. PhD
Institution: Purdue University
Degree Received: August 2018
Title: Performance of Finned Heat Exchangers after Air-side Fouling and Cleaning
Committee Chair: Eckhard Groll and Suresh Garimella

Air-side fouling of enhanced surface heat exchangers by particulate matter may significantly reduce their performance. Hence, the effect of particulate fouling and subsequent cleaning on the performance of finned heat exchangers is investigated. It is anticipated that heat exchanger geometry and operating conditions such as air velocity, air humidity, and concentration of dust in air will impact the process of fouling and subsequent performance degradation of heat exchangers.

In the experimental phase of research, heat exchangers being tested are installed in a wind tunnel where all air-side parameters can be controlled. ASHRAE standard test dust is injected into the air stream in a controlled manner leading to fouling of the heat exchanger. The mass of dust deposition on the heat exchanger is indirectly measured to quantify the extent of fouling of the heat exchanger. In addition, the pressure drop across and heat transfer through the heat exchanger are also measured to quantitatively evaluate degradation in performance due to fouling. A small set of in-situ cleaning strategies are attempted coupled with a standard detergent-based cleaning procedure to evaluate their efficacy.

In the modelling phase of research, a mathematical model is developed to predict the deposition rate and distribution of dust as a function of time using heat exchanger geometry and operating conditions as inputs. Published and measured experimental data are compared against model predictions. To improve prediction accuracy and fidelity of the model with experiments, fundamental measurements are necessary to acquire knowledge of the interaction parameters between the heat exchanger surface and the fouling agent. When this information is lacking, the use of estimated values or tuning factors becomes necessary.

It is proposed to extend the developed fouling model to predict the performance of fouled heat exchangers. The predicted fouled heat exchanger performance will then be used to estimate degradation in system performance due to fouling.

With this project, it is envisioned to predict the extent of fouling of fielded heat exchangers, and set target cleaning schedules based on the maximum degradation in performance of the heat exchanger that can be tolerated by the system in which the heat exchanger is installed. A comparison of prior-fouling and post-cleaning performances will enable an understanding of the efficacy of cleaning procedures. The experimental procedure developed as part of this research is proposed as a robust and repeatable test protocol for simulating heat exchanger fouling in laboratory conditions.

CHAPTER 1. INTRODUCTION

1.1 The Phenomenon of Fouling

The accumulation of dirt, scale, corrosion products or other material on the surfaces of heat exchangers is defined as fouling (Bott, 1988). The accumulated material may be of organic or inorganic origin. Epstein (1978) categorized fouling in six primary categories based on the dominant fouling mode.

1. Precipitation fouling or scaling is the precipitation of dissolved substances from a process fluid stream onto a heated heat transfer surface.

   For example, precipitation of calcium carbonate on the tube or shell side of water cooled condensers or formation of whey protein deposits on heat transfer surfaces in the dairy industry.
2. Particulate fouling is the deposition of fine suspended particles from a process fluid stream on a heat transfer surface.

   For example, soot and ash build up on boilers from combustion exhaust or fouling of air-cooled condensers in the HVAC industry due to atmospheric particulate matter.
3. Chemical reaction fouling is the deposition of products of chemical reactions in the process fluid on a heat transfer surface when the surface does not participate in the reaction.

   For example, coke fouling in the petroleum industry due to autoxidation and polymerization of hydrocarbons or fouling in nuclear reactors using organic coolants.
4. Corrosion fouling is the deposition of products of a chemical reaction between a heat transfer surface and process fluid on the participating surface.

   For example, corrosion in desalination plants or corrosion of heat exchangers due to high sulfur dioxide and water vapor content in process gases
5. Biological fouling is the attachment and growth of organisms on a heat transfer surface accompanied by the deposition of substances generated by said organisms.

   For example, growth of macroorganisms such as barnacles and mussels or biofilms consisting of colonies of microorganisms such as algae and bacteria in regions of low local flow velocities in water cooled heat exchangers.

6. Solidification or freezing fouling is the solidification of dissolved substances from a process fluid stream onto a cooled heat transfer surface.
   For example, solidification and deposition of paraffin wax in crude oil pipelines or frosting of heat exchangers in HVAC applications.

Precipitation fouling and solidification fouling are together categorized as crystallization fouling. Barring crystallization fouling, all modes listed above may contribute to air-side fouling of heat exchangers. Frosting, although not a mode of fouling per se, occurs due to freezing of water droplets on the heat transfer surface. It has a similar detrimental effect on the heat exchanger performance and is therefore listed above. Out of all modes listed above, particulate fouling is most commonly associated with gas-side fouling (Marner, 1990). The incidence of a single fouling mode is rare, and most fielded heat exchangers undergo fouling in multiple modes, especially when fouling on the air-side and tube-side are considered concurrently.

1.2 Impact of Fouling

Bott and Bemrose (1983) briefly suggest the annual cost of gas-side fouling in the United Kingdom to be $120 million. Their estimate was based on a study published by Thackeray (1979), and therefore it is unclear whether this estimate is in 1979 dollars or 1983 dollars.
A more detailed report published by Garrett-Price et al. (1984) divided costs incurred due to fouling in several components such as those paraphrased below.

1. Capital costs due to oversized or redundant equipment
2. Additional maintenance and cleaning costs
3. Lost energy costs and increased production costs due to increased energy consumption
4. Lost production costs due to additional downtime

The combined burden of tube-side and shell-side (or gas-side) fouling on the United States industry was extrapolated to be between $3 billion and $10 billion (in 1982 dollars).
Pritchard (1988) discussed the estimation of costs incurred due to heat exchanger fouling and concluded that such a cost estimate was difficult to obtain due to a lack of industrial data. This lack of data was attributed to the fact that fouling was unavoidable, and therefore plant designs accounted for inefficiencies related to fouling. Thus, there was a reluctance to employ effort to

collect data. Additionally, costs related to implementation of anti-fouling measures had to be weighed against costs incurred on account of reduced performance due to fouling. Thus, whether the first or second costs were the true financial impact of fouling was declared to be an open question. Nevertheless, detailed cost estimates for specific cases were presented. Some of the estimates of the cost of gas-side fouling are summarized in Table 1.1.

Table 1.1. Financial implications of fouling from Pritchard (1988).

Category		Associated cost
Capital costs		
	Overdesigned heat exchangers	Half of overdesigned heat exchanger surface area might be unnecessary.
	Installation costs	Between 2 to 10 times heat exchanger surface area depending on industry and location.
	Antifouling equipment	Cost of chlorination facilities intended to control biofouling in power plants in the U.S.A. could be as high as $267 million in 1983.
Fuel costs		
	Primary energy	$92 million annually for gas-side fouling in the petroleum industry, and $121 million annually for gas-side fouling in the cement industry in the U.S.A. in 1983. £10 to 20 million annually for fouling of boiler tubes in the power stations in the U.K. in 1979.
	Secondary energy	Refrigeration chillers in the U.S.A. were observed to consume 10 to 30% more kW per ton of capacity on account of fouling in 1980.
Maintenance costs		
	Cleaning	£30 million to remove fouling deposits in process plants in the U.K. in 1980. $2.1 billion annually due to gas-side fouling alone in the U.S.A. in 1982. £20 to 30 million to remove fouling from oil platforms in the North Sea in 1990.
	Preventive measures	£100 million annually in the U.K. for water treatment.
Lost production		$600 million annually to the U.S. power industry in 1983 due to corrosion. $108 million annually to the U.S. cement industry in 1982 due to gas-side fouling.
Safety		Elevated risk and incidence of component failure requiring stricter regulatory codes and personnel training.
Lost opportunities		Lack of knowledge and experimental data regarding fouling leading to overly conservative choices from design engineers.

Although the information provided in Table 1.1 is sparse and nonuniform, it can be seen that fouling costed different industries figures in excess of hundreds of millions in dollars or pounds sterling in the United States or the United Kingdom respectively. It can be reasonably estimated that the financial burden of fouling on the world economy is significant and can be quantified to be in excess of billions of dollars.

Smith and Dirks (1985) broke down the financial burden of heat exchanger fouling on the U.S. industrial sector into four categories. Capital costs due to special design considerations required to combat fouling related performance degradation amounted to between $1.04 million and $1.3 million annually. Energy costs associated with inefficient operation of plants were estimated to be between $750 million and $3.8 billion annually. Online and offline cleaning equipment and cleaning services were accounted for under maintenance costs amounting to $2.2 billion annually. Production losses due to downtime associated with fouled heat exchangers were estimated to be about $170 million annually. Thus, a conservative estimate of the annual cost of heat exchanger fouling to U.S. industry in 1984 was between $4.2 billion and $7.4 billion. All reported figures were for 1984.

Xu et al. (2007) estimated the cost of boiler and turbine fouling to China to be in the region of $4.68 billion in 2006, which was around 0.17% of contemporary Chinese GDP. This estimate is in line with Müller-Steinhagen et al. (2006) who suggested that the total financial burden of heat exchanger fouling could be as high as 0.25% of the GDP of industrialized countries.

This researcher was unable to obtain more recent studies investigating the financial implications of heat exchanger in the published literature. The lack of an updated cost estimate of heat exchanger fouling to industry was identified as a gap in the literature that could be fulfilled as part of this research, or as part of a future study.

1.3 Historical Fouling Research

One of the earliest publications on the topic of gas-side fouling as per a search on Google Scholar conducted on July 26, 2015 is Miller (1967). Mechanisms involved in the fouling of compact heat exchanger matrices used as gas turbine regenerators were investigated. One of the main conclusions drawn was that fouling was a two-stage process. Trace quantities of heavy hydrocarbons from combustion exhaust condensed on the heat transfer surface depositing as an adhesive coating. This layer then captured carbonaceous particulate matter. The synergetic nature

of fouling mechanisms and the role of prior fouling deposits in accumulation of particulate matter was revealed.

Another obscure report on gas-side fouling was published by Bott (1971) which the author of this work was unable to find despite many efforts. The report is mentioned here because the author of the original work, Dr. Theodore Reginald Bott, MBE, published many studies related to fouling of heat transfer surfaces and heat exchangers, and the aforementioned report seems to be one of his earliest attempts in this direction. Much of the earlier groundwork in this area of research was laid by Dr. Bott and his students in future publications.

Epstein (1978) published a review of studies into fouling of heat transfer surfaces and also various deposition and re-entrainment models. A brief review of fouling monitoring was also presented, which divided the process of monitoring into quantitative and qualitative assessments. The use of fouling curves as a way of characterizing the temporal behavior of fouling was identified and a few examples from the literature were presented. The six categories of fouling were described, and mechanisms by which deposition occurred in each category were discussed. Gravitational settling, thermophoresis, and electrophoresis had already been identified as mechanisms of particulate fouling, and the dependence of each mechanism on the particle size was mentioned. From the review of re-entrainment models, it can be seen that the concept of different mechanisms working in tandem already existed.

Marner and Suitor (1983) surveyed gas-side fouling in industrial heat transfer equipment and presented their results in form of a technical report published by the U.S. Department of Energy. A detailed overview of gas-side fouling was presented including a basic introduction to the phenomenon, and the proximate causes behind it. At the time of publication, research into gas-side fouling, as the name of the area of research suggests, focused on fouling of heat exchangers that used combustion gases as the process fluid. Various fuels combusted in different industries were listed and possible contributors to gas-side fouling in each exhaust stream were discussed.

Marner and Henslee (1984) published a report surveying measuring devices used to assess the level of gas-side fouling suffered by heat transfer surfaces. The surveyed devices were classified into different categories based on their functionality:

1. Heat flux meters measured the local heat transfer per unit area. A change in the local heat flux was correlated to a change in the local fouling resistance, which in turn was correlated to a local buildup of foulant.

2. Mass accumulation probes were used to quantitatively determine the mass of foulant accumulation at a certain location over time.
3. Optical devices were uncommon, and used the difference in the optical properties of heat transfer surfaces and foulant depositions to assess buildup.
4. Deposition probes were used to qualitatively investigate foulant depositions at a certain location for its chemical composition.
5. Acid condensation probes were cooled probes maintained at temperatures below the acid dew-point of the gas stream. The acid dew-point of the gas stream was correlated to the acid concentration in the gas stream. The acid deposition rate was also measured using such probes.

Epstein (1988) revisited the topic of modeling of fouling of heat transfer surface; however, the focus this time was on particulate fouling. Net fouling flux was defined as the net of deposition flux and re-entrainment flux of particles, while deposition comprised transport of particles towards the heat transfer surface and subsequent attachment. Particulate transport was divided into isothermal and non-isothermal mechanisms. Deposition flux of particles was calculated as,

$$\phi_d = k_t \left(c_b - c_s \right) \tag{1.1}$$

where, kt is the transport coefficient, cb is the bulk concentration of particles, while cs is the concentration of particles near the surface. It was assumed that all particles colliding with the surface adhered to it. Then, the concentration of particles near the surface would be 0. Equation (1.1) would then become,

$$\phi_d = k_d c_b \tag{1.2}$$

where, if the physical units of the different terms in the equation were analyzed, kt would be identical to kd, the deposition velocity.

Diffusion, inertia, impaction, surface roughness, and gravitational settling were identified as isothermal mechanisms of deposition, and expressions for deposition velocity by each mechanisms were derived. The Saffman lift force was identified as a possible source of error in the analysis of particle transport in turbulent flow near the surface. Thermophoresis and (thermal

gradient driven) electrophoresis were the non-isothermal deposition mechanisms analyzed. Particle adhesion was analyzed using a simple sticking probability or conducting a force balance based on surface forces. Multiple published studies using the stated analytical method for each mechanism were also cited, giving an idea of the development of these theories. The influence of bulk flow velocity on the deposition mechanisms was also explored. It can be seen that the modeling of fouling had already developed into an area of scientific research, and did not simply rely on measurement based correlations.

Concurrently, Bott (1988) published an article on gas-side fouling, but which focused specifically on heat exchangers rather the broader application area of heat transfer surfaces. Fouling was proposed to be the net action of transport of particles to the surface, adhesion of particles to the surface, and removal of particles from the surface. Particle transport to the surface was divide into two regimes: transport from the bulk flow to the boundary layer due to Brownian motion, eddy diffusion, and thermal diffusion; and transport across the boundary region correspondingly due to diffusion, inertial impaction, and thermophoresis. Mathematical expressions to quantify deposition due to mechanisms were discussed.

Marner (1990) published an extensive review of developments in the area of gas-side fouling. Four primary topics of knowledge were covered:

1. Theoretical analysis of fouling mechanisms
2. Analytical treatment of the impact of fouling on heat exchanger performance and metrics used to quantify fouling
3. Experimental investigations into gas-side fouling
4. Gas-side fouling measuring devices

Prior review articles were also briefly discussed. This article is, in the opinion of the author of this current work, presents a thorough treatment of the area of research covered under gas-side fouling, and covers almost all of the seminal works and developments in the topic. The progression of ideas can be seen from the literature review: initial studies focused on fouling of simple surfaces and due to one or two mechanisms, then the interaction of multiple mechanisms was investigated. Attention then turned to fouling of heat exchanger surfaces, which had complicated geometries, thus introducing difficulties in experimentation and the analytical treatment of gas-side fouling. The modification of purely analytical models by experimentally obtained coefficients is also evident. The use of fouling factors to account for additional flow resistance due to foulant buildup,

and the use of fouling resistances to account for additional thermal resistance due to deposition layers is also presented.

Similar reviews of gas-side fouling after Marner (1990) could not be found by the author of this current work. A simple analysis using the Create Citation Report on Web of Science reveals some interesting information. The first article published with 'air-side fouling' in its title was Petrov (1968), and the next article was Mason et al. (2002). All publications in the intervening time period have 'gas-side fouling' in their title. From the literature review, it is evident that the overwhelming majority of papers investigated fouling of heat exchangers with combustion gases as the process fluid outside the tubes. Air-side fouling of heat exchangers in refrigeration and air-conditioning applications can be considered as a relatively new sub-topic of research, and there is still much scope for broadening as well as deepening the knowledge base. The research described in this work attempts to explore this area.

1.4 Motivation

Most heat exchangers installed in the field experience air-side fouling. The degradation in performance of heat exchangers due to air-side fouling is a known problem faced by industry. Better understanding of the phenomenon of particulate fouling on the air-side of heat exchangers is the primary motivation behind this work. An evaluation of efficacy of cleaning processes to reverse the effects of fouling is also a driving factor behind this study. This effort is a series of projects conducted at Ray W. Herrick Laboratories, Purdue University investigating air-side fouling of heat exchangers. A continuing motivation behind this work is to develop institutional expertise in the area of heat exchanger fouling.

1.5 5 Objectives

This effort focuses on the following objectives:

1. Develop a standardized protocol to test performance of heat exchangers after air-side fouling by decoupling the phenomenon of fouling from the performance of the heat exchanger in fouled conditions.
2. Define test metrics to describe heat exchanger fouling.

3. Experimentally test heat exchangers after air-side fouling to quantitatively evaluate performance in clean and fouled conditions.
4. Investigate the effect of a change in operating conditions of the heat exchanger on fouling and the subsequent degradation in its performance and identify key parameters.
5. Develop a mathematical model as a tool to predict air-side fouling of heat exchangers as a function of its geometry and operating conditions.
6. Use the developed model to predict performance of the heat exchanger in a fouled condition to move away from a correlation based approaches towards more generalized models.

CHAPTER 2. DEFINING THE EXPERIMENTAL PROTOCOL BASED ON PUBLISHED FOULING STUDIES

2.1 Introduction

Epstein (1978) categorized fouling into 6 primary categories based on the dominant mode of deposition; *viz.* precipitation fouling (scaling), particulate fouling, chemical reaction fouling, corrosion fouling, biological fouling, solidification fouling. Barring precipitation fouling and solidification fouling, the other four modes may contribute to heat exchanger fouling on the air-side (or gas-side).

Much of the earlier research on gas-side fouling concentrated on power generation or waste heat recovery applications where combustion gases with high concentration of particulate matter were the process fluid. This is evidenced by Boll and Patel (1961), who analyzed corrosion mechanisms from the point of view of thermodynamics, and Miller (1967), who experimentally fouled gas turbine regenerators and observed the effect of surface geometry and air inlet temperature on the rate of degradation in their performance due to fouling. The term 'gas-side' fouling indicates the nature of applications under consideration where process fluid temperatures are high, the process fluid may contain corrosive vapors, and the particulate matter entrained in air is dominated by particulates whose source can be traced to combustion. One of the earliest studies referring to 'air-side' fouling of heat exchangers is Petrov (1968), who investigated effect of soot and fuel dust fouling on the heat transfer performance of air heater tube bundles. Insignificant deposits were observed on tube bundles, and deposition was reported to stabilize after a certain duration. Deposits were reported on rear faces of tube rows along with on frontal edges. This experiment still dealt with fouling due to particulates originating from combustion, and not ambient particulate matter. Cross and Cowell (1980) experimentally studied fouling on different types of automotive and industrial radiators and observed that fouling deposits were almost exclusively concentrated within the first few millimeters of the leading edge of the heat exchanger. It was inferred that louvered surfaces would show highest resistance to fouling. This also marked a broadening of research focus as automotive, air-conditioning, and refrigeration applications became relevant. The operating conditions, properties of suspended particulate matter, and concentrations of chemically reactive or corrosive substances entrained in the process fluid are different in these applications compared to the combustion-dominated applications. Consequently,

the nature of fouling occurring in these applications may be significantly different owing to differing deposition mechanisms.

This study is primarily concerned with dry particulate fouling occurring on heat exchangers that reject heat to the process fluid outside the tubes; most often air, and where the process fluid stream does not react with the heat exchanger surface.

2.2 Literature Review

2.2.1 Standards Related to Air-side Fouling of Equipment

ASHRAE Standard 52.2–2012 establishes test methods for evaluating performance characteristics of air cleaners, usually for ventilation equipment. Guidelines to construct a test apparatus, test materials to be used, and metrics to report air cleaner efficiency are also stated. SAE Standard J726–2002 established test methods for evaluating performance characteristics of air cleaners, usually in automotive applications. ISO Standard 5011:2014 superseded J726 and specifies uniform test procedures, conditions, equipment, and performance metrics to compare performance of air cleaners. ISO Standards 12103–1:1997 and 12103–2:1997 define test dusts to be used in such air cleaner tests. MIL–STD–810G in Method 510.6 (Sand and Dust) defines methods to evaluate the ability of material to resist the effects of dust in its operating environment. Test apparatus, test process, and test dust are described along with a method to analyze results. Thus, there exist a few standards that consider the interaction of suspended particulate matter with equipment that uses air as a process fluid. It is possible to use parts of these standards and apply them to testing of fouled heat exchangers.

2.2.2 Fouling Experiments in the Literature

Much variation can be observed in the published literature concerning experimental fouling of heat exchangers. Table 2.1 lists published studies and compares certain facets of the test procedure employed to experimentally foul heat exchangers in laboratory environments, viz. the method employed to simulate heat exchanger fouling, the operating conditions during the experiment, and the measurement of heat exchanger performance after fouling. In all studies, air is the process fluid outside the heat exchanger. All experiments were conducted in wind tunnels where the heat exchanger being tested was installed inside a wind tunnel and airflow was forced

through it without allowing bypass. Therefore, the air velocities reported are face velocities measured inside the wind tunnel at inlet to the heat exchanger.

Table 2.1. Comparison of published studies on basis of operating conditions, fouling method, and performance measurement.

Study	Heat Transfer Mode	Airflow Mode	Fouling Method	Evaluation of Fouled Performance
Bott and Bemrose (1983)	Both heat rejection to air stream and heat absorption from air stream (without moisture condensation)	Maintained constant throughout fouling period at values between 2.4 and 5.8 m/s (one constant value per test run)	Continuous; rate maintained constant at 21 or 37 g/min for usually 30 hours (sometimes up to 120 hours) *0.017 mm thick layer of liquid used to coat air filters applied to heat exchanger surface*	Periodically stop fouling and measure heat exchanger performance at a range of air velocities from 2.4 to 5.8 m/s
Zhang *et al.* (1990)	Both heat rejection to air stream and heat absorption from air stream (without moisture condensation)	Airflow rate allowed to decrease due to fouling	Continuous; maintained constant in each test run	Transient evaluation in fouled condition
Siegel (2002)	Unclear, but it seems isothermal	Maintained constant at 2 m/s	In batches; 25 g per batch till pressure drop doubled compared to clean case; rate not reported	In fouled condition, once after every batch of dust is used
Siegel and Nazaroff (2003)	Isothermal and heat rejection from air stream (with and without moisture condensation)	Maintained constant at 1.5, 2.2, and 5.2 m/s (one constant value per test run)	Continuous; rate and total duration unclear	No evaluation of fouled heat exchanger performance
Ahn *et al.* (2003)	Heat absorption from air stream	Maintained constant at 1 m/s	Obtain fouled heat exchangers installed in the field for durations between new and 15 years	In fouled condition, as-received from the field, at air velocity of 1 m/s

Lankinen *et al.* (2003)	Both heat rejection to air stream and heat absorption from air stream (with moisture condensation)	Maintained constant throughout fouling period	Continuous; rate maintained constant at 0.07 to 0.14 g/s for a total loading between 2.1 to 8.3 kg depending on fouling agent	In fouled condition at the end of fouling period at air velocities between 1.4 to 3.5 m/s
Pak *et al.* (2005)	Heat rejection to air stream	Maintained constant throughout fouling period at 1.53 m/s	Continuous; rate maintained constant at 100 g/hr for a total period of 3 hours	In fouled condition at the end of fouling period at air velocities between 0.5 to 2.0 m/s
Mason *et al.* (2006)	Isothermal	Airflow rate allowed to decrease due to fouling	Continuous; suspension density of fouling agent maintained constant at 1.5 g/m^3	Transient evaluation in fouled condition
Haghighi-Khoshkhoo and McCluskey (2007)	Heat absorption from air stream (with and without moisture condensation) and isothermal conditions	Unclear if maintained constant throughout fouling period	Continuous (in batches); maintained constant up to a fixed mass	In fouled condition at multiple points during fouling period 2.0, 2.5, 3.0, 3.5, 4.0, 4.5, and 5.0 m/s
Yang *et al.* (2007)	Heat absorption from air stream (with and without moisture condensation)	Maintained constant throughout fouling period at 2.54 m/s	Continuous; rate maintained constant at 100 g/hr for total of 6 hours	In fouled condition at the end of fouling period at air velocities of 1.52, 2.03, 2.54, and 3.05 m/s
Ali and Ismail (2008)	Heat absorption from air stream (with moisture condensation)	Maintained constant throughout fouling period	In batches, 100 g/hr at once till 300 g of fouling agent was used	In fouled condition after each batch at air velocities from 0.1 to 5.0 m/s
Bell and Groll (2011)	Heat absorption from air stream (with and without moisture condensation)	Maintained constant throughout fouling period at 2.8 m/s	Continuous; rate maintained constant at 100 g/hr for total of 6 hours	In fouled condition at the end of fouling period at air velocities of 1.0, 1.25, 1.5, 1.75, and 2.0 m/s

Bell *et al.* (2011)	Heat absorption from air stream (with and without moisture condensation)	Maintained constant throughout fouling period at 2 m/s	Continuous; rate maintained constant at 100 g/hr till a 600 g of fouling agent is used	In fouled condition once after 300 g fouling agent is used and once at the end of fouling period at different air velocities between 1.0 and 3.0 m/s
Malayeri *et al.* (2011)	Isothermal and heat absorption from air stream (without moisture condensation)	Maintained constant throughout fouling period at 10, 30, 70, or 120 m/s	Continuous, rate maintained constant at 2 g/hr for 4 to 6 hours or till pressure drop across heat exchanger reaches 18 Pa	Transient evaluation in fouled condition
Sun *et al.* (2012)	Both heat rejection to air stream and heat absorption from air stream (with moisture condensation)	Maintained constant throughout fouling period at 3.0 m/s	Continuous; rate maintained constant at 11.6 g/min for total of 4 hours (or until pressure drop across the heat exchanger doubled)	Transient evaluation of performance at same operating conditions as during fouling
Shi *et al.* (2012)	Heat absorption from air stream	Likely that airflow rate changed throughout fouling period, but not explicitly stated	Continuous; in–situ fouling, therefore rate dependent on parent system	At the end of fouling period (identified by stabilization of system operation parameters)
Walmsley *et al.* (2013)	Isothermal	Maintained constant throughout fouling period at 4.5 m/s	Continuous; rate maintained constant at 2.4 g/min	Transient evaluation in fouled condition
Obadina *et al.* (2014)	Isothermal	8.5, 12.4, 14.4, 16.3, and 24.4 m/s	Continuous; suspension density of fouling agent maintained constant at 0.5, 1.1, 1.6, or 2.2 g/m^3	Transient evaluation of pressure drop and measurement of sand retention at the end of each test
Zhan *et al.* (2016)	Isothermal	Maintained constant at 1, 2, and 3 m/s (one constant value per test run)	Continuous; rate maintained constant at 80, 160, or 280 kg/m^3 of airflow until saturation of foulant deposition	None

Hosseini *et al.* (2017)	Isothermal	Maintained constant at 1, 2, 3, 4, and 5 m/s (one constant value per test run)	Continuous (in batches); maintained constant up to a fixed mass	Transient evaluation in fouled condition

From the non-exhaustive summary of published studies in presented in Table 2.1, it is seen that experiments may be performed isothermally or the contribution of a temperature gradient between the air stream and heat exchanger surface to the phenomenon of fouling could be included in the experiment; and the presence of condensed moisture on the heat exchanger surface could be accounted for. Further, the evaluation of heat exchanger performance in fouled condition may be conducted at test conditions, or over a range of operating conditions. On the other hand, most studies report a constant air velocity throughout the fouling phase of the experiment. All these choices could potentially affect the process of fouling and thus make comparison of different experimental results difficult.

2.2.3 Fouling Agents in the Literature

Table 2.2 compares the choice of fouling agent made to simulate heat exchanger fouling in terms of substance and particle size. Since all studies are concerned with dry particulate fouling of heat exchangers on the air-side, all fouling agents are some variations of test dusts. The choice is informed by the heat exchanger application and the suspended particulates encountered by the heat exchanger in the field during routine operation.

Table 2.2. Comparison of test dusts used as fouling agents in the published literature.

Study	Fouling Agent	Particle Size
Bott and Bemrose (1983)	Precipitated calcium carbonate	Polydisperse; range : 3–30 µm
Zhang *et al.* (1990)	Calcium carbonate	Monodisperse; 5 and 12 µm
Siegel (2002)	SAE Coarse Test Dust	Not reported
Siegel and Nazaroff (2003)	Oil particles tagged with fluorescein	Monodisperse; range: 1–15 µm (approximately)
Lankinen *et al.* (2003)	Pure quartz (SAE J 726)	Polydisperse; range: 0–100 µm
	ASHRAE Standard Test Dust #1	Not reported
Pak *et al.* (2005)	ASHRAE Standard Test Dust #1	Not reported
Mason *et al.* (2006)	Sawdust	Polydisperse; range: 0.2–5 mm
Haghighi-Khoshkhoo and McCluskey (2007)	Wood shavings	Polydisperse; range: < 4 mm
Yang *et al.* (2007)	ASHRAE Standard Test Dust #1	Not reported
Ali and Ismail (2008)	Fouling materials collected from dirt evaporator coils of window-type air conditioners	Polydisperse; range: < 200 µm
Bell and Groll (2011)	ASHRAE Standard Test Dust #1	Not reported
	Arizona Road Test Dust	Polydisperse; range: < 80 µm
Bell *et al.* (2011)	ASHRAE Standard Test Dust #1	Not reported
Malayeri *et al.* (2011)	Soot particles	Polydisperse; range: 10–300 nm
Sun *et al.* (2012)	Masons hydrated limestone powder (type S)	Polydisperse range: 0.3–110 µm (approximately)
	Ground oats	Polydisperse; mass median diameter = 1067 µm
Shi *et al.* (2012)	Suspended particulates in flue gas from a coal fired boiler	Not reported
Walmsley *et al.* (2013)	Milk powder	Polydisperse; volume mean diameter = 104 µm
Obadina *et al.* (2014)	Sand according to MIL–STD–810G [10]	Polydisperse; 150–850 µm
Zhan *et al.* (2016)	Synthetic dust (presumably ASHRAE Standard dust)	Not reported
Hosseini *et al.* (2017)	Wood shavings	Polydisperse; range 1 µm–4 mm

It is observed that particulate matter with different compositions and size distributions has been employed in attempts to simulate heat exchanger fouling in laboratory environments. The dynamics of the transport of suspended particulates, the characteristics of the foulant deposits formed on the heat exchanger surface, the adhesion between the deposited particulates and the heat exchanger surface, and the effect of foulant deposits on the flow and thermal resistance of the heat exchanger may be affected by the characteristics of the fouling agent. Thus, the phenomenon of fouling and its impact on subsequent heat exchanger performance are strong functions of particle size and composition of the fouling agent. Therefore, the variability in choice of fouling agent, although important to bring out more experimental data regarding fouling, is not conducive to standardization of the test protocol.

Some of the fouling agents referred to in Table 2.2 are defined in standards published by organizations discussed at the beginning of Section 2.2.1. These test dust specifications are summarized in Table 2.3.

Table 2.3. Test dusts specified in standards.

Test Dust	Dust Composition	Particle Size Distribution
SAE Fine Test Dust (SAE Standard J726–2002)	Primarily silica and alumina with other metal oxides in small quantities	Polydisperse: 0–176 µm (54% by volume under 11 µm)
SAE Coarse Test Dust (SAE Standard J726–2002)	Primarily silica and alumina with other metal oxides in small quantities	Polydisperse: 0–176 µm (56% by volume under 44 µm)
A2 Fine Test Dust (ISO Standard 12103–1:1997)	Primarily silica and alumina with other metal oxides in small quantities	Polydisperse: 0–120 µm (50% by volume under 10 µm)
Arizona Road Test Dust	Synonymous with SAE Fine Test Dust and later with A2 Fine Test Dust (after ISO 12103-1 superseded SAE J726)	
ASHRAE Standard Test Dust #1 (ASHRAE Standard 52.2–2012)	72% by mass SAE Fine Test Dust	According to [7] or [9]
	23% by mass powdered carbon	Polydisperse: estimated to have a mean diameter of 101 nm based on specified CTAB surface
	6% by mass milled cotton linters	Polydisperse: ground using a knife shearing mill fitted with a 4 mm screen classifier
Blowing dust (US MIL–STD–810G)	Dust from a region of interest (preferred) or its analog or Red china clay or Silica flour	Polydisperse: < 150 µm (median diameter 20 ±5 µm)
Blowing sand (US MIL–STD–810G)	At least 95% by weight SiO_2	Polydisperse: 150–850 µm (median diameter 20 ±5 µm)

The above list is incomplete; ISO 12103–1:1997 defines other grades of test dusts; so does MIL–STD–810G. The test dusts included in Table 2.3 are primarily those that are considered in the published literature regarding air-side fouling of heat exchangers. There seems to be some agreement between the different standards regarding the particle size distribution of dust that is considered to be environmental dust. ASHRAE 52.2–2012 also defines average particle sizes for suspended particulates commonly observed in air. The composition and size distribution of test dusts can be compared against Table E–1 from the standard to estimate the kind of particulate matter being simulated by the test dust.

2.2.4 Fouling Metrics in the Literature

The metrics used to evaluate performance of a fouled heat exchanger and the method employed to report them also varies in the literature; these are summarized in Table 2.4.

Table 2.4. Fouling metrics in the literature.

Study	Fouled Heat Exchanger Performance Metric	Independent Variable
Bott and Bemrose (1983)	Friction factor, Colburn *j*–factor, fan power	Duration of experiment
Zhang *et al.* (1990)	Friction factor, Colburn *j*–factor, fan power, air-side heat transfer coefficient, fouling resistance, pressure drop (not the same for all experiments)	Duration of experiment
Siegel (2002)	Deposition fraction (ratio of mass of dust deposited on heat exchanger to total mass of fouling agent introduced into air stream)	Particle size
Siegel and Nazaroff (2003)	Pressure drop	Mass of dust deposited on heat exchanger
Ahn *et al.* (2003)	Pressure drop, cooling capacity	Duration of operation in the field
Lankinen *et al.* (2003)	Fouling factor, overall heat transfer coefficient, pressure drop, friction factor	Reynolds number of airflow
Pak *et al.* (2005)	Pressure drop, UA value	Air velocity
	Mass of test dust deposited on heat exchanger	Once after the experiment
	Pressure drop	Duration of experiment
Mason *et al.* (2006)	Time to foul, stop ratio for particles	Critical particle diameter for a heat exchanger
	Mass of test dust deposited on heat exchanger	Once after the experiment
Haghighi-Khoshkhoo and McCluskey (2007)	Fouling coefficient, tube-side ΔT	Air velocity; at multiple instances during a fouling test
	Pressure drop	Total mass of test dust used
	Mass of test dust deposited on heat exchanger	Once after the experiment
Yang *et al.* (2007)	Fouling factor for pressure drop and heat transfer	Air velocity; once after the fouling test
	Mass of test dust deposited on heat exchanger	Once after the experiment
Ali and Ismail (2008)	Change in air temperature and humidity across evaporator being tested, system COP	Air velocity
Bell and Groll (2011)	Pressure drop, rate of heat transfer	Air-side and tube-side mass flow rate
Bell *et al.* (2011)	Pressure drop, UA value	Air velocity

	Friction coefficient	Once after the experiment
Malayeri *et al.* (2011)	Fouling resistance, pressure drop	Duration of experiment
Sun *et al.* (2012)	Pressure drop, heat transfer effectiveness, overall heat transfer coefficient	Duration of experiment
Shi *et al.* (2012)	Fouling resistance; Heat transfer coefficient	Air velocity; Once after the fouling test
Walmsley *et al.* (2013)	Pressure drop	Duration of experiment
Obadina *et al.* (2014)	Pressure drop; Retention of fouling agent	Duration of experiment Once after the fouling test
Zhan *et al.* (2016)	Mass of test dust deposited on heat exchanger	Duration of experiment
Hosseini *et al.* (2017)	Pressure drop	Mass of test dust used; multiple times for a test run

Since the information reported by every study differs slightly from the rest, developing a physical model for fouling of heat exchangers using experimental data is difficult. The choice of the metric(s) should be made to convey maximum useful information about the experiment, the observed phenomenon of fouling, and the measured impact of fouling on heat exchanger performance.

2.2.5 Sensitivity of Fouling to Change in Heat Exchanger Design or Operating Conditions

The sensitivity of the phenomenon of fouling to a change in air-side or tube-side operating conditions has been investigated by multiple researchers. A change in operating conditions may be achieved as a complete reversal in the direction of heat transfer between air and the tube-side fluid, or as a change in a parameter such as air velocity, air humidity, concentration of suspended particulate in the air, etc. Experimental data for the effect of a change in heat exchanger design on fouling is available in the literature as well. A change in heat exchanger design may be achieved by a comparison between heat exchanger types such as finned tube and finned microchannel, or by a change in the type of fins such as a comparison between plain fins, wavy fins, and louvered fins, or by a change in geometric parameters such as fin density or tube diameter. Table 2.5 summarizes the current availability of measured data in the literature.

Table 2.5. Sensitivity of fouling to a change in heat exchanger design or operating conditions.

Study	Parameter varied	Main observations
	Bulk concentration of particulate solids in the air stream	Fouling rate is directly proportional to particulate concentration
Zhang *et al.* (1990)	Foulant particle size	Small particles enhance fouling
	Air velocity	Fouling is enhanced by higher air velocities
	Direction of heat flux in heat exchanger	Heat flux direction does not affect fouling
Siegel (2002) Siegel and Nazaroff (2003)	Foulant particle size	Deposition of smaller particles is low
Lankinen *et al.* (2003)	Fouling agent (composition and particle size distribution)	Fouling was strongly sensitive to choice of fouling agent
	Number of tube banks	Deeper heat exchangers accumulate more foulant
Pak *et al.* (2005)	Fin pattern and fin density	Fouling is sensitive to changes in these parameters
Mason *et al.* (2006)	Fin pattern, fin density, number of tube banks, arrangement of tube banks (staggered or inline)	Mass of fouling material collected in heat exchanger core and that collected on frontal face of heat exchanger are affected
Haghighi-Khoshkhoo and McCluskey (2007)	Foulant particle size	Larger particles are preferentially blocked by the heat exchanger; The fraction of particles blocked by the heat exchanger that penetrate the heat exchanger and are deposited in the core was some value between the smallest and largest particle size tested
	Presence of condensate on heat exchanger surface	Condensate tended to wash deposited foulant off the surface and ameliorate the impact of fouling
Yang *et al.* (2007)	Fin density	Heat exchangers with greater fin density tended to capture more dust
	Number of tube banks	Little correlation between heat exchanger depth and severity of fouling

	Fin pattern	Relatively small difference in fouling effects on between wavy and lanced fins
	Heat exchanger design	Finned microchannel heat exchangers are more susceptible to fouling than plate finned tube heat exchangers
Bell and Groll (2011)	Fouling agent (composition)	For foulant with more fibrous content, deposits tend to build up on the front face of the heat exchanger. For foulant with particulate content alone, deposition occurs on surface enhancements, especially near the stagnation region for airflow.
	Gas velocity	Increased gas velocity reduces particulate fouling
Malayeri *et al.* (2011)	Temperature gradient between bulk gas flow and heat transfer surface	Low temperature gradient reduces particulate fouling
	Complex geometric features on heat transfer surface	Increase in local heat transfer surface area reduces particulate fouling
	Foulant particle size	Heat exchangers clog readily when particle size is large relative to the fin spacing
Sun *et al.* (2012)	Fin density	Higher the fin density, faster the increase in airflow resistance (and by extension, the rate of fouling)
Shi *et al.* (2012)	Arrangement of tube banks (staggered or inline)	Staggered arrangement helps to lighten deposition as compared to inline arrangement
Walmsley *et al.* (2013)	Air temperature and relative humidity combination (humidity ratio maintained constant)	For low relative humidity, deposition is minimal
	Fin density	Greater fin density causes substantial increase in fouling
Obadina *et al.* (2014)	Air velocity	Increased air velocity increases fouling
	Bulk concentration of particulate solids in the air stream	Increased concentration increases fouling

	Fin density	High fin density is beneficial to particle deposition
Zhan *et al.* (2016)	Bulk concentration of particulate solids in the air stream	High particle concentrations are prone to result in particle deposition
	Air velocity	As air velocity increases, it first promotes and then restrains particle deposition
	Foulant particle size	Deposition enhances up to a critical particle size, and decreases beyond that
Hosseini *et al.* (2017)	Air velocity	Increase in flow velocity enhances deposition of small particles. Increase in flow velocity suppresses deposition of bigger particles.

2.3 Experimentation

The choice of the experimental procedure and the metrics used to quantify fouling and its impact will affect the experimental observations. No established standard currently exists that lays down guidelines for conducting fouling tests of heat exchangers. This is the primary reason behind the variation in choices made by researchers. The development of a standardized test protocol and specification of a standard fouling agent would help make fouling studies conducted in different laboratories consistent and comparable. It would also help the development of heat exchanger fouling models. When multiple researchers conduct experiments and report data in a similar manner, larger data sets are available to validate these models. With this in mind, an experimental procedure is designed that maintains many of the most commonly observed elements from the published literature, and seeks to report as much experimental data as possible. Consideration is given to whether the experimental procedure itself affects the observed outcome in any manner.

2.3.1 Overall Approach

It is proposed to separate the phenomenon of fouling from the impact of fouling on heat exchanger performance. Then, the mass (quantitative measurement) and distribution (qualitative evaluation) of foulant deposition on the heat exchanger is used to characterize the extent of fouling undergone by the heat exchanger; the flow and thermal performance of the heat exchanger characterize the performance of the fouled heat exchanger. This separation allows for development of physics-based heat exchanger fouling models whereby information about the extent of fouling is used to realistically model its impact on heat exchanger performance, instead of relying on empirical correlations.

2.3.2 Fouling Agent

The choice of fouling agent is critical because it can have a significant impact on the experiment. Ahn and Lee (2005) collected some heat exchangers (the exact number is unclear) that had been operating in the field for varying durations—between 3 and 14 years—and characterized the foulant depositions present on them. The finned-tube heat exchangers included both evaporators and condensers. The particulates present on the heat exchangers ranged in size from approximately 0.1–40 μm (based on size distribution plots) with mean diameters of 6.6–20.9 μm. The depositions on condensers comprised of particulates and fibers, whereas those on

evaporators were primarily particulates. A chemical analysis of the particulates revealed major constituents to be O, Si, Al, Fe, and Ca. Ali and Ismail (2008) collected foulant depositions from fielded evaporators and investigated its physical and chemical properties. The particle size distribution ranged from 0–200 µm with a mean diameter of approximately 77 µm, and included material from both organic and non-organic sources. The non-organic component was composed primarily of Al, Si, S, Ca, and Fe, which matches really well with the observations of Ahn and Lee (2005). High resolution images taken in both studies clearly show the presence of fibers. Thus, conclusions that can be drawn are that fouling agent should include both inorganic particulates (mainly metal oxides and silicates) and fibers, and that the particle size range should cover the submicron range, and at least extend up to 100 µm.

The composition of ASHRAE Standard Test Dust #1 is reported in Table 3. According to ISO 12103–1:1997, A2 Fine Test Dust—which makes up 72% by weight of the former test dust—comprises primarily of SiO_2, Al_2O_3, Fe_2O_3, Na_2O, and CaO. This combination of elements represents the composition of the foulant deposits observed by Ahn and Lee (2005) and Ali and Ismail (2008) fairly well. As part of this study, a sample of ASHRAE Standard Test Dust #1 was sent to Particle Technology Labs, Ltd. (Vinakos, 2015) for analysis. A particle size distribution and shape via image analysis was performed on the sample; raw data was reported in three categories—aggregate sample, only particulates, and only fibers.

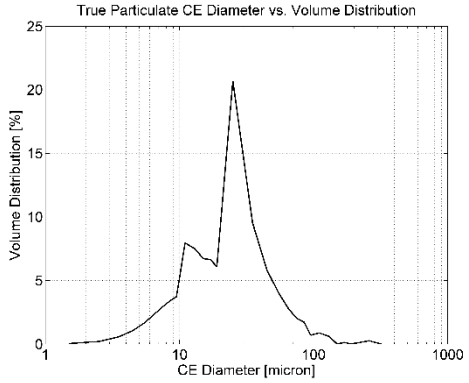

Figure 2.1. Volume distribution of true particulates versus circle equivalent diameter.

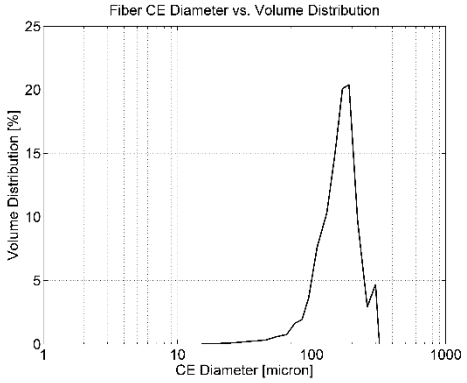

Figure 2.2. Volume distribution of fiber versus circle equivalent diameter.

Figure 2.1 and Figure 2.2 are independent volume distribution plots of the particulate and fiber content of the sample produced by the authors using raw data obtained from the analysis. The

particle size distribution can be seen to match the range observed by Ahn and Lee (2005) and Ali and Ismail (2008) fairly well. The carbon black content of the test dust could not be observed in the analysis due to it being in the submicron range. The resolution of the equipment used to analyze the sample did not extend to the submicron range. An aspect ratio analysis was also obtained for both of the above components, but is not reported here for brevity. Based on these analyses, ASHRAE Standard Test Dust #1 is believed to represent the fouling material encountered by heat exchangers and therefore suitable to be used as a fouling agent in laboratory experiments.

An additional point to be considered is the use of liquid coating on the heat exchanger surface as reported by Bott and Bemrose (1983), or the simulation of oil mist using diesel fuel as reported by Cowell and Cross (1980). These were observed to enhance the fouling rate and to improve the adhesion between the foulant deposition and the surface. To avoid the introduction of another variable in the experiments, the use of such methods was opted against in the current study. The choice of agent, its method of application, and the quantity of agent to be used would need further experimentation and standardization before any recommendation can be made about their use. Further, many of the studies reported in Section 2.2.2 did not employ any such method. The authors of this study have elected to investigate dry particulate fouling alone in the current effort.

2.3.3 Experimental Procedure

As stated in Section 2.3.1, the quantification of the phenomenon of fouling and its impact are proposed to be separated when conducting experiments. The mass of dust deposited on the heat exchanger is to be used to quantitatively assess the extent of fouling undergone by the heat exchanger. Photographs of the front and rear face of the heat exchanger can be used to get qualitative information about the distribution of deposition over the heat exchanger surface. The flow and thermal resistance offered by the heat exchanger are performance parameters to be monitored and correlated against the mass of deposited on the heat exchanger. Although these performance parameters are monitored continuously, even during the fouling periods, a steady state measurement is to be performed after each fouling period, which is then correlated with the mass of dust present on the heat exchanger. This is because many transients could exist during fouling periods, and it could be difficult to maintain all parameters constant and within variation limits. Airflow through the heat exchanger is not to be stopped between the fouling period and the steady state period; and no dust injection is to occur during the steady state measurement.

Performance parameters could be averaged over the duration of the steady state period and the reported.

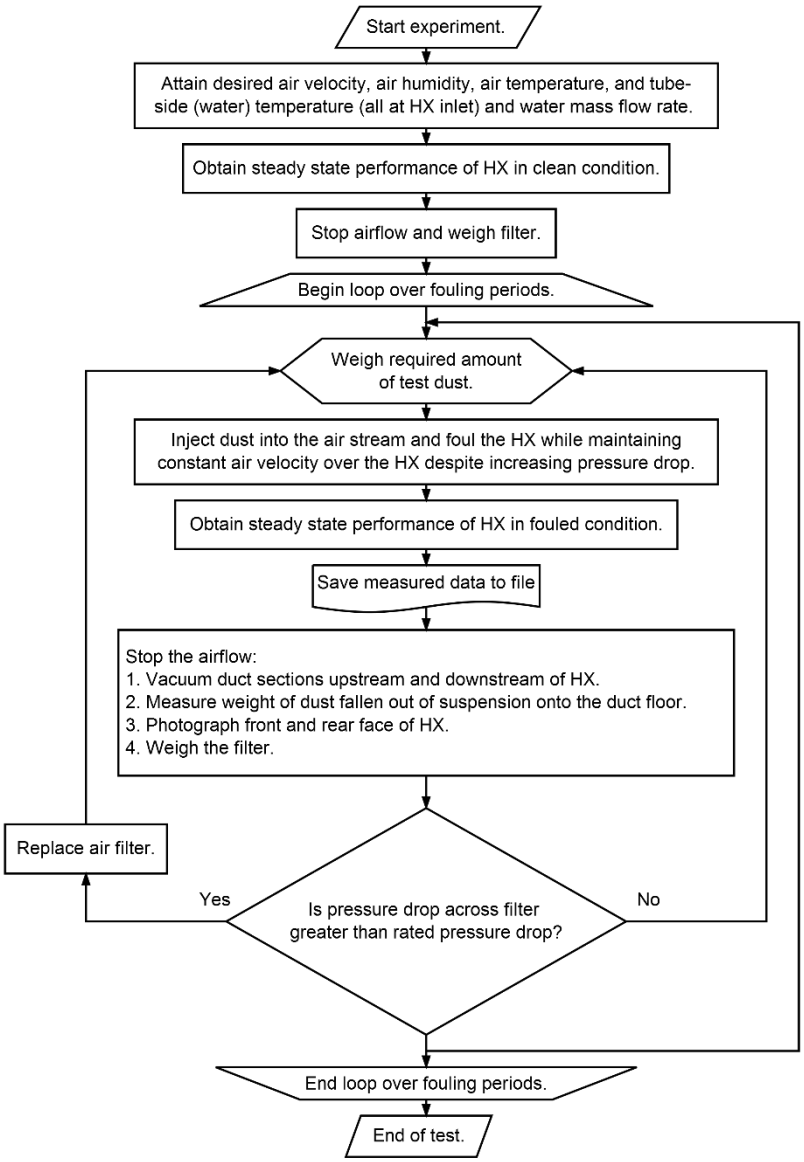

Figure 2.3. Flow chart of experimental procedure employed in this research.

The experimental procedure proposed in this research is outlined in Figure 2.3. Clearly, as deposition builds up on the heat exchanger, the flow resistance across the heat exchanger would increase, resulting in an increase in the pressure drop across it. According to standard fan curves, a constant speed blower would be able to deliver less airflow to the heat exchanger. This would then have a two-fold effect on the heat exchanger performance—the foulant deposition may cause an increase in the air-side thermal resistance to heat transfer, and the reduced airflow would cause

a further change in the air-side heat transfer coefficient. This compounding of effects would make it difficult to isolate the effect of changes in thermal resistance and flow resistance. Also, it is evident from the studies summarized in Section 2.2.5 that fouling is sensitive to changes in air velocity. Hence, a decision is made to maintain air velocity constant using a variable speed blower.

This experimental procedure assesses progressive buildup of foulant on the heat exchanger surface to evaluate whether the rate of buildup is affected by prior deposits present on the heat exchanger. Therefore, the fouling of the heat exchanger is proposed to be broken up into discrete periods of fouling or periods of dust injection, immediately followed by an assessment of the mass of deposition present on the heat exchanger and the performance of the heat exchanger after fouling. The airflow through the heat exchanger needs to be stopped to find the mass of deposition on the heat exchanger. This would result in an operation of the heat exchanger resembling cycling observed in many systems in the field. Such cycling has the potential to affect the fouling of the heat exchanger. As seen from the literature review presented in Section 2.2.2, many researchers foul the heat exchanger continuously without stopping the airflow through the heat exchanger. The assessment of fouled performance is done continuously, whereas the quantification of extent of fouling on the heat exchanger, if performed, is done once at the end of the experiment. Compared to the procedure in the literature, stopping the airflow, and restarting it may cause some dust to fall off the front face of the heat exchanger, especially if it were being held up by the airflow. Bott and Bemrose (1983) report having stopped periodically dust injection, but not the airflow, to measure heat exchanger performance in fouled condition. This was not observed to impact the experiment. On the other hand, Haghighi-Khoshkhoo and McCluskey (2007) report observing "a fall to the floor of a significant mass of particles from the heat exchanger surface" after stopping airflow through the heat exchanger. This deposition that contributed to the pressure drop was present not in the heat exchanger core, but only on the leading edges of the heat exchanger surface. The observation that "particles either passed through the exchanger, were blocked on the exchanger surface, or rebounded to the tunnel floor upon impact" was repeated in Hosseini *et al.* (2017). Mason *et al.* (2006) also acknowledge the existence of two distinct zones of deposition—the core and the leading face—and report proportion of particles collected in both zones for some test cases.

It is clear that the dust particles deposited on the front face of the heat exchanger may fall off once the force holding them in place, which is the airflow, stops. The experimental procedure

chosen is thus affecting the experiment. For heat exchangers operating in the field, cycling of airflow would be a usual occurrence. This experimental procedure is then chosen, despite its potential to affect the phenomenon being studied, because it represents those heat exchanger applications on which this study is focused with fidelity.

At the end of a fouling test run, some *in situ* cleaning procedures are performed to assess their efficacy. These include:

i. Reversal of airflow direction; air velocity maintained at value same as test run
ii. Short pulses of airflow (usually 30 seconds long) interspersed with periods of no airflow of equal duration; air velocity maintained at approximately same value as test run during periods when the blower is on
iii. High speed airflow with air velocity maintained at a value greater than that of the test run value (usually 3.5 m/s)

All procedures are to be conducted after each test run; however, the order in which these procedures are conducted should be switched around. As the amount of foulant deposition on the heat exchanger reduces, cleaning it requires greater effort. When the cleaning procedures are performed in a different order, the true efficacy of each procedure can be assessed.

At the end of a fouling test run and *in situ* cleaning procedures, heat exchanger should be thoroughly cleaned using hot water and a commercial coil cleaning agent. As reported in Bell *et al.* (2011), effective cleaning can only be performed using water with appropriate additives. The coil cleaner should be chosen based on the application stated by the manufacturer—heat exchanger design and material. Manufacturer guidelines are to be followed in the cleaning process.

2.4 Fouling Metrics

2.4.1 Test Metrics

In this study, *deposition fraction* is proposed to be used to quantify deposition of dust on the heat exchanger. This parameter was used by Siegel (2002), although Epstein (1988) used a parameter termed *fractional particle removal efficiency* and Mason *et al.* (2006) used a parameter termed as s*top ratio*, both of which are essentially defined in a similar manner.

$$D = \frac{m_{d,dep}}{m_{d,inj}} \tag{2.1}$$

The normalization of the mass of deposition on the heat exchanger by the mass of dust initially introduced into the wind tunnel helps to compare rates of deposition for experiments conducted at different operating conditions—even when the quantity of fouling agent used differs between test cases.

Measuring the mass of dust deposited on the heat exchanger may not be straightforward, as that would necessitate weighing the entire heat exchanger in clean and fouled condition. If that were not possible, instead of actually weighing the heat exchanger, the measurement could be performed indirectly. After each fouling period, duct sections upstream and downstream of the heat exchanger are to be vacuumed and the collected masses of dust are to be independently weighed to measure the mass of dust that falls out of suspension from the airflow. Additionally, the filter is to be weighed before and after each fouling period to calculate the mass of dust caught in the filter. An important assumption is necessary to make—the dust mass that escapes through the downstream filter is insignificant. Then, the definition of deposition fraction is slightly amended:

$$D = \frac{m_{d,dep}}{m_{d,inc}} \tag{2.2}$$

The mass of dust incident on the front face of the heat exchanger is calculated as:

$$m_{d,inc} = m_{d,inj} - m_{d,up} \tag{2.3}$$

The mass of dust deposited on the heat exchanger is calculated as:

$$m_{d,dep} = m_{d,inc} - m_{d,down} - \Delta m_{fil} \tag{2.4}$$

The deposition fraction corresponding to each fouling period is measured once after each fouling period.

Pressure drop across the heat exchanger is measured during each fouling period and the subsequent steady state period. This is a directly measured variable that reflects the flow resistance across the heat exchanger and requires no post-processing.

Heat exchanger effectiveness—a parameter reflecting the thermal resistance of the heat exchanger—is chosen to report the heat transfer performance of the heat exchanger. Any impact

of fouling deposition on the air-side thermal resistance would be reflected by the measured effectiveness of heat transfer. Heat exchanger effectiveness accounts for minor changes in mass flow rate of both fluids (air and water) and for changes in the temperatures of both fluids at inlet to the heat exchanger. Therefore, it provides a common basis to compare performance even when operating conditions change. The calculation of the air-side heat transfer coefficient requires detailed knowledge of the heat exchanger geometry on the air-side. On the other hand, the effectiveness is simple to calculate. The heat transfer effectiveness is calculated as:

$$\varepsilon = \frac{\dot{Q}_{act}}{\dot{Q}_{\max}} \tag{2.5}$$

2.5 Conclusions

A review of published manuscripts in the literature investigating air-side fouling of heat exchangers reveals much variability in the approach taken to conduct such experiments. This may, to some extent, be attributed to the complexity of the phenomenon, the occurrence of this phenomenon in the field in applications much different from each other, and the competing demands on experimentation—simplified, tightly controlled experiments may deepen understanding of the underlying phenomenon, but may not adequately represent the typical occurrence of the phenomenon in the field, and thus necessitate further experimentation to make the research practically applicable. In this research, an attempt is made to balance these needs. An experimental method to investigate air-side fouling of heat exchangers in a laboratory environment is proposed along with metrics to quantify the extent of fouling undergone by a heat exchanger and its impact on the performance of the heat exchanger. Measurements made from experiments conducted according to this procedure are described in the accompanying manuscript.

CHAPTER 3. EXPERIMENTAL INVESTIGATION OF AIR-SIDE FOULING OF A FINNED MICROCHANNEL HEAT EXCHANGER IN A LABORATORY ENVIRONMENT

3.1 Introduction

Deposition on surfaces from a moving fluid is hypothesized as being composed of three stages by Bott (1995):

i. Transport of the foulant or its precursors across the boundary layers adjacent to the deposition surface within the flowing fluid

ii. Adhesion of the deposit to the surface and to itself

iii. Transport of material away from the surface

Different mechanisms are proposed to be operative in each stage; multiple parameters are hypothesized to affect each mechanism. Properties of the fluid, characteristics of the flow, properties of the foulant, geometry of the surface, and interaction between the fluid and the foulant, and that between the foulant and the surface are all proposed to, in some measure, dictate occurrence and intensity of these mechanisms.

Montgomery (2013) stated that a successful design of experiments requires selection of response variable(s) that provide useful information about the process under study. Identification of factors that may influence the performance of the process or system under study, and the classification of parameters into design factors (the sensitivity of the experiment to changes in these factors is the focus of the study), factors to be held constant (the experiment is sensitive to changes in these factors, but this correlation is not of interest to the current study), and those factors allowed to vary is an important step in the design of experiments.

A high degree of control over air-side particulate fouling experiments is difficult to maintain, because a large number of factors affect the phenomenon with potential correlation between these factors. This complicates the classification of factors into three groups as defined above. A large range of dimension scales exist in the experiment—particle sizes in the foulant may be on the micrometer scale, whereas the heat exchanger dimensions and air velocity values may exist on the meter scale. This range introduces complexity to the measurement as well. In some cases, the

choice of which parameters are allowed to vary is informed by practical considerations, and not decided after a design of experiments type analysis.

3.2 Experimentation

Experiments conducted as part of this research are a continuation of similar efforts at Ray. W. Herrick Laboratories, Purdue University. Experience gained from earlier efforts informs research conducted in this research.

3.2.1 Experimental Setup

Figure 3.1 is a schematic of the L-shaped wind tunnel constituting the test stand used to generate the data reported in this study. The schematic is not to scale, and the actual distances between components or equipment depicted may be different than those shown in the schematic. The wind tunnel is located in Ray W. Herrick Laboratories, where the studies by Yang *et al.* (2007), Bell and Groll (2011), Bell *et al.* (2011) were also conducted. The test facility has undergone minor changes since the last of these studies were performed.

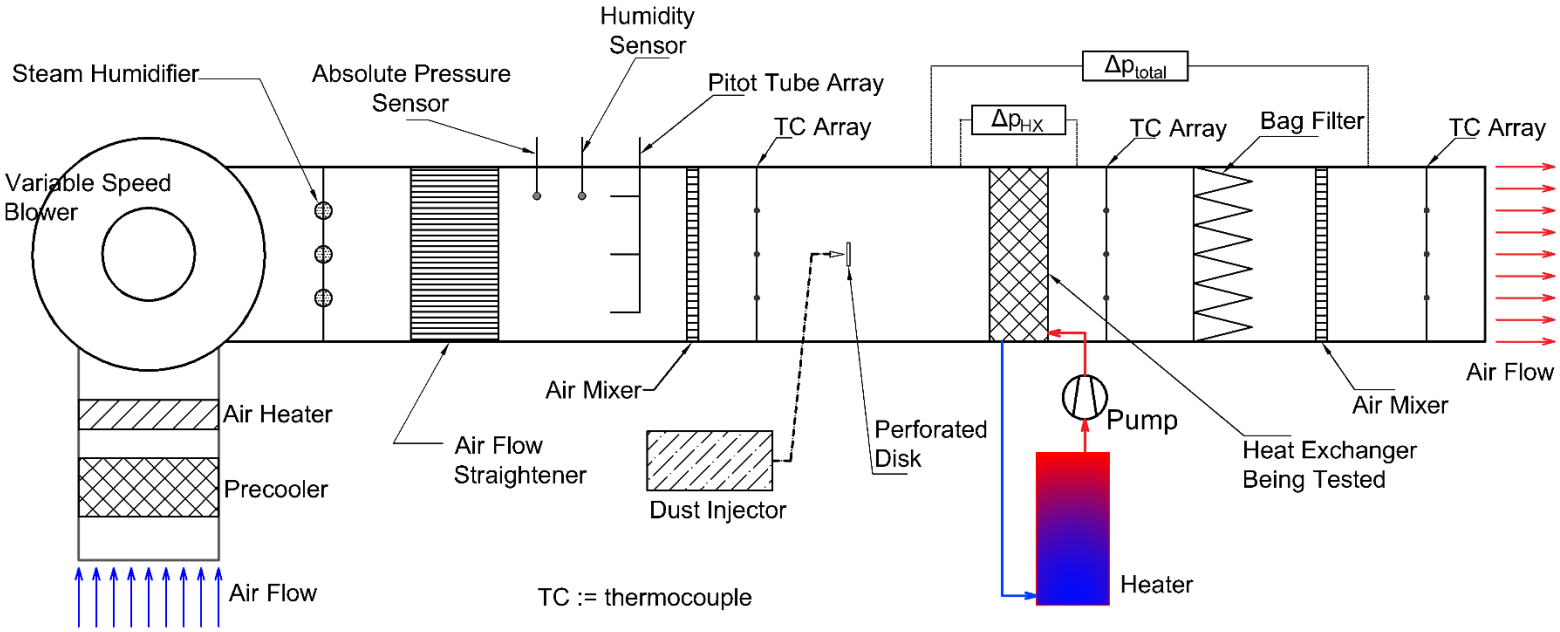

Figure 3.1. Schematic of test setup used in this study to conduct fouling experiments.

The wind tunnel is a square duct constructed using 1.22 m (4 feet) long flat metal sheets mounted on square brackets. The wind tunnel cross-section is 0.61 m × 0.61 m (2 feet × 2 feet). A centrifugal blower controlled by a variable frequency drive (Fuji Electric Frenic 5000P11S inverter) is used to force air through the wind tunnel. The inlet to the open loop wind tunnel is indoors, and it exhausts to the outdoor environment. A 10.55 kW (3 ton) direct expansion cooler can be turned on to cool the incoming air or for dehumidification. Three electrical resistance heaters of 5 kW (17.06 kBtu/h) capacity each can be used to reheat the airflow. These are capacity modulated using solid state relays. A steam humidifier is used to control the airflow humidity. An air straightener constructed as per ASHRAE 41.2–1997 is used to make the air velocity profile inside the duct more uniform and eliminate the effect of measurement equipment, fluctuations in fan rotation, and bends in the wind tunnel design on the airflow profile. A forced draft configuration, such as the one here, results in more non-uniformities in the airflow profile than induced draft configurations. An absolute pressure sensor and a humidity sensor are installed in close proximity with each other downstream of the air straightener. The humidity sensor provides two output signals—corresponding to the local relative humidity and temperature. These three measurements are used to calculate the local specific humidity. Since this study conducted experiments only in heat rejection mode, a second humidity sensor downstream of the heat exchanger was not necessary. The specific humidity of air must remain constant despite heating.

A Pitot tube array is installed downstream of the humidity sensor to measure air velocity. The array traverses the duct cross-section along its diagonal. The array enables measurement of dynamic or velocity pressure of the airflow at multiple points in the duct cross-section, thus helping to reduce errors in measurement due to a non-uniform air velocity profile. Robinson *et al.* (2004) raise some questions about the use of Pitot tubes in industry for measurement of air velocities based on a study conducted by the National Physical Laboratory, UK. The uncertainty in velocity measurement is determined by the measurement uncertainty of differential pressure measurement between the static and flow pressure ports. At low air velocities, uncertainty in measurement becomes comparable to the magnitude of the measured variable itself. This issue is also addressed in Bean and Hall (1999), where a minimum air velocity of 2.0 m/s (393.7 fpm) is suggested for use with Pitot tubes. An alternative way of measuring air velocities would be to use a nozzle chamber as described in ASHRAE 41.2–1997. However, this requires straight sections of duct of

prescribed length that could not be implemented in this study due to space constraints. Hence, a Pitot tube array is used to measure air velocity accepting a larger measurement uncertainty.

An air mixer constructed according to ASHRAE 41.2–1997 is used to eliminate any thermal stratification in the air stream. The air causes turbulence in the airflow and mixes the air stream to obtain temperatures close to the mass flux weighted average of the air stream. A 3×3 grid of K-type thermocouples is installed to measure air temperature at inlet to the heat exchanger. The true average temperature of the airflow is assumed to be a simple average of the 9 measurements. The heat exchanger is installed in a modular duct section that can be easily removed from the wind tunnel. A straight duct section more than 3.05 m (10 feet) long exists between the location of air temperature measurement and the front face of the heat exchanger.

There are two 3×3 K-type thermocouple grids downstream of the heat exchanger. The first grid, immediately after the heat exchanger, is used to gain qualitative information about the effect of fouling on heat transfer occurring in different tube passes of the heat exchanger. It is not used for calculating the heat transfer performance of the heat exchanger, because fouling may have significantly altered the air velocity profile in the duct. Then, a local–mass–flux–weighted average of the 9 temperatures would give the correct average temperature of the airflow. Local mass fluxes inside the wind tunnel are not measured in this study. The second grid is located downstream of a bag-type filter and a second air mixer, similar to the one upstream of the heat exchanger. The second air mixer ensures proper mixing and destratification of airflow. A simple average of the 9 thermocouples is then closer to the true average temperature of airflow.

Two differential pressure transducers are installed in the wind tunnel. One to measure the flow resistance—pressure drop—across the heat exchanger; one to measure the pressure drop across the heat exchanger and filter combination. The transducer installed across the Pitot tube ports, which is used to measure the velocity (dynamic) pressure of airflow is not a conventional differential pressure transducer. It produces an output signal directly corresponding to the air velocity assuming a standard air density of 0.075086 lbm/ft^3, calculated at 68 °F at a barometric pressure of 29.921 inch mercury. This density is provided by the manufacturer (Paragon Controls) in the submittal sheet for the sensor (model FT–1003 air velocity transducer). The dynamic pressure of airflow is calculated using this signal, and the true air velocity is then calculated in real time while conducting a test.

The bag filter is used to arrest dust particulates in the air stream that pass through the heat exchanger. In all experiments reported in this study, a synthetic bag filter with a MERV (Minimum Efficiency Rating Value) rating of 13 was used. According to ASHRAE Standard 52.2–2012, particulates in the size range of 0.30–1.0 μm are controlled using filters with MERV values in the range of 13–16. For purposes of this study and the foulant used, this efficiency was deemed to be sufficient.

3.2.2 Hot Water Loop

The heat exchanger is tested in heat rejection mode, *i.e.*, heat is rejected from the tube-side fluid, which in this case is distilled water, to the air stream. A hot water loop is used in this study to evaluate the heat transfer performance of the heat exchanger. It is already shown in Figure 3.1, but lacks details provided in Figure 3.2.

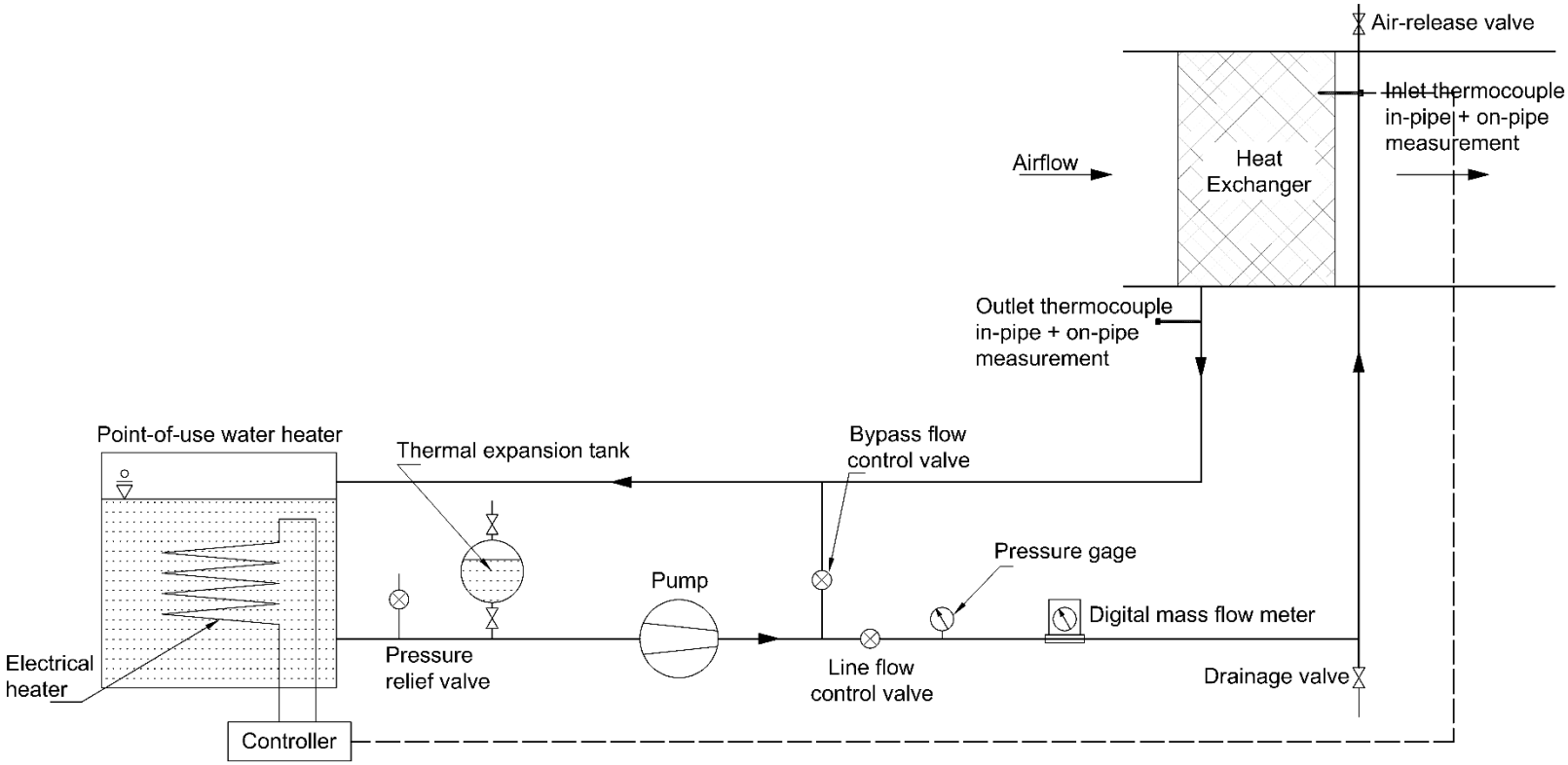

Figure 3.2. Schematic of hot water loop used in this study to measure heat transfer performance of heat exchanger.

The loop is constructed using standard L-type copper tubing of diameter 19.05 mm (3/4 inch). A rotary-vane circulating pump is used to maintain a fairly constant mass flow rate of water through the heat exchanger, regardless of changes in pressure head on the pump. Two simple flow control valves—one in–line and another one on a bypass line, are employed to control the flow rate of water delivered to the heat exchanger, while an Omega CN4000 series temperature controller is used to modulate the electric water heater to ultimately maintain a constant water temperature at inlet to the heat exchanger. A Coriolis mass flow meter is used to measure the flow rate of water in the circuit. Four T-type thermocouples are used to measure the water temperature at inlet and outlet of the heat exchanger—two at each end. Each measurement is an average of an in-pipe measurement using a probe type thermocouple, and an on-pipe measurement using thermocouple wires epoxied to the pipe surface using a highly conductive thermal epoxy. Care is taken to ensure that little debris or dust enters the water loop from outside, and efforts are taken to deaerate the piping prior to each test. This is to avoid tube-side fouling during the experiment and to accurately measure heat exchanger capacity respectively.

3.2.3 Dust Injector

The heat exchanger is actively fouled as part of the experiment to evaluate the impact of operating conditions on the phenomenon of fouling itself. The process of fouling takes place in the wind tunnel itself. A dust injector is used to introduce particulate dust to the air stream that flows through the heat exchanger. As this particulate–laden air stream passes through the heat exchanger, some of the particulates deposit on the air-side surface of the heat exchanger—thus simulating the process of fouling in the wind tunnel. The choice of quantity of dust to be introduced to the air stream influences the concentration of particulates in the air stream incident on the front face of the heat exchanger.

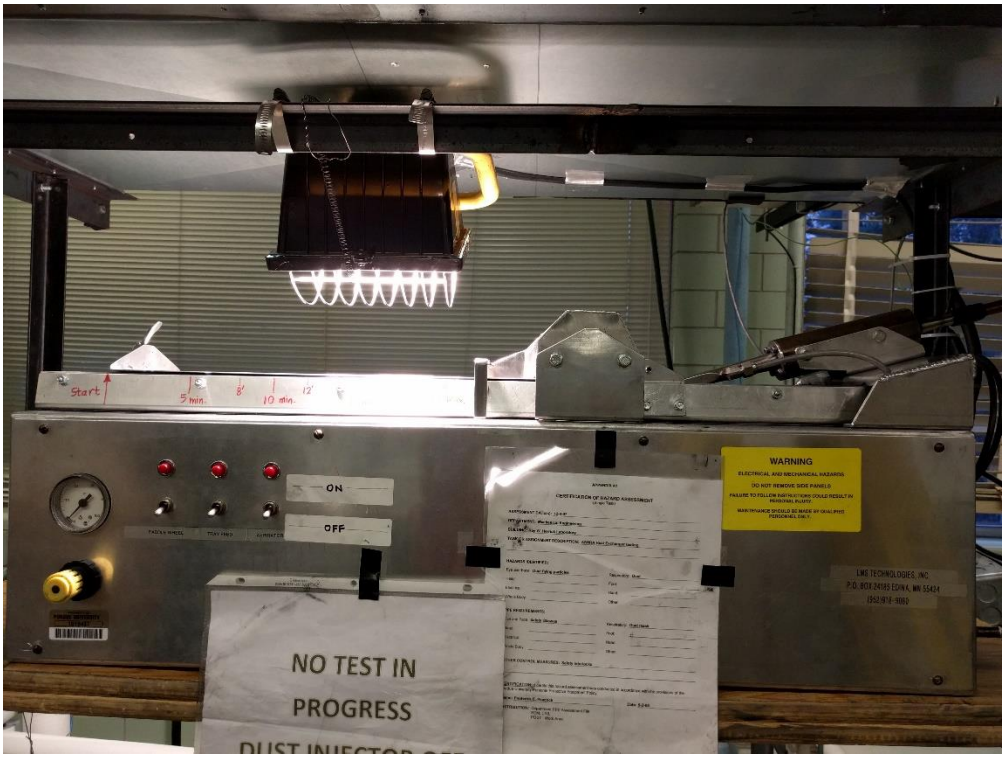

Figure 3.3. Photograph of dust injector used in this study to simulate heat exchanger fouling in the laboratory.

Figure 3.3 shows the dust injector manufactured by LMS Technologies, Inc., Bloomington, MN. ANSI/ASHRAE Standard 52.2–2012 states requirements for the dust feeder assembly including dust injector design, and ejector/venture dimensions. The desired quantity of dust is loaded on a flat tray. A high intensity halogen lamp—positioned just above the tray—is used to dry the dust being used as a fouling agent. This tray is located on top of the injector, and is mounted on top of a conveyor chain. The conveyer chain is driven by a geared motor that moves the tray forward at a speed of approximately 0.16 m (6.5 inches) in 10 minutes. A geared cylinder (seen approximately at top center of Figure 3) that functions as a metering wheel rotates just above the tray synchronized with its movement. As the tray moves forwards, the dust loaded on the tray is picked up between the teeth of the feeding cylinder, and fed to the inlet of a nozzle that can be seen on the top right of Figure 3. The nozzle is connected to a pressurized dry air supply whose pressure can be regulated. The nozzle aspirates the dust off the tray. The aerosol thus formed is then blown into the wind tunnel through copper tubing of diameter 12.7 mm (0.5 inch). The aerosol is blown through a perforated disc to ensure proper distribution of the dust in the duct cross-section. The dust thus blown mixes with the air stream that ultimately flows through the heat exchanger.

The front face of the heat exchanger is about 3.05 m (10 feet) away from the location of dust injection, and the flow geometry between the two locations consists of straight sections of constant area square duct.

A wet cloth was held at the front face of the heat exchanger, and dust was injected into the wind tunnel at different airflow velocities. Photographs were taken of the wet cloth, which demonstrated that the straight sections of duct allowed the flow to develop, and that dust is incident fairly uniformly over the entire front face of the heat exchanger regardless of operating conditions.

3.2.4 Measured Quantities and Measurement Uncertainties

An HP E1300A, B-size VXI mainframe is used to measure all output signals from the measurement instruments used in this study. The analog output signals produced by the different sensors/transducers installed in the experimental setup are wired to HP E1347A thermocouple multiplexers with on–board cold junctions. A total of 3 such multiplexers are used—each with 16 analog channels. National Instruments LabVIEW 2014 was the software interface used to record all the collected data. Thermophysical humid air properties, necessary to calculate the air velocity, were calculated at run-time using correlations provided in the ASHRAE Handbook of Fundamentals 2013. Thermophysical properties of water, necessary to calculate the heat transfer rate, are calculated at run-time by interfacing NI LabVIEW 2014 with REFPROP v9.0.

Table 3.1. Measured variables and corresponding measurement uncertainties.

Measured variable	Measurement instrument	Manufacturer stated uncertainty
Relative humidity of air at inlet to the heat exchanger	Rotronic HF43 relative humidity sensor	±1.0% RH
Air temperature at location of humidity measurement		±0.2 K
Absolute air pressure at location of humidity measurement	Omega PX177 absolute pressure transmitter	±1.72 kPa
All air temperatures upstream and downstream of the heat exchanger and filter	3×3 grid of Omega K-type thermocouples	±2.2 K each
Air velocity	Paragon Controls model FT-1003 air velocity transducer	±0.03 m/s
Pressure drop across the heat exchanger	Setra 264 differential pressure transducer	±2.49 Pa
Pressure drop across the heat exchanger and filter combination		±24.91 Pa
All water temperatures at inlet and outlet of heat exchanger	Omega T-type thermocouples with special limits of error	±0.5 K
Water mass flow rate	MicroMotion R025S Coriolis mass flow meter	0.5% of reading
Dust mass	Adam CBK bench scale model 16a	±1.0 g
Cold junction temperature	HP E1347A thermocouple relay multiplexer	±0.3 K
DC voltage	HP E1326B multimeter with relay multiplexers for an aperture of 20 ms over 1 power cycle	±1.0 mV ±0.15% of reading
Electrical resistance		±28.2 mΩ ±0.025% of reading

Table 3.1 presents the experimental variables measured while conducting a test and their corresponding uncertainties. Some of the manufacturer data were originally provided in USCS units, which were converted to the metric system before reporting in Table 3.1.

3.2.5 Test Matrix

Three main parameters are chosen to be varied to evaluate their impact on heat exchanger fouling—air humidity, air velocity, and suspended particulate concentration. The test matrix

followed in this study is designed to vary only one out of three parameters in each test group, maintaining the other two constant. The total dust injected per fouling period is also maintained constant within a group of tests. If prior foulant depositions affect future heat exchanger fouling, then more dust injected in the last fouling period may affect fouling that occurs in the current period. Researchers such as Zhang *et al.* (1990) and Mason *et al.* (2006) report having observed two distinct fouling regimes—nucleation fouling and bulk fouling—the former having a low rate of deposition and occurring due to deposition of large particles. The latter regime was hypothesized in Mason *et al.* (2006) to occur when the deposited large particles act as nucleation sites for smaller particles, which would otherwise not deposit on the surface. Moore (2009) proposed a similar acceleration in the rate of fouling occurring due to fibers deposited on heat sinks. It is possible that this could be extended to compact heat exchangers as well. If this were to occur in the current experiments as well, comparing the progression of fouling between different experiments—even in the same group—would be difficult. Therefore, the dust injected into the wind tunnel per fouling period is maintained constant within a test group.

Table 3.2. Experimental parameters maintained constant for all experiments.

Experimental variable	**Value**	**Unit**
Air temperature at inlet to heat exchanger	24	°C
Water temperature at inlet to heat exchanger	60	°C
Mass flow rate of water	30	g/s
Total number of fouling (and subsequent steady state) periods	6	—

Table 3.2 lists experimental parameters that were maintained constant for all test cases in all test groups.

Table 3.3. Test matrix for which results are presented in this study.

Test index		Relative humidity	Air velocity	Rate of dust injection	Time period of dust injection	Dust injected per fouling period	Total airflow over the heat exchanger per fouling period	Dust concentration in air during fouling period
		%	m/s	g/hr	min	g	m^3	mg/m^3
1	A	50	1.5	120	30	60	1003.4	59.8
	B			60	60		2006.7	29.9
	C†			15	240		8026.8	7.5
	D			7.5	480		16053.6	3.7
2	A	60	1	100	60	100	1337.8	74.8
	B	70						
	C†	75						
	D	80						
	E†	90						
3	A	50	1	60	60	60	1337.8	44.8
	B		1.5	90	40			
	C		2	120	30			
	D†		2.5	150	24			

Table 3.3 represents the fouling test matrix and the three main groups into which the experiments were divided. Test runs marked with the symbol † were conducted twice to ascertain repeatability of the measurements and of the test procedure.

The choice of which parameters to vary, and which to hold constant is informed by the data in the experimental literature about the effect of some of the above operating parameters on heat exchanger fouling as well as theory of particulate deposition on heat transfer surfaces. For example, Zhang *et al.* (1990) report that greater air velocities and greater bulk concentration of suspended particulates in the air stream both enhanced fouling on a finned–tube heat exchanger. In their experiments, the air velocity was allowed to decrease with buildup of deposition. The measurements are then reported by normalizing them to a single Reynolds number. Müller-Steinhagen *et al.* (1988) evaluated the effect of operating conditions including air velocity, particle size, and particulate concentration on fouling using a fouling probe. Fouling probes are much different in geometry to heat exchangers, and therefore extrapolating from their data to heat exchangers is difficult. The overall fouling behavior was reported to be similar regardless of changes in operating conditions—fouling resistance asymptotically reached a constant value; however, this value was different for different cases. The time required to reach this asymptotically constant value also differed. Based on their experiments, Haghighi-Khoshkhoo and McCluskey (2007) expected the rate of introduction of dust into their wind tunnel to have "no effect on the fouling process apart from duration to saturation", where saturation is the state at which no change is observed in the total foulant deposition present on the heat exchanger or the measured fouling resistance of the heat exchanger. Bott and Bemrose (1983) also varied air velocity and rate of dust injection in their experiments, but made no comparative observations.

Walmsley *et al.* (2013) in their experiments held the humidity ratio constant at 60 g/kg but changed the air temperature at inlet to the heat exchanger (maintaining a constant value per test run). This meant the value of relative humidity varying between 27 to 75% between test runs. From published photographs of their heat exchanger in fouled condition, it is apparent that the severity of fouling deposition increases monotonically with an increase in relative humidity, and the sensitivity of this severity to a change in relative humidity is greater at larger values of relative humidity. They report that "The stickiness level of milk powder is a determining factor in the severity of deposition and pressure drop increase." It can be surmised that they infer a relationship between the humidity of air and the stickiness of milk powder. Zhan *et al.* (2016) report that an

increase in concentration of suspended particulate in air flowing through the finned tube heat exchanger being tested led to an accelerated accumulation of foulant deposition on the sample. However, the total particle deposition weight per unit area of heat exchanger reached approximately similar values asymptotically. Thus, the time required to reach a *saturated* state changed, but the *saturation states* did not show a large difference. A change in air velocity, on the other hand, led to different values of particle deposition weight per unit area of heat exchanger. The trend was mixed—air velocity was reported to "first promote, and then restrain particle deposition as it increased".

The effect of changes in heat exchanger geometry such as number of tube rows and fin pitch was compared in Pak *et al.* (2005) and Yang *et al.* (2007), whereas the differences between fouling of plate–finned–tube heat exchangers and finned–microchannel heat exchangers were investigated in Bell and Groll (2011). Variation due to the choice of fouling agent is also reported in the literature; relevant studies can be found in the companion manuscript. For this study, the heat exchanger geometry and fouling agent were not varied, although fouling is known to be sensitive to them.

Bott (1988) presents an overview of the different mechanisms by which particulates (the dispersed phase in a continuous medium such as air) deposit on heat transfer surfaces. Inertial impaction, an important mechanism in heat exchanger fouling, is a strong function of the velocity of airflow. The issue of particle agglomeration—which would affect deposition—is raised; size distribution of the suspended dust is hypothesized to affect particle agglomeration. The concentration of suspended dust could also affect particle agglomeration, ultimately affecting heat exchanger fouling. Therefore, the sensitivity of fouling to both these parameters is investigated in this study. A similar reasoning is behind the choice of relative humidity at inlet to the heat exchanger as the third parameter to be varied. Since air temperature at inlet to the heat exchanger is maintained constant, a change in relative humidity implies a proportional change in the specific humidity, as long as ambient pressure does not vary significantly. In addition, changes in air velocity and air humidity could affect the characteristics of layers of dust deposited on the heat exchanger such as porosity and the adhesive forces between them and the heat exchanger surface. This could then affect deposition that occurs on top of these layers.

3.2.6 Heat Exchanger Cleaning Procedure

At the end of a fouling test run, an attempt is made to clean the heat exchanger by implementing the *in situ* cleaning procedures described in the companion manuscript. Once the *in situ* cleaning sequence is complete, the modular heat exchanger section is unmounted from the wind tunnel, and thoroughly cleaned using hot water and a commercial coil cleaning agent. The coil cleaner is intended for use on finned microchannel heat exchangers fabricated using aluminum. The safety data sheet for the cleaner is retrieved from the manufacturer website (NU–Calgon, 2013). Manufacturer guidelines are followed in the cleaning process.

3.2.7 Heat Exchanger Under Investigation

The heat exchanger being tested as part of this research is an automotive condenser and has a finned microchannel design. The condenser is manufactured by Denso International America, Inc. for the air-conditioning system installed on a 2014 Dodge Ram truck 6.7L. On the refrigerant side, the heat exchanger is divided in two sections—the condenser (top) and the subcooler (bottom). The tube-side fluid enters the condenser section through a header, and flows through the heat exchanger in a single pass. It then collects in a header on the other side of the heat exchanger, and flows into the subcooler section. The tube-side fluid flows through the subcooler section in a single pass as well, and returns to the inlet side. The inlet and outlet headers are physically distinct. Characteristics of the heat exchanger are listed in Table 3.4.

Table 3.4. Characteristics of finned microchannel heat exchanger tested subjected to air-side fouling in this research.

Dimension	**Value**	**Unit**
Finned width	609.6 (24)	mm (inch)
Finned height (total)	555.6 (21–7/8)	mm (inch)
Condenser section	400 (15–3/4)	mm (inch)
Subcooler section	155.6 (6–1/8)	mm (inch)
Finned depth	19 (3/4)	mm (inch)
Liquid channel height		
Condenser section	1.09 (0.043)	mm (inch)
Subcooler section	3.0 (0.118)	mm (inch)
Fin density	9.5	$inch^{-1}$
Fin thickness	0.051 (0.002)	mm (inch)
Fin height	5.309 (0.209)	mm (inch)

3.3 Data Analysis

3.3.1 Test Metrics

The deposition fraction, as defined in the companion manuscript is the metric used to quantify the extent of air-side particulate fouling undergone by the heat exchanger. The impact of fouling is characterized in terms of the hydraulic resistance and thermal resistance—hydraulic resistance reflected by the air-side pressure drop across the heat exchanger, and thermal resistance reflected by the heat exchanger effectiveness.

All thermophysical properties are evaluated using CoolProp v5.0.7. The change in the choice of fluid property database used in data reduction versus that used during experimentation is for convenience. The actual heat transfer rate is calculated using the water-side measurements, because it is the measurement with lesser uncertainty than the air-side measurement. The air-side measurement is used as a check to compare with the water-side measurement, and to ensure the lack of leaks or heat loss through the duct walls. Actual heat transfer rate is calculated as:

$$\dot{Q}_{act} = \dot{m}_w \times \left[h_w\left(T = T_{w,in}, p = p_w\right) - h_w\left(T = T_{w,out}, p = p_w\right) \right] \tag{3.1}$$

Water is assumed to be incompressible, and a change in its pressure is assumed to have an insignificant effect on its enthalpy. It is to be noted that the maximum change in pressure on the water-side from the heat exchanger inlet to outlet does not exceed 275.8 kPa (40 psi). A simple check performed using CoolProp v5.0.7 reveals a possible deviation in enthalpy calculation on the order of 0.1%. The maximum possible heat transfer is calculated using:

$$\dot{Q}_{\max} = \dot{m}_w \times \left[h_w\left(T = T_{w,in}, p = p_w\right) - h_w\left(T = T_{a,in}, p = p_w\right) \right] \tag{3.2}$$

The maximum heat transfer rate calculation is based on the maximum available temperature gradient in the heat exchanger and the minimum mass flow rate:

$$\begin{aligned} \Delta T_{\max} &= T_{w,in} - T_{a,in} \\ \dot{m}_{\min} &= \min\left(\dot{m}_w, \dot{m}_a\right) \end{aligned} \tag{3.3}$$

3.3.2 Data Reduction

The Data Acquisition System (comprising the different sensors and transducers, data acquisition device, and software interface) organized to measure analog output signals communicated by the different sensors/ transducers installed in the experimental setup was designed to scan all channels on the multiplexer approximately once every two seconds. Since values of measured variables were not required at this high frequency, all raw values were first averaged over one (1) minute long periods. Fouling periods are characterized by highly transient values of air velocity, usually increasing pressure drop across the heat exchanger, and therefore processed values of all variables are recorded at this frequency. Then, all calculated quantities as described in the current section and in Section 4.1 are evaluated using these processed values of measured variables. All data is processed in a commercial numerical computation package—MATLAB 2015b.

In addition to the fouling metrics described in the companion manuscript Section 4.1, and evaluated as described in Section 3.3.1, an additional set of calculations are performed using the raw data. The air–side heat transfer rate is calculated to perform a heat balance on the heat exchanger, and function as a check on the water–side measurements.

The humidity ratio of air at inlet to the heat exchanger is calculated using the measured relative humidity as follows:

$$\omega_{a,in} = \omega_a\left(T = T_{a,in}, \phi = \phi_{a,in}, p = p_{a,in}\right) \tag{3.4}$$

Since the heat exchanger is always operated in heat rejection mode, where the tube–side fluid (water) rejects energy in the form of heat to air, no change is anticipated in the humidity ratio of air across the heat exchanger. Thus:

$$\omega_{a,out} = \omega_{a,in} \tag{3.5}$$

The air–side enthalpies are obtained as:

$$\begin{aligned} h_{a,in} &= h_a\left(T = T_{a,in}, \omega = \omega_{a,in}, p = p_{a,in}\right) \\ h_{a,out} &= h_a\left(T = T_{a,out}, \omega = \omega_{a,out}, p = p_{a,out}\right) \end{aligned} \tag{3.6}$$

The absolute pressure sensor upstream of the heat exchanger is used to measure absolute (static) pressure of air at inlet to the heat exchanger. The differential pressure sensor installed across the

heat exchanger and filter combination is used to obtain local pressure downstream of the heat exchanger—where the outlet air temperature is measured.

$$p_{a,out} = p_{a,in} - \Delta p_{total} \tag{3.7}$$

The density of air at inlet to the heat exchanger is calculated from:

$$\rho_{a,in} = \rho_a \left(T = T_{a,in}, \omega = \omega_{a,in}, p = p_{a,in} \right) \tag{3.8}$$

The velocity pressure from the Pitot tube array is mechanically averaged. This measured value is used to calculate air velocity in the wind tunnel at inlet to the heat exchanger as follows:

$$V_{a,in} = \sqrt{\frac{2 \times \Delta p_{Pitot}}{\rho_{a,in}}} \tag{3.9}$$

The mass flow rate of air at inlet to the heat exchanger is then given by:

$$\dot{m}_{a,in} = \rho_{a,in} \times A_{wind\ tunnel} \times V_{a,in} \tag{3.10}$$

The air–side heat transfer rate is then calculated using:

$$\dot{Q}_{air} = \dot{m}_{a,in} \left(h_{a,out} - h_{a,in} \right) \tag{3.11}$$

During steady state periods, the airflow is much more stable, and there are small changes in measured variables over time. To compare heat exchanger performance in fouled condition at different degrees of fouling occurring at different operating conditions, all points in steady state period data are again averaged over the entire period to obtain a single value as representative of the heat exchanger steady state performance.

3.3.3 Uncertainty Analysis

During steady state periods, the airflow is much more stable, and there are small changes in measured variables over time. To compare heat exchanger performance in fouled condition at different degrees of fouling occurring at different operating conditions, all points in steady state period data are again averaged over the entire period to obtain a single value as representative of the heat exchanger steady state performance.

Propagation of measurement uncertainty to estimate errors in calculated quantities was performed according to JCGM 100:2008. An analysis of bias or systematic errors is performed to

calculate Type B uncertainty whereas the analysis of precision or random errors is performed to calculate Type A uncertainty. In the assessment of Type B uncertainty, it is assumed that the instrument accuracy quoted by the manufacturer of the instrument is characterized by a uniform rectangular distribution. Type A uncertainty is assessed for every set of measurements comprising raw values of variables measured over one (1) minute long periods. Since measurements are sampled at approximately once every two seconds, the measured data form a subset of the full population of which an estimate of the mean value is desired. The Student's *t*–distribution is used to approximate the distribution of this mean. An expanded combined uncertainty value is calculated for every measured variable. This uncertainty is then propagated through the data reduction procedure described in sections 4.1 and 4.2 to obtain uncertainty values for all calculated quantities. The computation necessary to calculate measurement uncertainty is performed in MATLAB 2015b as well. The uncertainty values expressed for the steady state data are averaged uncertainty values of all variables over the entire steady state period using the uncertainty values calculated for every one (1) minute long set of measurements within the steady state period.

3.4 Test results

3.4.1 Detailed Measurements for One Test Run

Detailed set of results are presented for one sample test run—test 2B. A transient plot of measured air velocity *airspeed* , pressure drop across the heat exchanger Δp_{coil} , and mass of fouling agent (test dust) introduced into the wind tunnel $m_{dust,injected}$ is presented in Figure 3.4. The *X*–axis is the running time of the test. It must be noted that the values plotted on the graph have been averaged over one (1) minute long intervals, as described in Section 3.3.2.

It must also be noted that the plot shown in Figure 3.4 has been *stitched together*. The dust injector used to introduce test dust into the wind tunnel has a tray on which test dust is loaded before being aspirated. This tray has a total travel time of twenty (20) minutes, *i.e.*, the dust injector can be operated for only twenty minutes without stopping. Thus, when fouling periods last longer than twenty (20) minutes, the process of dust injection must be conducted in batches. The first batch of test dust is weighed and uniformly loaded on the tray. When all the test dust from this first batch has been injected into the air stream in the wind tunnel, a second batch of test dust is weighed and uniformly loaded on the tray. The airflow in the wind tunnel and the flow of hot water

through the heat exchanger are maintained constant through this intermission in dust injection. An effort is made to keep this gap in dust injection during the fouling period as small as possible—below five (5) minutes. A further reduction in this intermission is not possible, because some time must be allowed for the test dust to be dried using the lamp positioned above the tray. This intermission is recorded during testing, and the raw data measured during such intermissions is removed from that associated with the respective fouling periods. When data analysis is performed for the fouling periods, only values of variables measured during the time when the dust injector is functioning are included. The plot shown in Figure 3.4 presents this filtered data.

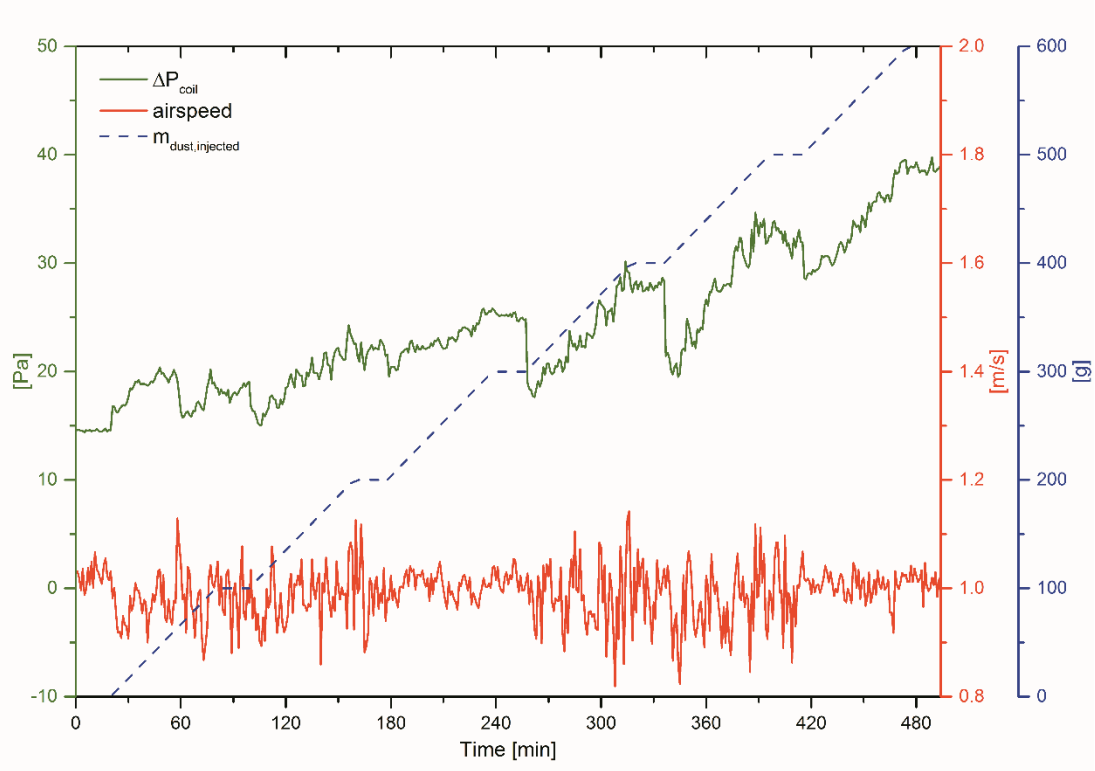

Figure 3.4. Transient plot of variables related to flow resistance across the heat exchanger.

The first part of the plot from time 0 minutes to 20 minutes is the steady state measurement of the performance of the heat exchanger in clean condition. After 20 minutes, flows of air and water through the heat exchanger are stopped, and panels from the duct wall are pulled out to weigh the filter and to vacuum the duct floor upstream and downstream of the heat exchanger. Then, from time 20 minutes to 80 minutes is the first fouling period. The mass of test dust injected into the wind tunnel increases from 0 g to 100 g. It can be seen that the air velocity through the wind tunnel is unstable during the fouling period, and so is the pressure drop measured across the

heat exchanger. From time 80 to 100 minutes is the first steady state measurement of the performance of the heat exchanger in fouled condition. The plot of mass of test dust injected into the wind tunnel stays flat through the steady state period. At 100 minutes, flows of air and water through the heat exchanger are once again stopped to perform the same actions as those after the zeroth steady state period (clean heat exchanger). It can be seen that as airflow through the heat exchanger is stopped at the end of a steady state measurement and restarted to begin the next fouling period, there is often a marked drop in pressure drop across the heat exchanger. It is hypothesized that this is due to the fact that some test dust is held up against the front face of the heat exchanger due to the force of airflow in the wind tunnel. Once this airflow stops, these particles fall off the face of the heat exchanger. The quantity of particles falling off the front face of the heat exchanger varies between test runs and also within a single test run. Figure 5 shows photographs of the duct floor immediately upstream of the front face of the heat exchanger. Such photographs are taken every time that airflow through the heat exchanger is stopped after a steady state period. The photographs Figure 3.5 and Figure 3.6 are from test run 2B, while a photograph from test run 2C is shown in Figure 3.7 as a point of comparison. The last photograph is an extreme case; most fouling tests show deposited test dust falling off the front face of the heat exchanger to a lesser degree.

Figure 3.5. Duct floor upstream of heat exchanger after first fouling period in test 2B.

Figure 3.6. Duct floor upstream of heat exchanger after sixth fouling period in test 2B.

Figure 3.7. Duct floor upstream of heat exchanger after sixth fouling period in test 2C.

It is also seen from Figure 3.5, Figure 3.6, and Figure 3.7 that the magnitude of fluctuations in measured duct air velocity change within the duration of the experiment. As the downstream filter clogs up with test dust that passes through the heat exchanger, the pressure drop across the filter increases. The wind tunnel blower must deliver airflow against this pressure head. The rising resistance to airflow through the duct, in addition to the secondary airflow being introduced into the wind tunnel by the test injector, contributes to the unsteady nature of air velocity—especially during fouling periods. When the pressure drop across the filter exceeds the maximum pressure drop recommended by the manufacturer, the filter is replaced. To avoid the stopping and restarting of airflow at times other than the end of steady state periods, this replacement is performed only when the airflow through the heat exchanger is stopped as part of the test procedure. This restriction, in some cases, leads to durations of testing where the pressure drop across the filter exceeds manufacturer replacement guidelines. Although this exacerbates the unsteady nature of air velocity, it is favorable than the introduction of an arbitrary pause in any test run.

As expected from published data in the literature, pressure drop measured across the heat exchanger increases monotonically as the total mass of dust injected into the air stream from the beginning of the test run increases. As dust deposits on the heat exchanger surface, flow area is blocked, and resistance to airflow increases. Since air velocity in the duct is maintained constant, pressure drop increases. Figure 3.8 to Figure 3.13 present photographs taken of the front face of the heat exchanger at various times during the test run.

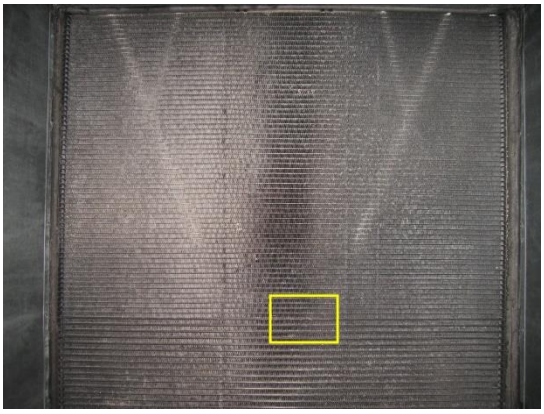

Figure 3.8. Location of photograph on the front face of the heat exchanger.

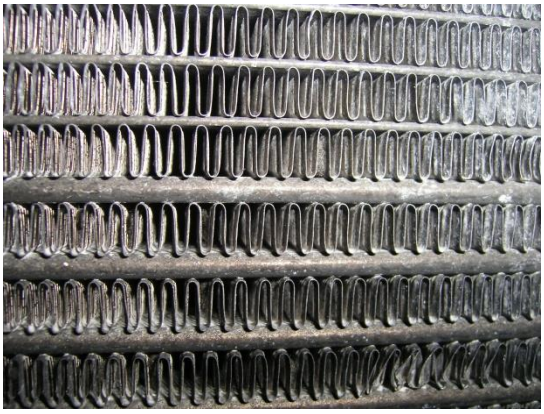

Figure 3.9. Clean heat exchanger.

Figure 3.10. After second fouling period.

Figure 3.11. After fourth fouling period.

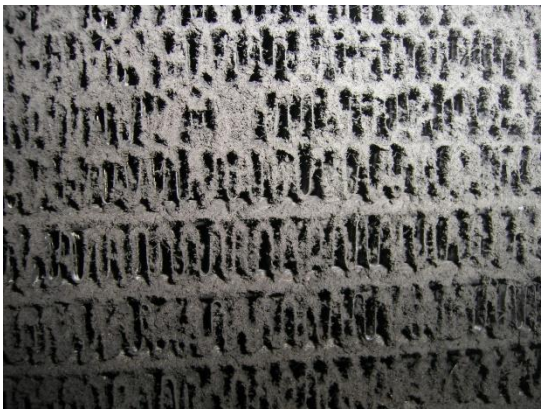

Figure 3.12. After sixth fouling period.

Figure 3.13. After in–situ cleaning by reversal of airflow direction.

Figure 3.8 shows the location on the front face of the heat exchanger where this set of photographs are taken. Figure 3.9 shows a close–up of the heat exchanger in clean condition, whereas Figure 3.10 to Figure 3.12 show the progressive buildup of foulant deposition on the heat exchanger. Figure 3.13 shows the same location after an attempt at *in situ* cleaning of the heat exchanger by reversal of airflow direction. It is seen that some of the deposition on the leading edges of fins and microchannel tubes is dislodged; however, foulant deposits are still seen inside the airflow channels.

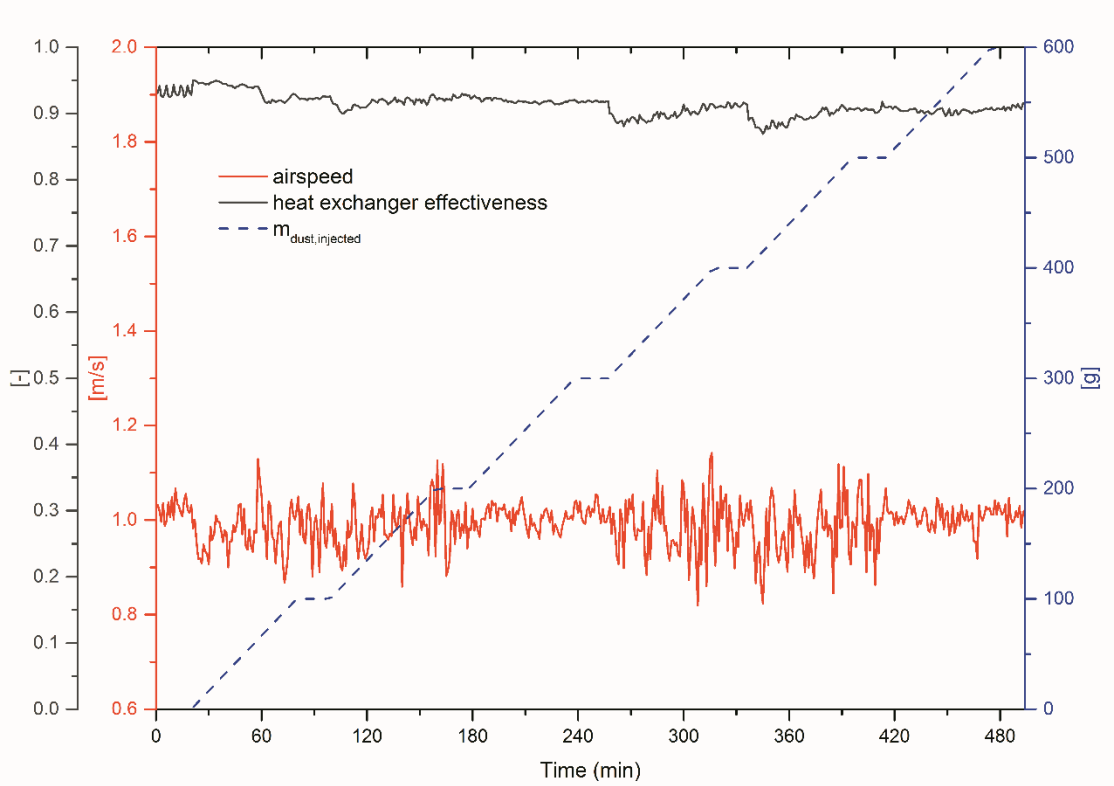

Figure 3.14. Transient plot of variables related to thermal resistance through the heat exchanger.

Figure 3.14 presents a *stitched together*, transient plot of filtered measured data (*cf.* explanation for Figure 3.4) of variables characterizing the thermal resistance to heat transfer through the heat exchanger. The mass of dust injected into the air stream in the wind tunnel increases during fouling periods, and remains unchanged during steady state periods. It is seen that the heat exchanger effectiveness shows little change throughout the duration of the experiment. This is because air velocity at the front face of the heat exchanger is maintained constant for the test run by increasing the speed of the blower. Then, the only impact of fouling is a possible

reduction in heat transfer surface area, and thermal resistance due to a layer of foulant deposition. From these results, it can be inferred that *for the defined operating conditions*, the thermal performance of the heat exchanger suffers little degradation.

The mass of test dust dislodged from the heat exchanger during the in situ cleaning methods is measured by vacuuming the duct floor upstream and downstream of the heat exchanger and by measuring the change in weight of the downstream filter. The efficacy of the cleaning procedure is characterized by the ratio of the mass of test dust removed from the heat exchanger to the mass of test dust present on the heat exchanger at the beginning of cleaning. In this case, statistics related to the cleaning methods are presented in Table 3.5.

Table 3.5. Efficacy of cleaning method during test run 2B.

Cleaning method	**Air velocity**	**Duration of cleaning procedure**	**Dust mass present on heat exchanger**	**Dust mass knocked off heat exchanger**	**Fraction of displaced dust**
	m/s	min	g	g	%
Reversal of airflow direction	1.0	2	156.8	33.6	21.4

After the multi–pronged attempt at *in situ* cleaning as described in Section 3.3.3 of the companion manuscript, the heat exchanger section is removed from the wind tunnel, and is cleaned as described in Section 3.2.6. From visual and mass–based assessment of the amount of foulant deposition still present on the heat exchanger, it is concluded that *in situ* cleaning is not sufficient, and a wet cleaning of the heat exchanger with some coil cleaner is necessary to remove all foulant deposition present on it.

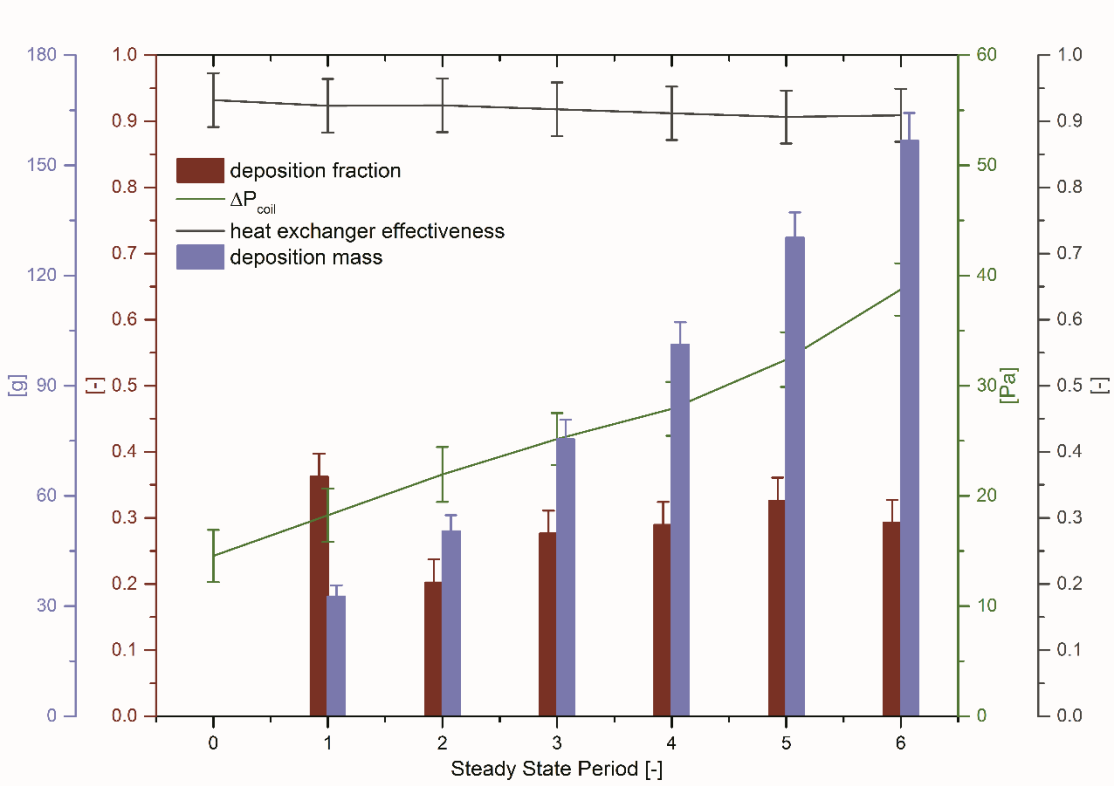

Figure 3.15. Steady state performance of the heat exchanger in clean and in fouled condition.

The performance of the heat exchanger during steady state measurements is presented in Figure 3.15. It is evident that the total mass of foulant deposition present on the heat exchanger increases after each fouling period, and so does the pressure drop across the heat exchanger. The change in the heat exchanger effectiveness from clean heat exchanger to fouled heat exchanger after six (6) fouling periods is within measurement uncertainty, and no conclusions can be drawn. The pressure drop across the heat exchanger largely tracks the increase in total mass of dust deposited on the heat exchanger.

The deposition fraction plotted on the graph is calculated for each fouling period independently—thus, its value represents the rate of fouling of the heat exchanger for each fouling period. No meaningful conclusion can be drawn from the trend observed in the value of deposition fraction. In all test runs, the deposition fraction for the first fouling period is observed to have the highest value. However, the value of deposition fraction for successive fouling periods does not always follow a monotonically increasing or decreasing trend. From this, it may be inferred that fouling already present on the heat exchanger does not strongly affect fouling occurring in subsequent fouling periods. It must be stressed that this conclusion is valid *for the current*

combination of heat exchanger geometry and operating conditions, and a larger, similarly collected experimental data set is required to make a broader statement.

The actual mass of dust deposited on the heat exchanger in the six fouling periods is 32.6, 17.8, 25.0, 25.8, 29.2, and 26.4 g. During every fouling period, about 10 g of dust out of the 60 g introduced into the wind tunnel by the dust injector is observed to fall out of suspension upstream of the heat exchanger. This is the sum total of the dust that falls out of the air stream before ever reaching the front face of the heat exchanger, or is held against the front face of the heat exchanger, but falls down after airflow is stopped. The decision to measure these together is taken because of inability to reliably separate dust from the two sources. A qualitative assessment of the quantity of dust that is trapped against the front edges of fins and tubes by the force of the airflow can be made from photographs taken of the duct floor immediately upstream of the heat exchanger after every steady state period. The relatively insignificant change in this measurement for successive fouling periods suggests a relatively reliable dust injector and dust injection process.

The mass of dust fallen out of suspension downstream of the heat exchanger is about 5 g per fouling period. Dust that passes through the heat exchanger may settle on the duct floor downstream of the heat exchanger. A dust particle may collide with the layer of foulant already present on the heat exchanger, and knock particles of dust off their deposition sites. Both these may contribute to this mass of dust vacuumed from the duct floor downstream of the heat exchanger.

Table 3.6 lists periodwise, steady state measured data for test run 2B. The pressure drop across the heat exchanger at the end of the test run is about 2.7 times that of the clean heat exchanger. Since a variable speed blower is used, the heat transfer performance and capacity of the heat exchanger does not suffer. Since the mass flow rate of hot water through the heat exchanger, the temperature of water at inlet to the heat exchanger, and temperature of air at inlet to the heat exchanger is maintained constant, the heat exchanger effectiveness can be used to comment on the capacity of the heat exchanger as well. If a constant speed blower were to be used, the airflow through the heat exchanger would decrease substantially resulting in a much reduced capacity. This would likely impact the performance of the system in which the heat exchanger is installed as well.

Table 3.6. Steady state data for test run 2B.

Steady state period	**Periodwise deposition fraction**	**Total dust deposition mass on heat exchanger**	**Pressure drop across heat exchanger**	**Heat exchanger effectiveness**
	—	g	Pa	—
clean			14.54 ±2.37	0.93 ±0.04
1	0.36 ±0.03	32.6 ±3.1	18.24 ±2.43	0.92 ±0.04
2	0.20 ±0.04	50.4 ±4.3	21.94 ±2.49	0.92 ±0.04
3	0.28 ±0.03	75.4 ±5.3	25.16 ±2.37	0.92 ±0.04
4	0.29 ±0.03	101.2 ±6.1	27.91 ±2.45	0.91 ±0.04
5	0.33 ±0.03	130.4 ±6.8	32.37 ±2.49	0.91 ±0.04
6	0.29 ±0.03	156.8 ±7.5	38.73 ±2.38	0.91 ±0.04

3.4.2 Parametric Test Runs

A comparison of measurements from test runs from each group defined in Table 3.3 is presented in the following sections. All results presented use similar terminology. The cumulative deposition fraction is calculated according to:

$$D_{cumulative} = \frac{\sum_{i=1}^{6}\left(m_{d,dep}\right)_i}{\sum_{i=1}^{6}\left(m_{d,inc}\right)_i} \tag{3.12}$$

The pressure drop and heat exchanger effectiveness values plotted on graphs that correspond to a *fouled heat exchanger* are values measured during the last steady state period—at the end of a test run. Measurements denoted as corresponding to a *clean heat exchanger* are made during the zeroth steady state period. This comparison is seen as an indicator of the degradation in the thermal and hydraulic performance of the heat exchanger due to fouling.

3.4.3 Sensitivity of Fouling to a Change in Dust Concentration During Test Runs

A comparison of experimental measurements from Group 1 (*cf.* Table 3.3) of test runs is presented in Figure 9. For all test runs in Group 1 (*cf.* Table 3.3), it is seen that measured pressure drop across the heat exchanger at the same face air velocity is greater for a fouled heat exchanger than for a clean heat exchanger. It is also seen that as air velocity is maintained constant despite fouling, the measured heat exchanger effectiveness for a fouled heat exchanger are lower than that for a clean heat exchanger, although the change in the measured value is on the same order of magnitude as the measurement uncertainty. When assessing the impact of an increase in fouling rate (or concentration of fouling agent in air), it is seen that there is a small increase in cumulative deposition fraction at higher fouling rates. The change in cumulative deposition fraction is not observed to significantly affect heat exchanger effectiveness; pressure drop across the fouled heat exchanger is observed to track the increase in dust deposition on the heat exchanger. When assessing the repeatability of measurements, attention is focused on measurements from test run 1C (15 g/hr). The two test points are plotted adjacent to each other in Figure 3.16. Pressure drop measurements from the repeated tests for the clean heat exchanger are within measurement uncertainty. The cumulative deposition fraction is slightly higher for one of the test runs; the pressure drop across the fouled heat exchanger shows a far greater increase for the test run corresponding to the higher value of measured cumulative deposition fraction. The test run with

the lower measured pressure drop value was conducted in March 2016, whereas the one with the higher measured pressure drop value was conducted in June 2016. The test runs were conducted using fouling agent from different batches. For the iteration of test run 1C conducted in March 2016, mass of test dust injected during the second fouling period is 55 g, which is 5 g less than the corresponding entry in Table 3.3 (= 60 g). Thus, the total mass of test dust injected into the wind tunnel for the March 2016 iteration of test run 1C is 355 g, whereas that injected into the wind tunnel for the June 2016 iteration of test run 1C is 360 g. This difference is also reflected in the total mass of dust incident on the front face of the heat exchanger after all fouling periods. However, the total mass of dust deposited on the heat exchanger for both iterations differs by an amount larger than 5 g; thus this deviation cannot alone be held responsible for the difference in the cumulative deposition fraction between the two iterations. It is noted that all deposition fraction calculations are based on *actual* masses, and thus any deviations are accounted for in these calculated values.

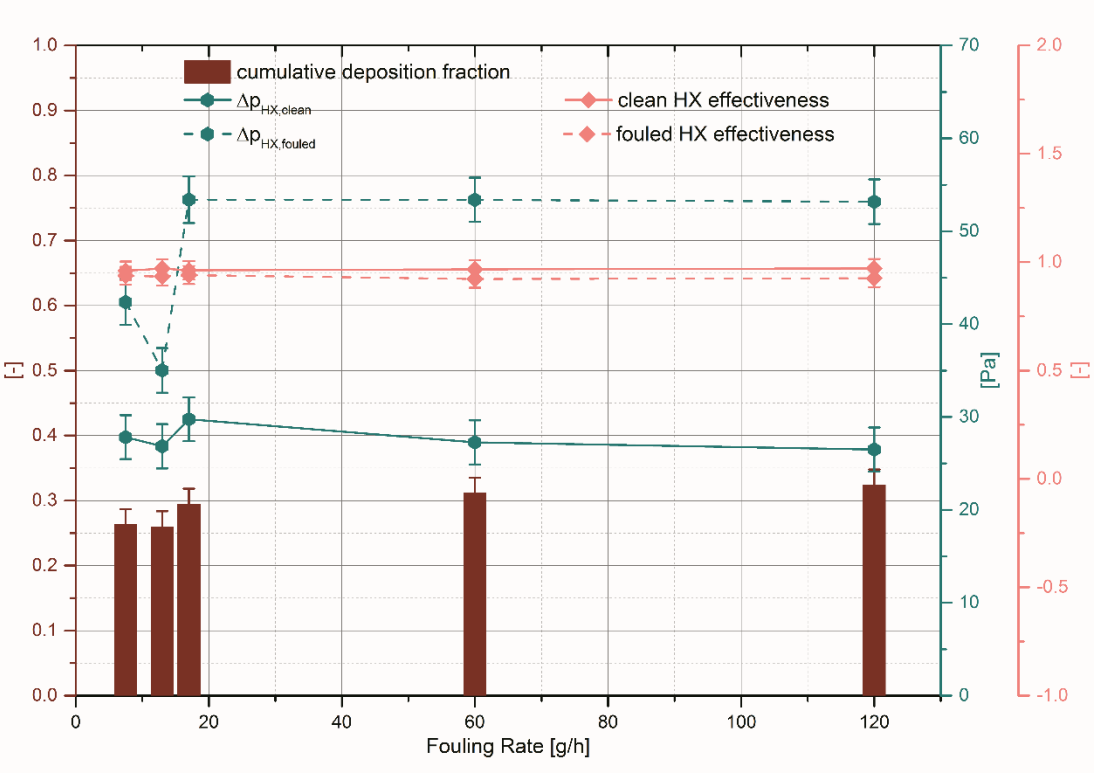

Figure 3.16. Measurements from Group 1 (*cf.* Table 3.3) of test runs.

As qualitative assessment of the measured cumulative deposition fraction, Figure 3.17and Figure 3.18 compare the front face of the heat exchanger after the last steady state period at the end of the

test run. Photographs from test run 1A and 1D are presented since the largest difference in deposition fraction exists between them. It can be seen that deposition occurs to a larger extent in test run 1D than in test run 1A.

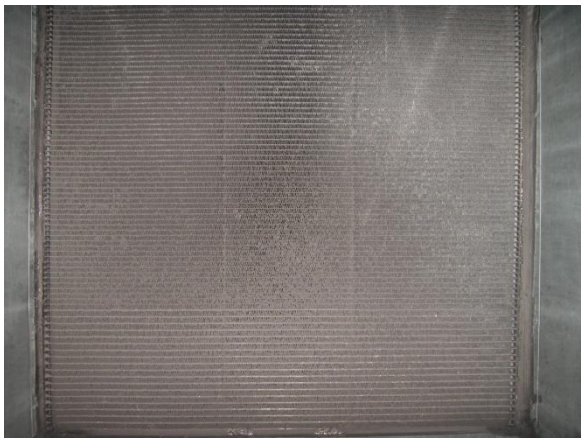

Figure 3.17. Test run 1A.

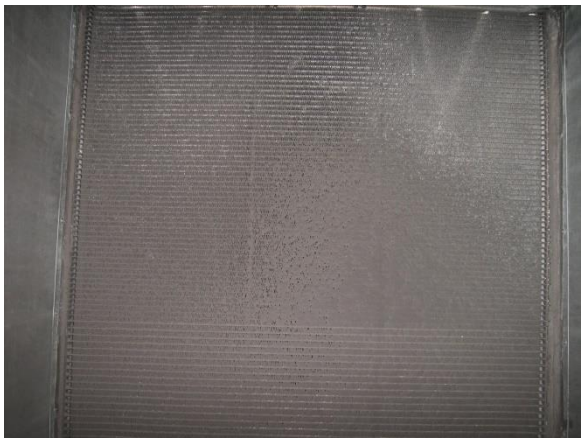

Figure 3.18. Test run 1D.

3.4.4 Sensitivity of Fouling to a Change in Relative Humidity During Test Runs

A comparison of experimental measurements from Group 2 (*cf.* Table 3.3) of test runs is presented in Figure 3.19. Here again, it is observed that pressure drop across a fouled heat exchanger is greater than that across a clean heat exchanger. On the other hand, heat transfer effectiveness of a fouled heat exchanger is slightly lower than that for a clean heat exchanger; however, this change is again on a similar order of magnitude as the measurement uncertainty. The pressure drop across the fouled heat exchanger roughly tracks the mass of foulant deposition on the heat exchanger. It is observed that the cumulative deposition fraction tends to increase as the humidity of air at heat exchanger inlet increases, reaches a peak value near 75% to 80% relative humidity, and decreases with a further increase in the humidity of air at heat exchanger inlet. To ascertain the veracity of measured data, two test runs are repeated in Group 2 (*cf.* Table 3.3). The repeated tests are plotted adjacent to each other on the graph in Figure 3.19. The measured cumulative deposition fraction for both test runs with an inlet relative humidity of 90% is fairly similar, so is the measured pressure drop across the fouled heat exchanger. Thus, the measurements can be repeated. In the interest of comprehensive reporting of data, the measurements plotted in Figure 3.19 at 90% relative humidity were made in September 2014 (higher value of cumulative deposition fraction) and September 2015 (lower value of cumulative deposition fraction). The test

dust used came from different batches of purchased foulant. The cumulative deposition fraction for the test runs repeated at 75% relative humidity at inlet to the heat exchanger, however, differs. The larger deviation is between the pressure drops measured across the fouled heat exchanger—in terms of trend with respect to foulant deposition. The pressure drop corresponding to the fouled heat exchanger with lower value of cumulative deposition fraction is higher. The test run with the lower pressure drop value was conducted in August 2014; the repeated test run was conducted in May 2015. The second anomaly is that the pressure drop across the fouled heat exchanger is lower at 70% relative humidity than at 60% relative humidity although the cumulative deposition fraction at 70% relative humidity is greater than that at 60% relative humidity.

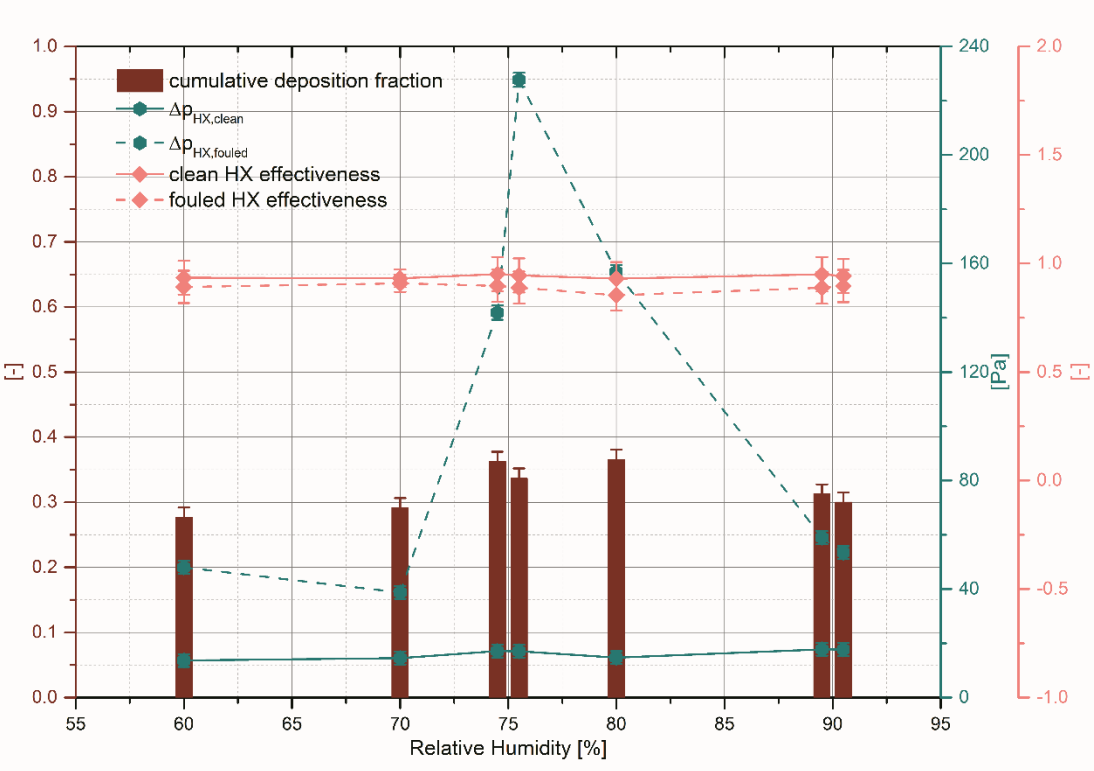

Figure 3.19. Measurements from Group 2 (*cf.* Table 3.3) of test runs.

A series of photographs are presented in Figure 3.20 to Figure 3.26. All photographs are of the front face of the heat exchanger taken after the last fouling period for test runs from Group 2 (*cf.* Table 3.3). The fact that foulant deposition is greater for test runs 2C and 2D than for other test runs is evident from these photographs. Since the total dust mass injected per test run is maintained constant, cumulative deposition fraction and total foulant deposition after all fouling periods are equivalent. These photographs are presented as qualitative verification of measured

cumulative deposition fractions. The photographs can only capture dust deposited on the front face of the heat exchanger. Since some foulant deposition could occur inside the airflow channels, small differences in deposition fraction cannot be reliably predicted by observing photographs—but the difference between foulant deposition at the end of test run 2A and that at the end of test run 2D is evident in Figure 3.20 to Figure 3.26.

Figure 3.20. Test run 2A.

Figure 3.21. Test run 2B.

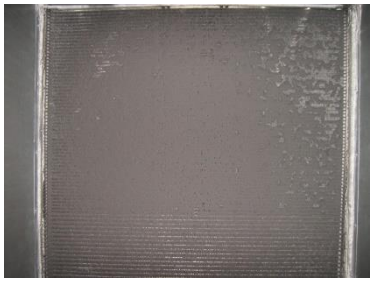

Figure 3.22. Test run 2C; lower pressure drop measured (2014).

Figure 3.23. Test run 2C; higher pressure drop measured (2015).

Figure 3.24. Test run 2D.

Figure 3.25. Test run 2E; higher pressure drop measured (2014).

Figure 3.26. Test run 2E; lower pressure drop measured (2015).

It is noted that all photographs in Figure 3.20 to Figure 3.26 are taken after airflow is stopped, but pressure drop across the fouled heat exchanger and heat exchanger effectiveness are based on

steady state periods directly following fouling periods without any break in airflow. Similarly, the quantitative assessment of foulant deposition is performed after airflow through the heat exchanger is stopped. Thus, there exists a time lag between the measured data and the photographs presented in Figure 3.20 to Figure 3.26. Therefore, a second set of photographs are presented in Figure 3.27 to Figure 3.30. These photographs are of the duct floor directly upstream of the heat exchanger after airflow is stopped at the end of a test run (after the steady state period following the last fouling period). The region of the wind tunnel floor focused on here is as wide as the front face of the heat exchanger, and extends about 0.1 m (4 inches) upstream from its front face. It is likely that most of the dust deposited in this region is held up against the frontal edges of fins and tubes and falls out of suspension once airflow stops.

Figure 3.27. Test run 2C; lower pressure drop measured (2014).

Figure 3.28. Test run 2C; higher pressure drop measured (2015).

Figure 3.29. Test run 2E; higher pressure drop measured (2014).

Figure 3.30. Test run 2E; lower pressure drop measured (2015).

It may be inferred from Figure 3.27 and Figure 3.28 that a larger mass of dust was being held up against the frontal edges of fins and tubes during the last steady state period of the 2014 iteration of test run 2C compared to the 2015 iteration. The consequences of this phenomenon, however, are contrary to the measured pressure drop value. A larger fraction of dust being held up against

the front face of the heat exchanger would serve to elevate the measured pressure drop but not be counted in the deposition fraction (since it is not *deposited on the heat exchanger surface*). An assessment of the mass of test dust that falls out of suspension upstream of the heat exchanger shows that this remains relatively constant throughout a test run. For instance, the mass of test dust that reaches the front face of the heat exchanger in each fouling period for the 2014 iteration of test 2C is 87.2, 87.6, 88.6, 88.6, 87.8, 83.6 g for the six fouling periods. A similar assessment for the 2015 iteration of test 2C reveals that these figures are 101.8, 85.2, 78.6, 87.0, 85.0, 83.6 g. The cause for this deviation is that excess test dust was injected into the wind tunnel during the first fouling period. This is because the fouling agent contained, as received, clumps and aggregates of its fibre content. This blocked the dust injector feeder wheel and nozzle, and the dust injection process had to be suspended while the dust injector was cleaned. While the dust injector was cleaned, the mass of test dust still present in it was measured. Based on the mass of test dust vacuumed from the dust injector, the mass of test dust actually injected into the wind tunnel was back–calculated. The mass was then loaded on the dust injector and the fouling period was conducted to its completion. Due to the interruption, the mass of dust injected into the wind tunnel, and subsequently, the mass of test dust incident on the front face of the heat exchanger is inflated for the first fouling period. The fact that more fouling agent was used during the 2015 iteration of test 2C may have caused the pressure drop measurement disproportionately greater in relation to the cumulative deposition fraction. The degraded quality of fouling agent may have affected this measurement as well. It is noted that all deposition fraction calculations take *actual* masses into account, and thus any deviations are accounted for.

3.4.5 Sensitivity of Fouling to a Change in Air Velocity During Test Runs

A comparison of experimental measurements from Group 3 (*cf.* Table 3.3) of test runs is presented in Figure 3.31. The trend of pressure drop across a fouled heat exchanger being greater than that across a clean heat exchanger is consistent in this group of measurements; so is the insignificant difference in heat exchanger effectiveness for a fouled heat exchanger versus a clean heat exchanger (when face air velocity for the heat exchanger is maintained constant). It is seen from the test results, that as the face air velocity (which is the air velocity incident on the front face of the heat exchanger) is increased, the cumulative deposition fraction reduces. Pressure drop across the fouled heat exchanger tracks the mass of foulant deposition on the heat exchanger

surface. Test run 3D is repeated in Group 3 (*cf.* Table 3.3)—its measurements are plotted adjacent to each other in Figure 3.31. The cumulative deposition fraction measured at the end of the test run is similar for both iterations. The pressure drop measured across the fouled heat exchanger at the end of the test run, is however, significantly different. The test run with smaller measured pressure drop across the fouled heat exchanger was conducted in November 2015, while that with the larger measured pressure drop across the fouled heat exchanger was conducted in December 2015. Test dust from the same purchased batch was used for both iterations. About the same total mass of test dust is incident on the front face of the heat exchanger for both iterations.

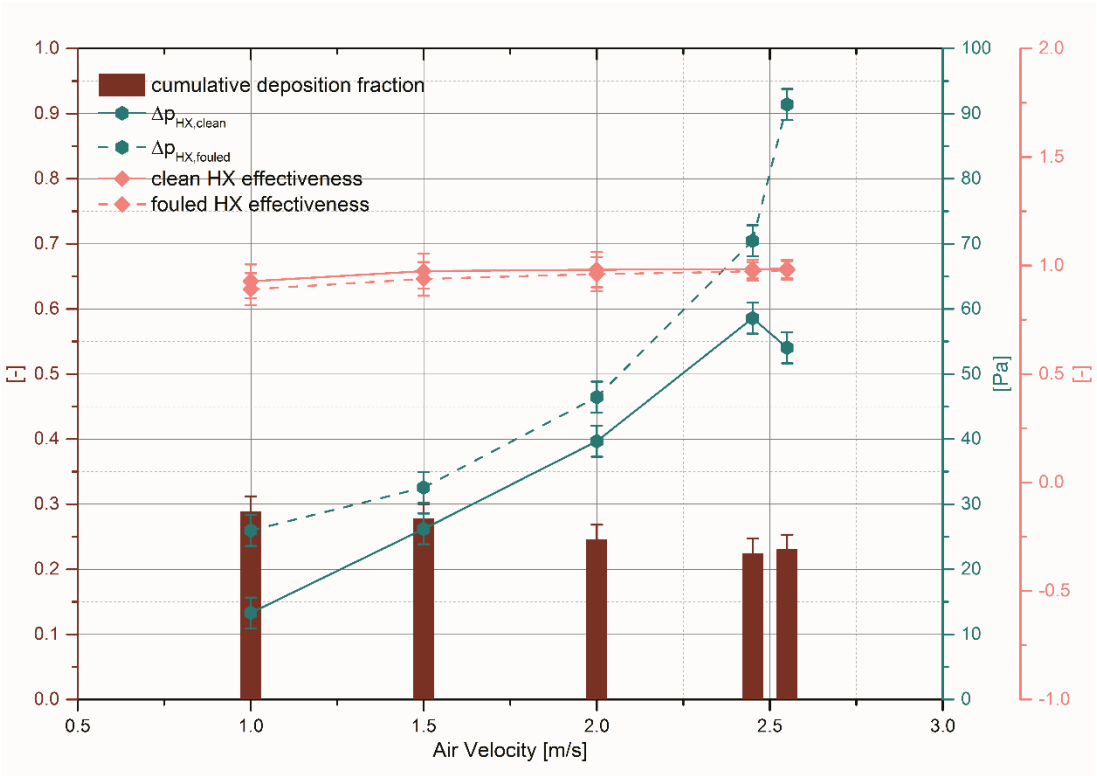

Figure 3.31. Measurements from Group 3 (*cf.* Table 3.3) of test runs.

Photographs of the front face of the heat exchanger after the last steady state period are presented for test runs 3A, and both iterations of test run 3D in Figure 3.32 to Figure 3.34 as qualitative assessment of the extent of foulant deposition on the heat exchanger. Photographs for both iterations of test run 3D are presented in Figure 3.33 and Figure 3.34, and it can be seen that there is no significant difference in the extent of fouling between the two iterations. The decrease in deposition for test run 3D versus test run 3A can also be seen from these photographs. The photographs presented in Figure 3.33 and Figure 3.34 do not demonstrate clear evidence to explain

the difference in measured pressure drop across the fouled heat exchanger. The total mass of test dust injected into the wind tunnel during each iteration, and the mass of test dust incident on the front face of the heat exchanger during each iteration are both fairly similar.

Figure 3.32. Test run 3A.

Figure 3.33. Test run 3D; smaller pressure drop (November, 2015).

Figure 3.34. Test run 3D; larger pressure drop (December, 2015).

3.4.6 Single Speed Blower Test

All measured data reported in Sections 3.4.3, 0, and 3.4.5 is from test runs where a constant face air velocity at the heat exchanger is maintained by increasing the blower speed. To investigate the effect of reducing air velocity on the phenomenon of fouling and the subsequent performance of the fouled heat exchanger, a test run is conducted by setting a constant blower speed and allowing the face air velocity at the heat exchanger to change. The experimental procedure outlined in Section 2.3.3 of the previous chapter is followed for this test run as well, with one important change. Instead of maintaining a constant face air velocity at the heat exchanger, the blower speed is always set to the same speed (by setting the variable frequency drive at the same frequency value).

Figure 3.35 presents steady state measurements for this test run. Trends observed in results presented in Section 3.4.1 are both observed to undergo significant changes here. Pressure drop measured across the heat exchanger decreases as the test run progresses, even as total mass of

foulant deposition on the heat exchanger increases. This is because the air velocity through the heat exchanger reduces. The heat exchanger effectiveness is measured to reduce as a consequence of a reduction in air velocity, and as per established theory, the air-side heat transfer coefficient. In accordance to the trend observed in Section 3.4.5, as air velocity decreases, deposition fraction tends to increase. The measured deposition fraction shows this trend; their values decrease as the test run progresses—although this increase is within measurement uncertainty.

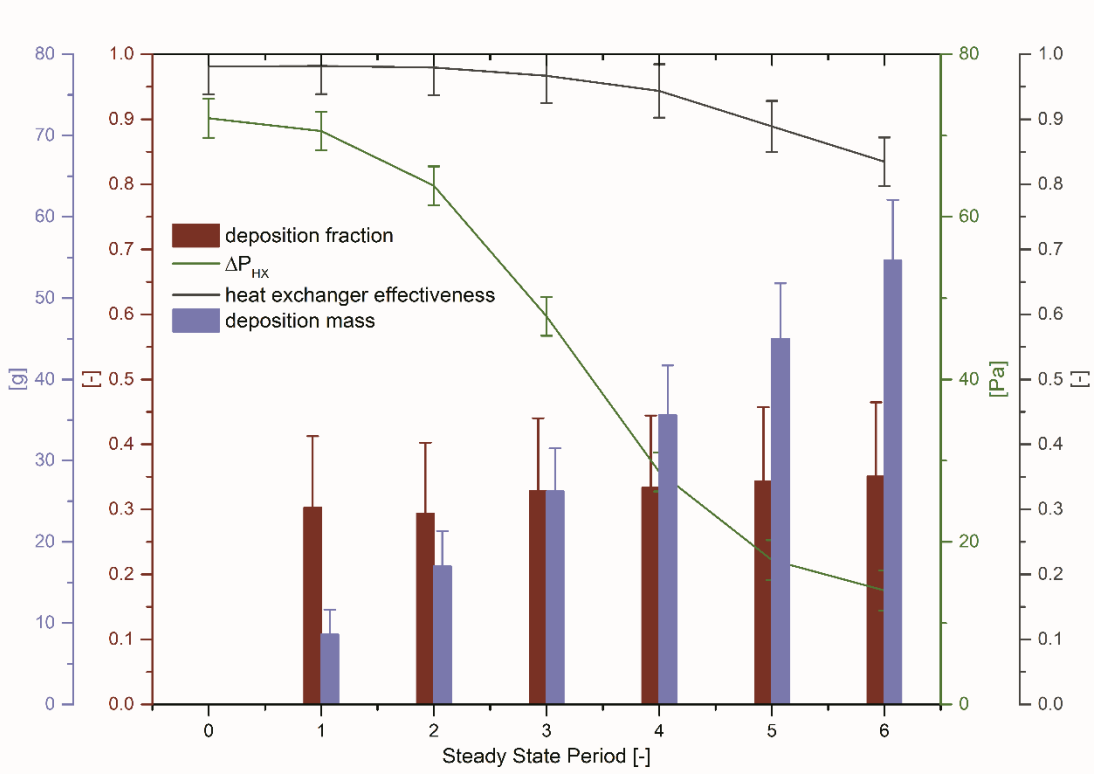

Figure 3.35. Steady state performance of the heat exchanger in clean and in fouled condition.

Figure 3.36 presents a transient graph of experimental variables related to flow resistance across the heat exchanger. Fouling periods can be identified as those regions where the slope of the plot corresponding to the mass of test dust injected into the air stream is positive. Steady state periods can be identified as those regions where the slope of this plot is zero (0). This plot is *stitched together* from discontinuous measurements as well (see Section 3.4.1). One very apparent effect observed in the graph is that the pressure drop across the heat exchanger and the face air velocity decrease continuously during fouling periods and stay relatively steady during steady state periods. There is a clear increase in face air velocity for each fouling period following the steady state measurement. As discussed in Section 3.4.1, some of the dust is held up against the front

edges of tubes and fins. It contributes to flow resistance during the steady state measurement, however falls off the front face once airflow stops. Thus, for the subsequent fouling period, there is a reduction in flow resistance. Since this is a single speed blower test, a reduction in flow resistance causes an increase in air velocity through the heat exchanger and thus an increase in pressure drop measured across the heat exchanger. Since the blower is restarted at the same speed (and not to achieve a fixed face air velocity) after each time it is stopped, this effect is exaggerated.

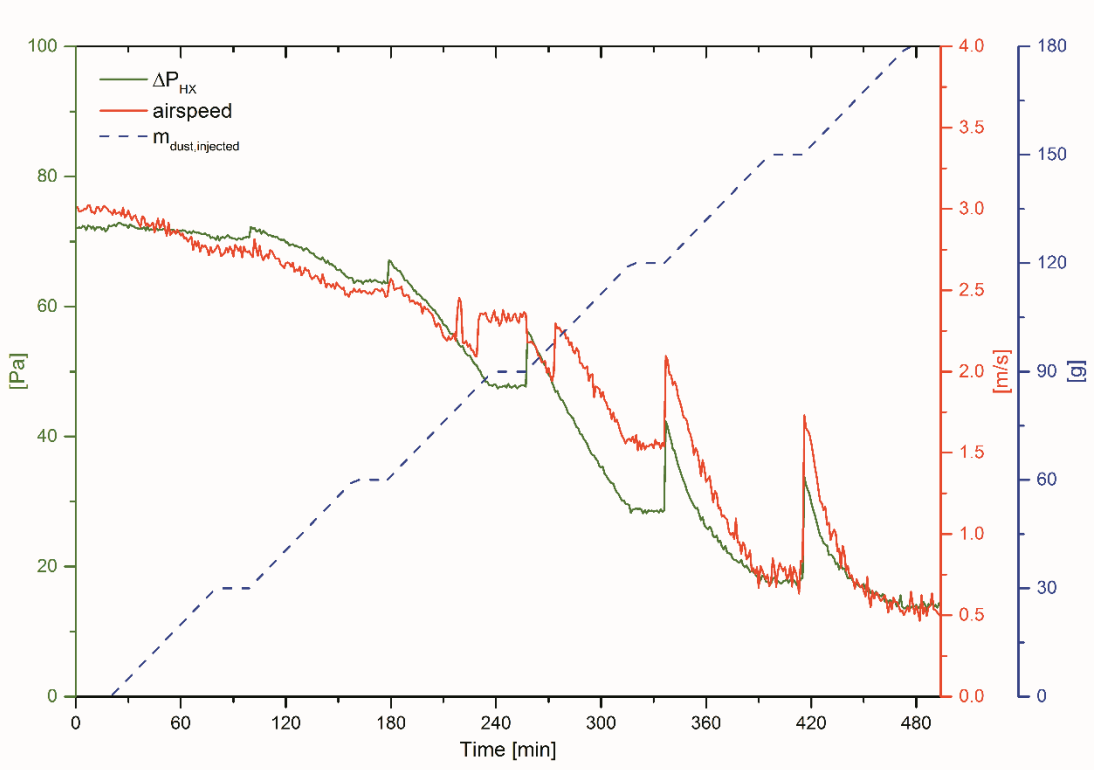

Figure 3.36. Transient graph of experimental variables related to flow resistance across the heat exchanger.

Figure 3.37 presents a transient graph of experimental variables related to thermal resistance through the heat exchanger. Fouling periods and steady state periods can be identified similar to Figure 3.36. Again, this plot is *stitched together* from discontinuous measurements (see Section 3.4.1). Similar to remarks made about Figure 3.36, the face air velocity for the heat exchanger experiences sharp increases for every fouling period following a steady state measurement. This is reflected in the value calculated for the heat exchanger effectiveness as well. Figure 3.36 and Figure 3.37 can be observed as representing actual performance of a heat exchanger when undergoing fouling in the field, as long as the heat exchanger is installed in a system with a single speed blower.

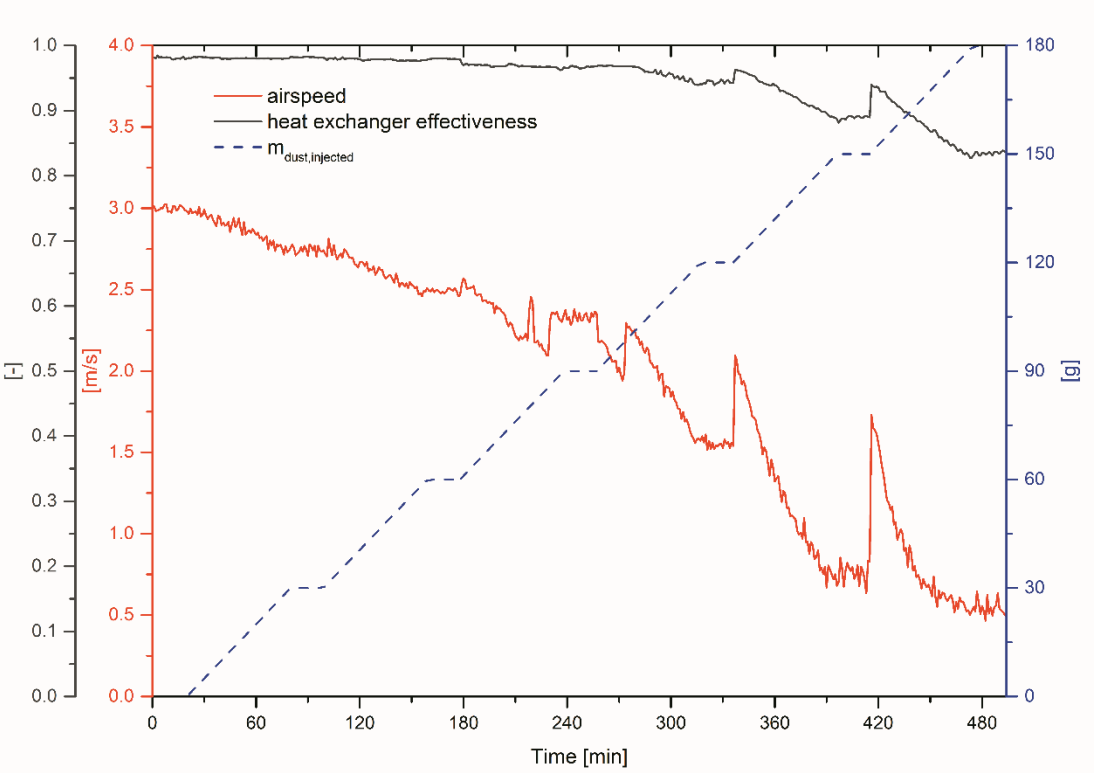

Figure 3.37 Transient graph of experimental variables related to thermal resistance through the heat exchanger

3.4.7 Efficacy of Cleaning Methods

Section 2.3.3 from the previous chapter describes *in situ* cleaning methods attempted for some of the test runs. In general, it is observed that the efficacy of the cleaning process is a function of the amount of foulant deposition present on the heat exchanger before the cleaning process is initiated. However, across different test runs, reversal of airflow direction is more efficacious than the other methods. It is noted that the construction of the wind tunnel is such that reversing the direction of airflow in the entire duct is impossible. Therefore, the modular duct section that the heat exchanger is installed in is reversed and then reconnected with the duct. The wind tunnel blower is operated as before. As a result, the airflow direction through the heat exchanger *is* reversed. Experimental data measured when conducting *in situ* cleaning of the heat exchanger is presented in Table 3.7.

Table 3.7. Experimental measurements on cleaning methods.

Test run	Rank in cleaning sequence	Cleaning method	Air velocity	Duration of cleaning procedure	Dust mass present on heat exchanger	Dust mass knocked off heat exchanger	Fraction of displaced dust
			m/s	min	g	g	%
3D (Dec. 2015)	1	High speed airflow	3.5	3	77.8	8.0	10.3
	2	Pulsed airflow	2.5	1 × 3	69.8	0.0	0.0
	3	Reversed airflow	2.5	3	69.8	7.8	11.2
1A	1	Pulsed airflow	1.5	1 × 3	107.8	5.2	4.8
	2	High speed airflow	3.2	3	102.6	28.6	27.9
	3	Reversed airflow	1.5	3	74.0	8.2	11.1
1B	1	Pulsed airflow	1.5	1 × 3	103.8	8.0	7.7
	2	High speed airflow	2.5	3	95.8	14.2	14.8
	3	Reversed airflow	1.5	3	81.6	12.4	15.2
1C (Mar 2016)	1	High speed airflow	3.2	3	84.4	27.4	32.5
	2	Pulsed airflow	1.5	1 × 3	57.0	1.0	1.8
	3	Reversed airflow	1.5	3	56.0	3.2	5.7
1C (Jun 2016)	1	Reversed airflow	1.5	3	97.4	12.6	12.9
	2	Pulsed airflow	1.5	1 × 3	84.8	1.8	2.1
	3	High speed airflow	3.1	3	83.0	18.2	21.9
1D	1	Reversed airflow	1.5	3	87.2	12.4	14.2
	2	High speed airflow	3.1	3	74.8	18.0	24.1
	3	Pulsed airflow	1.5	1 × 3	56.8	0.4	0.7

3.5 Discussion

3.5.1 Quality of Fouling Agent

Inconsistent quality of test dust is a problem encountered in the course of this research. Some samples of fouling agent (as purchased/received) contain large clumps where the fibre content has formed aggregates in which particulate content accumulates. These clumps cannot be broken down in course of the usual test procedure. Figure 3.38 and Figure 3.39 compares a homogeneous, well–mixed sample with a non–homogeneous sample containing aggregates. These block the feeder wheel in the dust injector or choke the injector nozzle, thus breaking down the experiment. An attempt is made to break down the clumps using a paint mixer, however, this attempt is abandoned for two reasons—the attempt is unsuccessful, and it is expected that the post–mixed test dust characteristics would be different from those of the fouling agent sample as received.

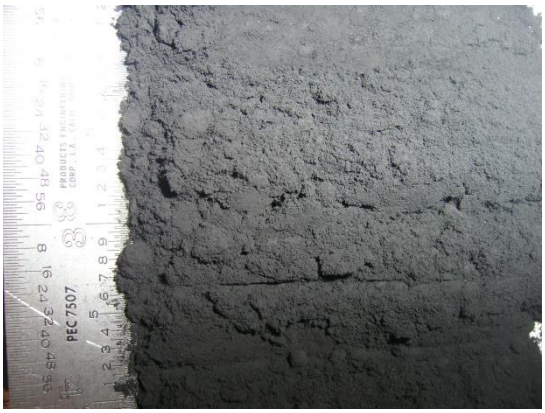

Figure 3.38. Test dust sample without clumps.

Figure 3.39. Test dust sample with clumps.

To assess the test dust in greater detail, two samples of purchased fouling agent were sent to an external laboratory to conduct a particle size and shape analysis—once in June 2015, and once again in August 2016. Particle Technology Labs, IL conducted an imaging analysis on a submitted sample of test dust employing a Malvern Morphologi G3 instrument (Malvern Instruments, Ltd., 2015). The analysis provided information about the particulate content and fibre content of the test dust separately. Particle size plots of the particulate content and fibre content of the test dust samples are presented in Figure 3.40 to Figure 3.43. The distinction between true particulate content and fibre content is made by defining cut off values for elongation (> 0.90), solidity (< 0.70), circularity (< 0.49), and fibre length (> 80.0 µm).

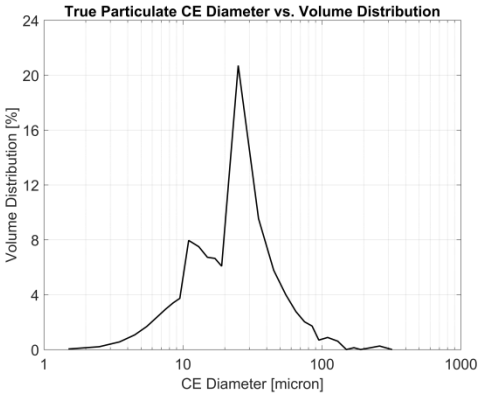

Figure 3.40. Volume based particle size distribution of particulate content of test dust (Vinakos, 2015).

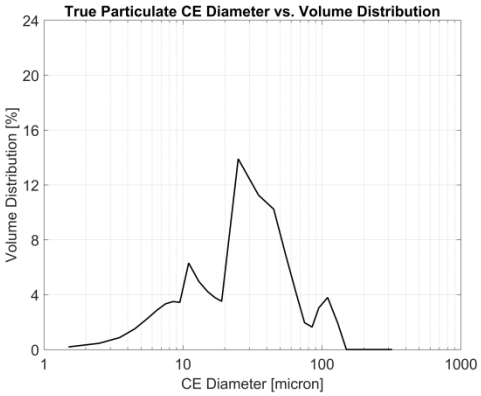

Figure 3.41 Volume based particle size distribution of particulate content of test dust (Vinakos, 2016).

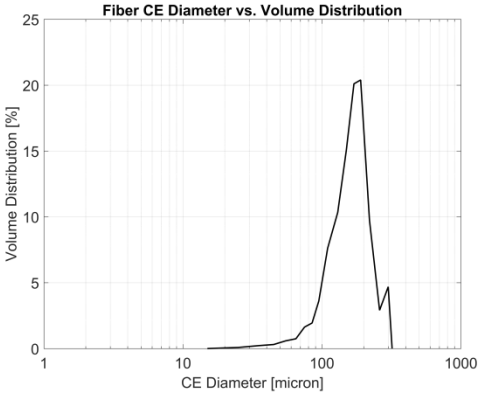

Figure 3.42 Volume based particle size distribution of fibre content of test dust (Vinakos, 2015).

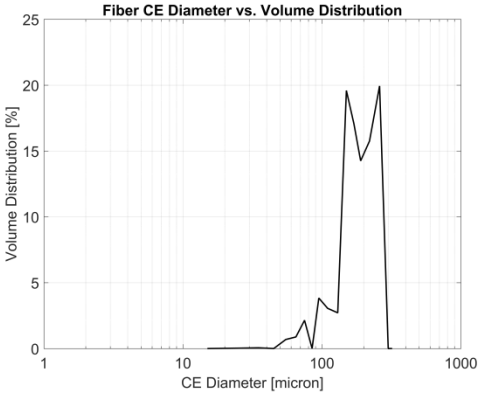

Figure 3.43 Volume based particle size distribution of fibre content of test dust (Vinakos, 2016).

It is evident from the graphs that there is variability between the two samples, and this variability may have some impact on the phenomenon of fouling. It is stressed that ANSI/ASHRAE Standard 52.2–2012 does not define an exact particle size distribution for ASHRAE Standard Test Dust #1; neither does ISO 12103–1:1997 define an exact particle size distribution for A2 Fine Test Dust (which is a component of ASHRAE Standard Test Dust #1). Thus, this variability is to be expected. It is difficult to quantify the impact of this variability in the particle size distribution of the fouling agent on this research. Some of the inconsistencies in the measurement results, *e.g.* the differences in repeated measurements, may result from this variability.

3.5.2 Operation of Blower in Wind Tunnel

As discussed in Section 3.2.1, the method chosen to measure air velocity is not ideal for the range of air velocities encountered in the course of this research and for the experimental setup. As the pressure drop across the heat exchanger rises, the pressure head on the blower increases. Some of the measurements are conducted at combinations of pressure head on the blower and airflow rate that lie in the unstable region of the fan curve. The blower installed in the duct is a Buffalo Forge type BL, size 300, single inlet fan. The fan curve characteristics are obtained through personal communication with the manufacturer. The blower being throttled into the stalled region may drive some of the unsteady pressure and flow. In addition, the current test setup is a blow through flow configuration—where the blower is upstream of the heat exchanger (restriction to airflow). This configuration tends to deliver airflow with high turbulence levels at fan exit (P. Lawless, Ph.D., Xcelaero Corporation, personal communication, September 13, 2013). The combination of these three factors may explain the fluctuating nature of measured duct air velocity plotted in graphs presented in this manuscript. It may also introduce uncertainty in the measurement of air velocity—uncertainty that cannot be mathematically represented because of difficulty in characterizing it accurately.

3.5.3 Filtration Efficiency

As stated in Section 3.2.1, the bag filter used downstream of the heat exchanger has an MERV value of 13. Table 3.8 presents particle removal efficiency necessary for a filter to be filter rated at an MERV value of 13 as a function of particle size. It is reproduced from Table 12–1 given in ANSI/ASHRAE Standard 52.2–2012.

Table 3.8. Particle removal efficiency of a filter as a function of particle size.

MERV (Minimum Efficiency Reporting Value)	**Composite Average Particle Removal Efficiency, E [%]**		
	Particle Size Range 0.3 to 1.0 µm	Particle Size Range 1.0 to 3.0 µm	Particle Size Range 3.0 to 10.0 µm
13	$E < 75$	$90 \leq E$	$90 \leq E$

ISO 12103–1:1997 states an approximate particle size distribution based on volume for A2 Fine Test Dust—a component of the fouling agent used in this research. This distribution is reproduced in Table 3.9.

Table 3.9. Particle size distribution of A2 Fine Test Dust.

Size µm	**Cumulative maximum volume fraction** %
1	2.5 to 3.5
2	10.5 to 12.5
3	18.5 to 22.0
4	25.5 to 29.5
5	31 to 36
7	41 to 46
10	50 to 54
20	70 to 74
40	88 to 91
80	99.5 to 100
120	100

As can be seen from Table 8, some fraction of the test dust lies in the particle size range for which arrestance efficiency is lower than 75% (*cf.* Table 3.9). In addition, the carbon black component of the test dust lies in the particle size range for which arrestance efficiency is lower than 75% as well (*cf.* Table 2.3 of previous chapter, Table 3.8). As stated in Section 3.4.1, the calculation for deposition fraction assumes that no dust particles escape the downstream bag filter. Based on particle removal efficiencies for filters rated at MERV values of 13, this assumption is not entirely accurate and introduces error in the measurement—again, an error that cannot be mathematically represented as a measurement uncertainty because it is difficult to characterize.

In addition, the manufacturer of the pleated bag air filter used in this study (AAF Flanders, Louisville, KY) requires the maximum pressure drop across the filter to be 498.2 Pa (2.0 inWC). While measurements reported in this study were being made, the pressure drop across the filter exceeded this maximum value. Since the dust injection process cannot be stopped before completion of a fouling period, this usage of bag filters outside of the recommended pressure drop range could not be avoided. The filtration efficiency of the bag filters may deviate from the rated MERV 13 during usage at pressure drops in excess of the recommended maximum value—which may affect the accuracy of calculated deposition fractions.

3.6 Conclusion

A finned microchannel heat exchanger is experimentally investigated for air-side particulate fouling. The sensitivity of the phenomenon of fouling to changes in operating conditions is experimentally evaluated, and measurements are reported. Efficacy of various *in situ* cleaning

procedures is experimentally assessed. A detailed analysis of factors impacting the measured data is presented as well.

CHAPTER 4. PREDICTIVE MODEL FOR FINNED TUBE HEAT EXCHANGERS

4.1 Literature Review

One of the earliest attempts to experimentally characterize air-side fouling of heat exchangers with complex fin and tube surface geometries was reported by Bott and Bemrose (1983), who experimentally fouled a four-row, four-pass spiral wound finned tube heat exchanger using precipitated calcium carbonate dust. The tests performed indicated that the Colburn-*j* factor and friction factor of the heat exchanger were influenced by fouling. The ratio of the instantaneous friction factor to its initial value asymptotically reached a constant value with progressive fouling. The difficulty in predictive modeling of such air-side fouling behavior, specifically at the scale of a complete heat exchangers has hindered the development of universal models. Instead, heat exchanger fouling models are developed based on various related studies that investigate fouling of representative heat transfer surfaces, and focus on one or two selected deposition mechanisms. Thus, reasonable accuracy can only be expected when modeling fouling of these specific surfaces under certain operating conditions for which the predominant deposition mechanisms are captured.

Waldmann and Schmitt (1966) modeled the thermophoresis and diffusiophoresis of aerosols and provided analytical expressions for thermophoretic and diffusiophoretic velocities of particles. Goldsmith and May (1966) experimentally measured particle deposition due to these mechanisms on flat plates. A test section was constructed out of two parallel plates between which a temperature or water-vapor gradient was maintained as necessary. Derjaguin *et al.* (1966) also modeled diffusiophoresis and thermophoresis of aerosol particles. These analyses were valid for small particles (particle radius smaller than the mean free path of gas molecules), which were assumed to not affect the flow field in their vicinity, and for large particles (particle radius much larger than the mean free path), which do affect the gas flow field around them. Annis *et al.* (1973) extended the range of applicability of earlier diffusiophoresis models, specifically for particle radii on the same order of magnitude as the mean free path of the gas molecules. Pilat and Prem (1975) used the models developed by Waldmann and Schmitt (1966) to analyze particle collection efficiency of a water droplet due to thermophoresis and diffusiophoresis, in addition to the effects of inertial impaction and Brownian diffusion.

Davies (1966) first analyzed particle deposition due to turbulence by modeling particle transport from the bulk fluid to the boundary layer by turbulent diffusion and deposition in the laminar sublayer under free flight. Sehmel (1970, 1971, and 1973) modeled turbulent deposition of particles from boundary layers adjacent to the surface. An important contribution was the inclusion of particle eddy diffusivities; it was found from experimental data that particle eddy diffusivity was greater than the fluid eddy diffusivity due to turbulence. Cleaver and Yates (1976) analyzed the deposition of particles by modeling their transport across the viscous sub-layer in a turbulent boundary layer. They also accounted for re-entrainment of particles by analyzing the local wall shear stress and turbulent bursts, and analyzed the limiting cases of gravity-dominated and inertia-dominated deposition. Later advances leveraged numerical modeling approaches, such as Kallio and Reeks (1989), who calculated particle trajectories in turbulent boundary layers to calculate particle deposition velocities in pipe flow.

Based on the foundational models discussed above that considered deposition due to individual mechanisms, comprehensive fouling models were developed for more realistic situations and flow geometries. Epstein (1988) modeled the phenomenon of particulate fouling of flat heat transfer surfaces due to various individual particle deposition mechanisms. The paper reviewed the different mechanisms of particle deposition driven by diffusion, inertia, impaction, gravitational settling, and thermophoresis, and presented analytical models to calculate the deposition velocity of particles for each mechanism. Deposition velocity is the velocity at which a particle approaches a surface from the free stream before finally depositing on it. This velocity may, for many mechanisms, be in a direction other than that of the primary fluid flow. Bott (1988) used a deposition velocity to model fouling of heat exchangers, with this velocity being defined as the mass flux of particles from the bulk flow to the surface on which deposition is being analyzed for fouling, normalized by the aerosol concentration. The transport of particles was separated into two types of phenomenon: transport across the bulk flow region toward the boundary layer and surface (Brownian motion, eddy diffusion, and thermophoresis) and transport across the boundary layer to adhere on the surface (particle diffusion, inertial impaction, and thermophoresis). The lack of good-quality experimental data was identified as a limitation for assessment of the model accuracy and simplifying assumptions made.

Siegel and Nazaroff (2003) accounted for the individual mechanisms as described above and developed a model to predict deposition of particles in a diameter range of 0.01 to 100 μm on wavy

fin-tube heat exchangers. The contribution of each deposition mechanism to the overall deposition fraction was deterministically calculated, except in the case of deposition due to turbulence, where a Monte Carlo simulation method was utilized. Experiments were conducted to measure the deposition fractions of monodisperse oil particles at different air velocities. The model predicted Brownian motion to be the dominant deposition mechanism for particles in the diameter range of 0.01-1 μm, while impaction on the leading edge of fins was predicted to be dominant in the 1-10 μm range. For the range of 10-100 μm, gravitational settling, impaction on tubes, and deposition due to turbulence were all contributing factors. The model showed qualitative agreement with experimental data, but underpredicted the extent of fouling at higher velocities and for larger particles.

The current work extends previous modeling approaches to include additional deposition characteristics in order to better represent the physical situation and improve prediction accuracy. In particular, the modeling enhancements include superimposition of the different fouling mechanisms, prediction of the distribution of deposits on the heat exchanger surface along the streamwise direction, analysis of the effects of accumulated deposits on subsequent fouling, and adaption of the previous modeling approach to different heat exchanger geometries. A comparison of model predictions with published experimental data is presented.

4.2 Model Description

The current modeling approach builds upon the deposition mechanisms considered by Siegel and Nazaroff (2003). The Siegel and Nazaroff (2003) [SN] model accounted for fouling of heat exchangers through inertial impaction on fins and tubes, gravitational settling, and deposition due to Brownian motion, turbophoresis, thermophoresis, and diffusiophoresis as described below:

1. Inertial impaction on fins and tubes accounts for the deposition that occurs when particulate matter in air flows around obstacles such as fins and tubes. If the inertia of a particle is high, it may not perfectly follow streamlines of air. The path that the particle moves along may lead to a collision with the obstacle further leading to deposition.
2. Gravitational settling accounts for deposition of particles under gravity. The larger the mass of a particle, the greater displacement due to gravity. If this displacement is large enough, the particle will settle onto the floor of the airflow passage.

3. Deposition due to Brownian motion accounts for the collision with and subsequent deposition of particles on heat exchanger surfaces due to random motion. This random motion, caused by momentum transferred to these particles by collisions with air molecules, is dominant in small particle sizes.
4. The presence of turbulence in the airflow causes movement of particles away from high turbulence zones. This is due to a gradient in the momentum transferred to the particles from collisions with air molecules. As the particles move in directions orthogonal to airflow, they may encounter heat exchanger surfaces and deposit.
5. Thermophoretic deposition also occurs due to a gradient in the momentum transferred to particles due to collisions with air molecules. However, this gradient is explained by a temperature gradient present in the airflow as a result of operation of the heat exchanger itself.
6. Diffusiophoretic deposition occurs due to the motion of particles under the action of diffusive forces. These diffusive forces result from moisture concentration gradients present in air. Most air-cooled heat exchangers operate in environments with a moderate amount of humidity. As air is heated or cooled, the moisture bearing capacity changes, causing a change in the moisture concentration in air. Diffusive fluxes of moisture and air lead to lateral particle motion toward surfaces.
7.

In the SN model, fouling of the tubes and fins of a heat exchanger is modeled for a finite number of distinct particle sizes, and the aggregate particulate deposition is calculated based on the particulate matter composition in the air stream. Using the detailed description of the model published by Siegel (2002), the model was first replicated to ensure consistency with these publications. The SN model is then modified and adapted to achieve certain objectives as described in Section 4.2.3.

4.2.1 Universal Modeling Assumptions

The following assumptions are applicable to all the fouling mechanisms considered in this model:

1. Dust particles suspended in the air are perfectly spherical solid particles with a known size distribution based on mass;

2. The density of individual dust particles and the bulk density of the aggregate deposited particulate matter differ by a constant factor;
3. The effective particle density of the particulate suspension in the air stream can be represented by a weighted mean of the constituent particle densities based on the mixture composition;
4. Every collision between particles and heat exchanger surfaces is assumed to be perfectly inelastic, *i.e.*, every collision results in adhesion of the particle to the surface; a separate model for particle adhesion is not implemented;
5. There is no re-entrainment of particles into the air stream after initial deposition;
6. Deposition occurs on both lateral side surfaces of the fins, and on the front edges of fins; the trailing one-quarter area of the tube surfaces remains free of fouling;
7. No fouling mechanism causes the transport of particles transverse to the bulk streamwise direction in a direction opposite to gravity; and
8. The particulate suspension in the air stream maintains a uniform spatial distribution as it flows through the heat exchanger, *i.e.*, there exists no spatial gradient in the suspended particulate concentration.

4.2.2 Deposition Fraction

Deposition fraction is used to quantitatively evaluate the extent of fouling of the heat exchanger surface. It is a mass-based, non-dimensional number defined as:

$$deposition\ fraction = \frac{mass\ of\ dust\ deposited\ on\ the\ heat\ exchanger}{total\ mass\ of\ dust\ entering\ the\ front\ face\ of\ the\ heat\ exchanger} \tag{4.1}$$

Conversely, the penetration fraction is a quantity used to evaluate the amount of particles which are able to pass through the heat exchanger without depositing:

$$penetration\ fraction = 1 - deposition\ fraction \tag{4.2}$$

4.2.3 Motivation and Description of Modifications to the Siegel-Nazaroff [SN] Model

The flow chart of the analytical model used to predict fouling of HVAC&R heat exchangers is presented in Figure 4.1. The model has been implemented in MATLAB, a commercially available algorithm development environment. Microsoft Excel is used to provide inputs to the model and record outputs. The model consists of simplified mathematical, deterministic calculations of the deposition fractions for particles of a specific size due to each deposition mechanism (except deposition due to turbulence, which is a probabilistic calculation). The penetration fractions for each particle size are then calculated and multiplied to find the aggregate penetration fraction for a given particle size. This is possible because all deposition mechanisms (except thermophoresis and diffusiophoresis) are assumed to be independent of one other, which can be justified by the observation that specific mechanisms dominate in unique and discrete ranges of particle size.

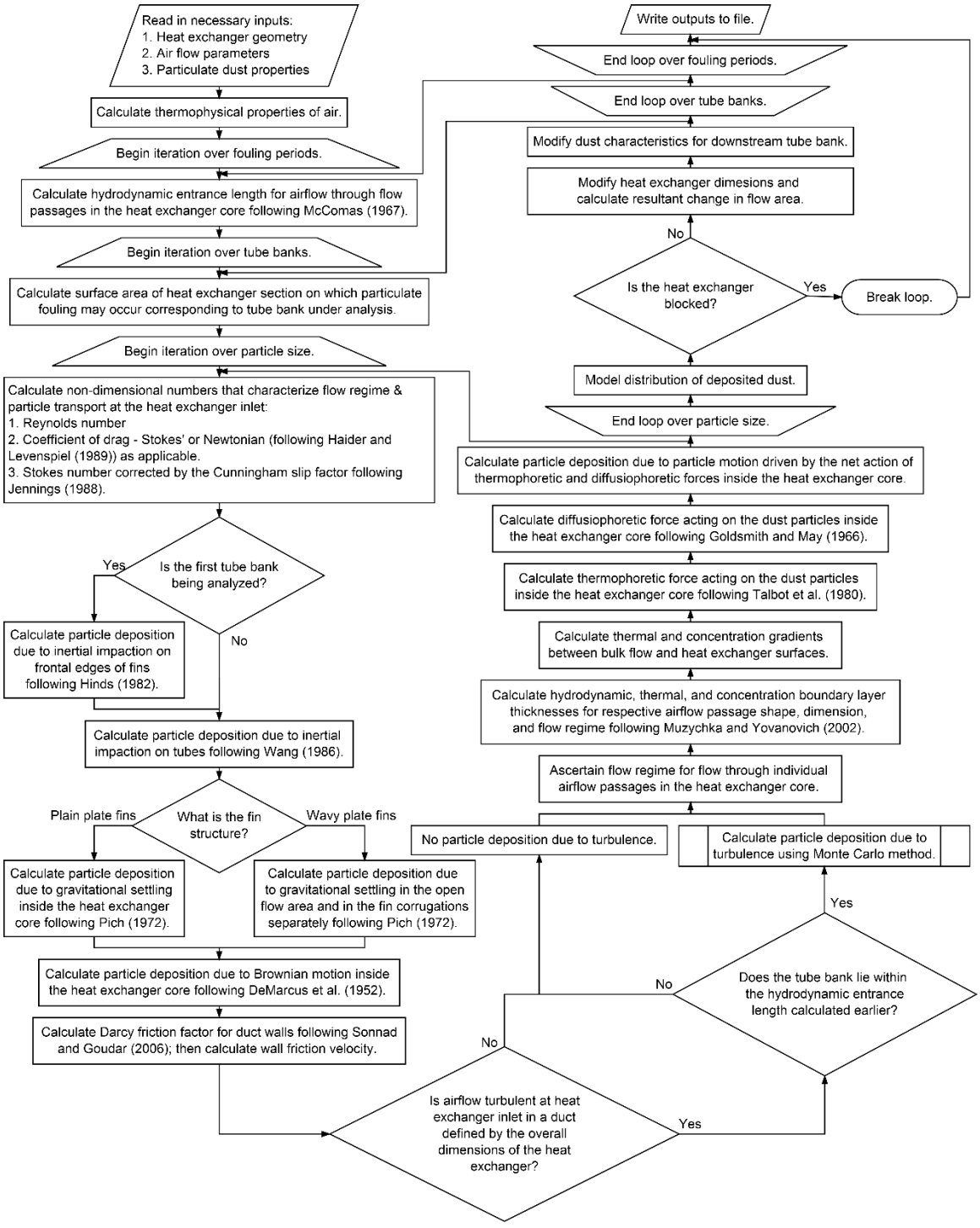

Figure 4.1. Flow chart of analytical model developed to predict fouling of a finned tube heat exchangers.

Figure 4.2 describes the naming convention used to denote directions relative to the duct.

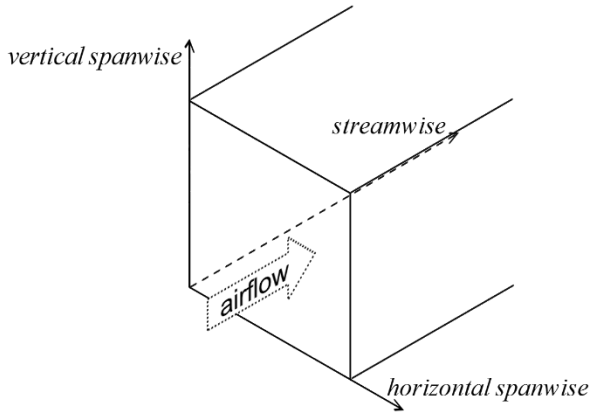

Figure 4.2. Naming convention used to denote directions with respect to the duct.

Table 4.1 lists some of the key equations used in the model to analyze the deposition mechanisms.

Table 4.1. Important equations used to calculate deposition due to each mechanism in the current model.

Deposition Mechanism	Equation for Deposition Fraction		Definitions	
Inertial impaction on fins (Hinds, 1982)	$D_{fin} = \min\left(1\ ,\ St_{fin} \cdot \frac{\pi}{2}\right) \times \frac{t'_{fin} \cdot corf}{S_{fin}}$	(4.3)	$St_{fin} = \tau_{p,x} \cdot \frac{U_{duct}}{t'_{fin}}$	(4.4)
Inertial impaction on tubes (Wang, 1986)	$D_{tube} = \min\left\{1\ ,\ \frac{2}{\pi} \times \tan^{-1}\left[0.8\left(St_{tube} - \frac{1}{8}\right)^{0.8}\right]\right\} \times \frac{D'_t}{P_t}$	(4.5)	$St_{tube} = \tau_{p,x} \cdot \frac{U_{duct}}{D'_t}$	(4.6)
Gravitational settling (Pich, 1972)	$D_{gra,plain-fins} = \frac{u_s \cdot P_l}{U_{hx} \cdot N_t \cdot P_t}$ $D_{gra,open} = \frac{u_s \cdot P_l \times \left(S_{fin} - H_w\right)}{U_{hx} \cdot N_t \cdot P_t \times \left(S_{fin} - t'_{fin} \cdot corf\right)}$ $D_{gra,corr} = \frac{u_s \cdot P_l \times \left(H_w - t'_{fin} \cdot corf\right)}{\left(\frac{P_w - 2 \cdot L_f / corf'}{2}\right) \times U_{hx} \times \left(S_{fin} - t'_{fin} \cdot corf\right)}$ $D_{gra} = D_{gra,open} + D_{gra,corr}$	(4.7)	$corf' = \sqrt{1 - \frac{1}{corf^2}}$	(4.8)
Brownian diffusion (DeMarcus and Thomas, 1952)	$D_{bro} = 0.91489 \times \exp\left(-2.827785 \cdot \phi\right) + 0.059245 \times \exp\left(-33.5 \cdot \phi\right) + 0.025865 \times \exp\left(-227.672 \cdot \phi\right)$	(4.9)	$\phi = \frac{8 \cdot D \cdot P_l}{3 \cdot U_{hx} \cdot \left(S_{fin} - t'_{fin}\right)^2}$	(4.10)

Turbulence-related mechanisms

(adapted from Siegel and Nazaroff, 2003)

$$D_{ent,i} = \mathrm{P}\left(\frac{\tau_{imp,ent,i}}{\tau_{p,i}} < 1\right)$$

$$D_{tur,i} = \mathrm{P}\left(\frac{\tau_{imp,tur,i}}{\tau_{p,i}} < 1\right)$$

$$D_{turb} = \mathrm{P}\left[\left(D_{ent,x} \cup D_{pho,x}\right) \cup \left(D_{ent,y} \cup D_{pho,y}\right) \cup \left(D_{ent,z} \cup D_{pho,z}\right)\right] \quad (4.11)$$

$$\tau_{p,i} = \frac{\left|u_{p,i} - u_i\right| \cdot m_p}{F_{drag,i}}$$

$$\tau_{imp,ent,i} = \frac{dist_i}{u_{p,i}} = \frac{dist_i}{\bar{u}_i + u'_p} \quad (4.12)$$

$$\tau_{imp,pho,i} = \frac{dist_i}{\bar{u}_i + u_{pho,i}}$$

Thermo- and diffusiophoresis

(Goldsmith and May, 1966, and Talbot, *et al.*, 1980)

$$F_{diff} = -\frac{\sqrt{M_{wv}} \times D_{wv,air}}{x_{wv} \times \sqrt{M_{wv}} + x_{air} \times \sqrt{M_{air}}} \times \frac{1}{p_{p,wv}} \times \nabla p_{wv} \cdot 3\pi \cdot \mu_{air} \cdot d_p \quad \text{for } Kn < 0.6$$

$$F_{diff} = -\frac{D_{wv,air} \times \left(M_{wv} - M_{air}\right)}{\rho_{air} \cdot N_A} \times \nabla n_{wv} \cdot 3\pi \cdot \mu_{air} \cdot d_p \quad \text{for } Kn \geq 0.6$$

$$F_{ther} = -\frac{6\pi \cdot \mu_{air} \cdot \nu_{air} \cdot d_p \cdot C_s \times \left(k_{air} / k_p + C_t \cdot \mathrm{Kn}\right) \nabla T_{air}}{\left(1 + 3 \cdot C_m \cdot \mathrm{Kn}\right) \times \left(1 + 2 \cdot k_{air} / k_p + C_t \cdot \mathrm{Kn}\right) \times T_{air}}$$

$$D_{ther+diff,fin} = \frac{2 \cdot P_l \cdot w_{ther+diff}}{U_{hx} \times \left(S_{fin} - t'_{fin} \cdot corf\right)}$$

$$D_{ther+diff,tube} = \frac{D'_t \cdot \nu_{ther+diff}}{U_{hx} \times \left(P_t - D'_t\right)}$$

$$F_{diff} + F_{ther} = F_{drag} \quad (4.13)$$

$$F_{drag} = \frac{C_D}{C_C} \cdot \frac{\pi}{8} \cdot \rho_{air} \cdot d_p{}^2 \cdot w_{ther+diff}{}^2 \quad (4.14)$$

$$\nu_{ther+diff} = w_{ther+diff}$$

4.2.3.1 Drag Force on a Particle

We use a correlation for the drag force acting on a particle, given by Haider and Levenspiel (1989), which is valid for particle Reynolds numbers up to 2.6×10^5 and also for non-spherical particles. This gives the current model the capability to be expanded to model the deposition of fibers. The SN model used a correlation given by Seinfeld and Pandis (1998).

Drag forces resist against the motion of particles in a fluid medium. The usual formulation to calculate the drag force acting on a spherical particle moving through a medium is used, which depends on C_D, the dimensionless drag coefficient that varies with the Reynolds number of the particle. The correlation presented by Haider and Levenspiel (1989) is used to calculate the drag coefficient. The analysis of flow in the Stokes and Newtonian regimes assumes that the relative velocity of the fluid medium at the surface of the particle is zero, *i.e.*, a no-slip boundary condition. However, for particles whose size approaches the mean free path in the fluid medium, there is slip between the particle and fluid molecules at this surface that reduces the drag force acting on the particle. The Cunningham correction factor is used to account for this slip according to the correlation presented by Jennings (1988). The value of the slip correction factor reduces to 1 as the particle size increases. The mean free path in air has been calculated as given by Jennings (1988). The new correlation used to calculate drag force is reflected in Equation (4.14) in Table 4.1.

4.2.3.2 Zone-based Modeling of Gravitational Settling

Deposition due to gravitational settling is typically accounted for in most prior models, but usually for channels of constant streamwise cross-section. For wavy finned-tube heat exchangers, on the other hand, the air is split into paths that flow either through the fin corrugations or through the open spaces between fins. These regions offer different distances for the particle to travel before settling. The settling surface orientations also differ, and hence the two regions must be analyzed separately, as shown in Figure 4.3.

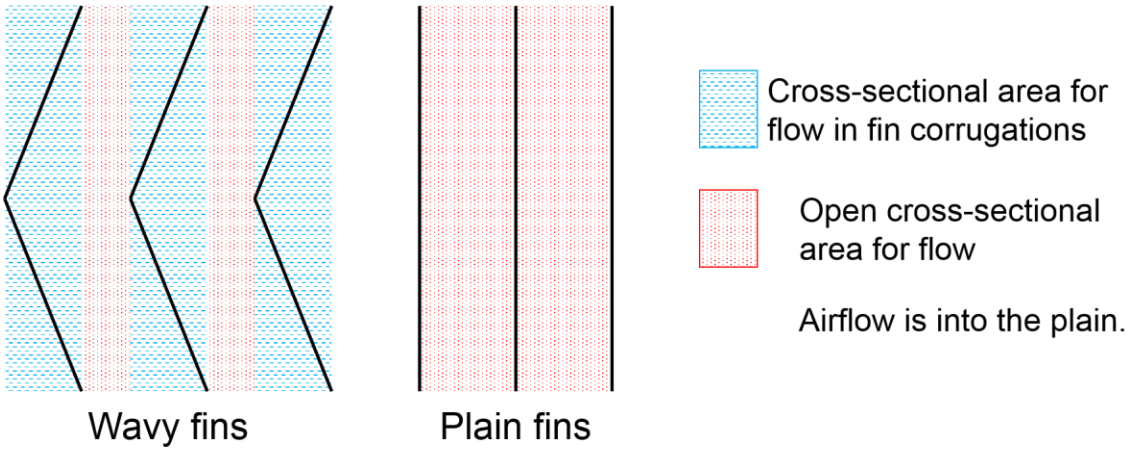

Figure 4.3. Schematic division of airflow passages into distinct gravitational settling zones.

Particulate matter in the open zone (filled in with a red dotted pattern) will deposit on the floor of the heat exchanger by gravitational settling after traveling a distance much greater than the pitch of the wavy fins. On the other hand, particulate matter in the fin corrugation zone (filled in with a blue dashed pattern) will deposit on the wavy fins. The maximum distance a particle would have to settle under gravity before it encounters a deposition surface that is on the order of the pitch of the wavy fins. These zones are modeled separately and the total deposition by gravitational settling is the sum of the deposition in both zones. Equations (4.7) and (4.8) in Table 4.1 describe the procedure followed in the model to analyze deposition by gravitation settling.

4.2.3.3 Deposition due to the Combined Effect of Thermophoresis and Diffusiophoresis

Thermophoresis, the motion of dispersed particles in a fluid medium due to a temperature gradient, occurs in a direction towards regions of lower temperature. Diffusiophoresis, the motion of dispersed particles due to a dissolved component concentration gradient in a fluid medium, occurs in a direction towards a lower concentration region. For a heat exchanger surface that is rejecting heat to the air stream, the temperature gradient established in the air would repel particles away from heat exchanger surface; there would be no appreciable concentration gradient for any water vapor present in the air. Conversely, for a heat exchanger surface that is absorbing heat from the air stream, the temperature gradient would attract particles to the heat exchanger surface. Water vapor present in the air may condense on the surface to establish a concentration gradient that also attracts particles the surface. The thermophoretic and diffusiophoretic forces would act on suspended particulates of a similar size range in the same direction and tend to be on the same

order of magnitude (Pilat and Prem, 1976). Goldsmith and May (1966) performed experiments to test whether thermophoresis and diffusiophoresis could be analyzed independently in this scenario, and reported that the forces acting on particles due to these two effects could be superimposed for aerosol deposition in helium or air. Assuming mutual independence between thermophoresis and diffusiophoresis may lead to an overprediction in the deposition rate because a certain particle could deposit under the combined action of both thermophoresis and diffusiophoresis.

Prediction of deposition due to thermophoresis (according to Talbot *et al.* (1980)) and diffusiophoresis (according to Goldsmith and May (1966)) is combined by superimposing the thermophoretic and diffusiophoretic forces. The net force acting on a particle in the direction of surface is calculated, from which the net deposition velocity towards that surface is obtained. This velocity is used to calculate the deposition fraction of particles due to the net action of these two mechanisms. Equations (4.13) and (4.14) in Table 4.1 describe the calculation procedure employed in the model to find deposition due to net action of thermophoresis and diffusiophoresis.

4.2.3.4 Deposition due to Turbulence

Particle transport due to turbulence is assumed to occur in two distinct ways – first due to entrainment in fluid flows occurring in turbulent flow but not in laminar flow and second due to turbophoresis. In the first sub-mechanism, dust particles are assumed to be entrained in secondary flows (flows in directions other than the streamwise direction of bulk flow) resulting from formation of eddies and also in flows caused by random bursts of turbulent fluctuation velocity. Turbophoresis, the motion of dispersed particles in a fluid medium due to a difference in the local turbulence intensities, transports particles from regions of high turbulence towards regions of low turbulence. The analysis of deposition due to turbulence in the base model used turbulence statistics from a direct numerical simulation of fully developed turbulent flow between parallel plates published by Moser *et al.* (1999). To better match operating conditions of fielded heat exchangers and experiments, data should be extracted from simulation of representative duct geometries. The SN model considered deposition by turbulence as a two-dimensional phenomenon: deposition on fins from random velocity bursts in the horizontal spanwise direction and turbophoretic deposition on tubes in the streamwise direction for a heat exchanger installed in a duct with horizontal airflow. Turbulence in the vertical spanwise direction was assumed to not cause significant deposition. This assumption is logical for plain plate finned tube heat exchangers

on account of the much smaller area available for deposition in the vertical spanwise direction as compared to that available in the horizontal spanwise direction. However, the fin corrugations in wavy finned tube heat exchangers could potentially provide surface area for particles to deposit owing to turbulence in the vertical spanwise direction as well. The SN model assumed that turbulence from bulk flow in the duct does not persist into the airflow in the channels between the fins. Thus, deposition due to turbulence was only due to entrainment in random velocity bursts. For purposes of assessing the effect of the persistence of turbulence, turbulence from the upstream duct was alternatively assumed to persist through the entire depth of the heat exchanger; calculation of deposition with this turbophoresis was reported as an upper limit on deposition from turbulence-related mechanisms. While the narrow airflow channels should lead to some laminarization of the airflow, , an absence of detailed turbulence data for airflow inside heat exchangers prevents the analysis of deposition due to turbulence induced by roughness elements and fin discontinuities within the heat exchanger itself (distinct from duct turbulence persisting inside the heat exchanger).

Figure 4.4 is a flow chart of the subroutine developed to predict particle deposition due to turbulence. Table 4.2 presents key equations used in the subroutine. The general approach for predicting deposition due to turbulence in the current study is similar to that used by Siegel and Nazaroff (2003) and uses a Monte Carlo simulation. However, because turbulence is a three-dimensional phenomenon, the modeling of deposition due to turbulence is extended to three dimensions for both sub-mechanisms, as opposed to the two-dimensional approximation used in the SN model. Turbulence causes large deposition fractions for large particle sizes, and the extension of the analysis of deposition due to turbulence to three dimensions has a measureable influence on the total deposition fraction predicted. Turbulence statistics were reported by Gavrilakis (1992) and Huser and Biringen (1993) in all directions, and provided the numerical data necessary to perform this analysis. Regression curves were fitted to reported turbulence statistics such as primary and secondary velocity profiles, RMS values of turbulent fluctuation velocities in all directions, and Reynolds stress profiles in all directions. Instantaneous turbulent fluctuation velocity was randomly sampled from a normal distribution about a mean of 0 and a standard deviation equal to the rms value of turbulent fluctuation velocity. Deposition due to turbulence in the additional vertical spanwise direction is modeled similarly to that in the horizontal spanwise and streamwise directions. The turbophoretic deposition is not used to define an upper limit on

deposition due to turbulence-related mechanisms as was done in the SN model; instead, its contribution is included in the prediction of actual deposition, instead of as an uncertainty estimate. The model approximates the hydrodynamic entrance length to be the the length over which the duct turbulence persists inside the heat exchanger core. If the entrance length is greater than the depth of the first tube bank in the heat exchanger, then duct turbulence is assumed to persist inside the heat exchanger for the entire depth of the tube bank. The entrance length is approximated by the expression applicable for flow through rectangular ducts from McComas (1967). Equations (4.11) and (4.12) from Table 4.1 and Equations (4.15), (4.16), and (4.17) from Table 4.2 describe the computation procedure used to estimate deposition due to turbulence-related mechanisms.

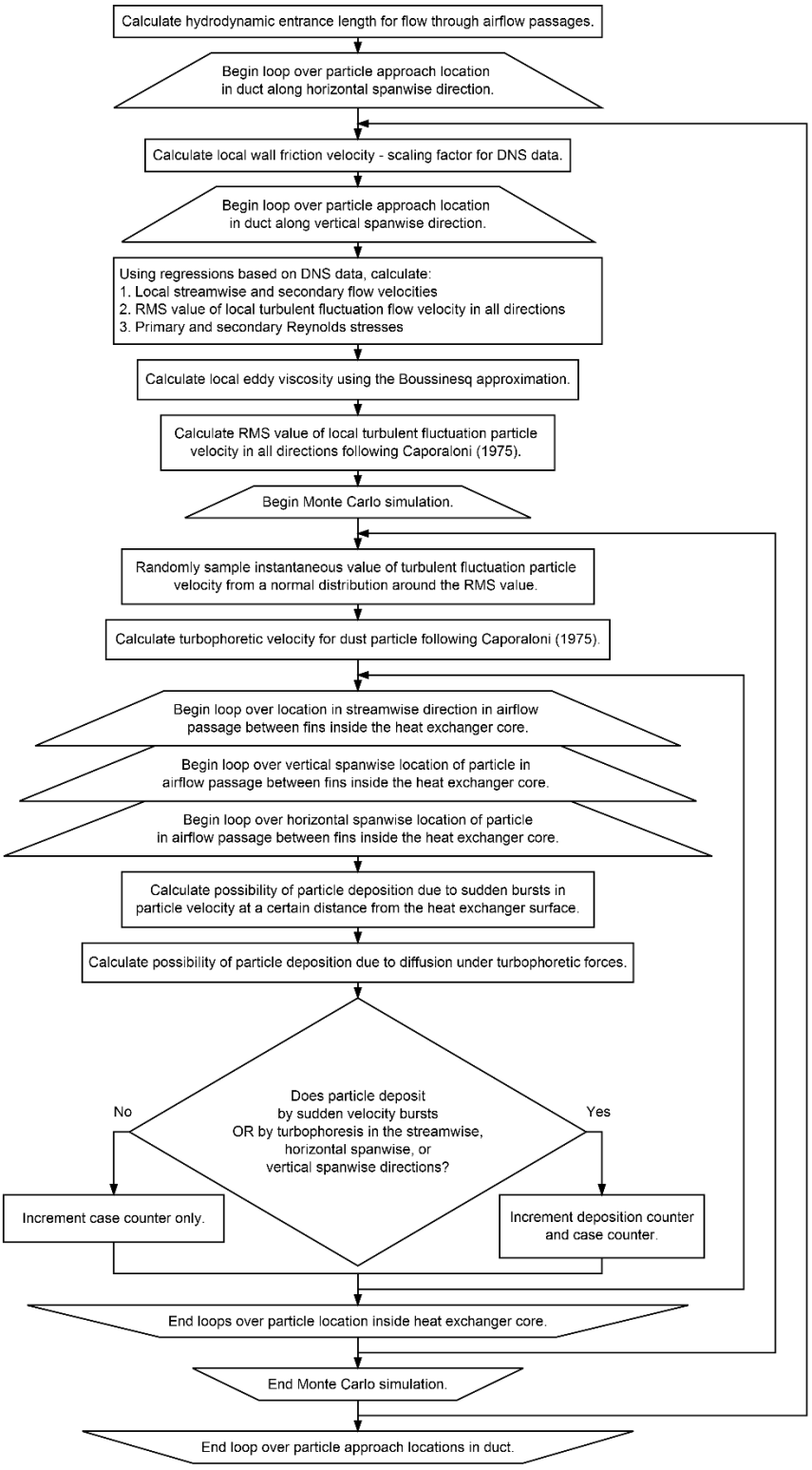

Figure 4.4. Flow chart of stochastic method employed to predict fouling of a heat exchanger due to air-side turbulence.

Table 4.2. Additional equations used in the model to analyze deposition due to turbulence.

Variable Evaluated	Equation	
Turbophoretic velocity (Caporaloni, *et al.*, 1975)	$u_{pho,i} = -\tau_{p,i} \frac{\partial u'^2_{rms,i}}{\partial x}$	(4.15)
Particle turbulent fluctuation velocity (Caporaloni, *et al.*, 1975)	$u'^2_{p,rms,i} = K u'^2_{rms,i}$ where, $K = \frac{aJ_{fl,i} + b^2}{aJ_{fl,i} + 1}$ such that $a = \frac{36\mu_{air}}{\left(2\rho_p + \rho_{air}\right) d_p^2}$ and $b = \frac{3\rho_{air}}{2\rho_p + \rho_{air}}$	(4.16)
Lagrangian (or diffusion) integral scale of times (Caporaloni, *et al.*, 1975); Eddy diffusion coefficient (or eddy viscosity or turbulent viscosity) (Boussinesq approximation)	$J_{fl,i} \approx \frac{\nu_{t,air}}{u'^2_{rms,i}}$ where $-\overline{u'_i u'_j} = \nu_{t,air}\left(\frac{\partial \bar{u}_i}{\partial x_j} + \frac{\partial \bar{u}_j}{\partial x_i}\right)$	(4.17)

4.2.3.5 Time-Stepping to Account for the Effect of Previously Deposited Dust on Subsequent Fouling

Based on fouling experiments performed on a compact heat exchanger using sawdust, Mason *et al.* (2002) proposed distinct temporal regimes in the process of fouling of a heat exchanger. The increase in pressure drop across the heat exchanger as a function of time was divided into three phases. In the first *nucleation fouling* stage, the pressure drop increased gradually, and was followed by a second *transition fouling* stage, and finally with a *bulk fouling* stage during which the pressure drop increased very rapidly. Since saw dust was continuously injected into the air stream passing through the heat exchanger, this dependence on time reflects a dependence of the fouling rate on the extent to which the heat exchanger had been previously fouled. It was proposed that larger particles were deposited preferentially in the nucleation fouling stage. These deposits then acted as nucleation sites to trap smaller particles that would have otherwise passed through a clean heat exchanger.

House dust is a heterogeneous mixture of organic and inorganic particles/fibers of different sizes. Common sources of fibers in the air are paper, glass wool, wood, textiles (Butte and Heinzow, 2002), human hair and animal fur. Moore (2009) studied the accumulation of fibrous dust on high-fin-density heat sinks. Due to the small fin pitches, fibers formed bridges between adjacent fins. The webbed structures formed were able to trap progressively finer particles, thus accelerating the process of fouling. In the case of compact finned heat exchangers, which are becoming increasingly common in HVAC&R applications, a similar phenomenon could lead to increasing rates of fouling as a function of dust already present on the heat exchangers. Ahn and Lee (2005) report similar findings occurring in prefilters; accumulated fibers form dust-cake layers that act as a secondary filtration medium and can collect particles smaller than the filter pore sizes. In the same study, photographs of fouled condenser and evaporator heat exchangers, which had been in service for periods between 3 to 14 years showed a significant presence of fiber and particulate agglomeration between the fins.

There are several other potential particulate-agglomeration-dependent deposition mechanisms. As air passages inside the heat exchanger become blocked by deposited dust, the distance that particles need to travel to impact upon the heat exchanger surface decreases. Surface deposits may also increase the turbulence inside the heat exchanger (Yang *et al.*, 2007). These factors may contribute to progressively faster fouling of the heat exchanger over time. Bott and

Bemrose (1983) also asserted that the rate of deposit buildup is a function of the thickness of the foulant layer, which causes a change in the flow area and pattern through the heat exchanger, thus affecting the individual deposition phenomena. Hence the pressure drop across a fouled spiral wound finned tube heat exchanger increased at different rates depending on the dust concentration in the air stream (which influences the actual thickness of the deposited layer at the same deposition fraction). This deposit buildup mechanism is easily adapted into the deposition model, and done in the present work.

While there is no formal testing standard, experiments typically evaluate the fouling of heat exchangers by injecting dust into an air stream flowing through the heat exchanger at a set rate and duration. The injection of dust is then stopped and steady-state performance is measured in a fouled condition (Bott and Bemrose, 1983, Siegel, 2002, Yang et al., 2007, Bell and Groll, 2011, Haghighi-Khoshkhoo and McCluskey, 2007, Pak *et al.*, 2005, Bell *et al.*, 2011, Lankinen *et al.*, 2003). Bott and Bemrose (1983) claimed that the periodic nature of this testing approach does not affect the phenomenon of fouling. The deposition of dust on the heat exchanger is also evaluated by stopping air flow through the heat exchanger and measuring the mass of dust deposited. Continuous heat exchanger performance may also be measured to obtain transient behavior data as the surfaces are progressively fouled during testing (Bott and Bemrose, 1983 and Sun *et al.*, 2012).

To mimic this experimental procedure for which data is available for comparison, dust deposition is modeled in discrete time periods corresponding to the periods of dust injection in the current approach. The modeling procedure approximates integral accumulation of dust by summing the deposition after each time step. When one time period ends, the total additional mass of dust deposited on the heat exchanger is calculated, and heat exchanger flow path dimensions are modified to reflect the contraction due to fouling. This is achieved by artificially increasing the fin thickness and tube diameter of the heat exchanger per the distribution of dust. The parameters dependent on the dimensions of the heat exchanger for flow past fins and tubes are recalculated based on the new dimensions. The model also checks for total blockage of flow passage due to fouling after a time step and returns a notification if this condition is reached.

4.2.3.6 Streamwise Distribution of Deposited Dust

Large variations in the local streamwise distribution of deposited dust have been observed experimentally in the literature. Yang *et al.* (2007) and Bell and Groll (2011) observed that a majority of the fouled dust gets deposited on the front face of the coil, and photographs showed that rear faces remained clean. Pak *et al.* (2005) reported that dust accumulated more at the leading edges of fins, and that dust particles formed bridged shapes which reduced the front-facing open flow area. Ahn and Lee (2005) reported that the fouling deposits were observed to have been formed within 5 mm of the frontal air inlet to the heat exchanger surface, while the rear faces were fairly clean. Other experimental observations of concentrated fouling at the front face of the heat exchanger have been reported by Sun *et al.* (2012) and Ali and Ismail (2008).

The increase in pressure drop across the heat exchanger due to fouling is likely determined by deposition in this region. Similarly, if the front rows of the heat exchanger are heavily blocked due to dust deposition, the remaining rows of the heat exchanger could potentially remain clean while the heat exchanger would still not function properly. It is evident that modeling the distribution of the dust deposition inside a heat exchanger is important to predict the extent of fouling and the effect that fouling has on performance, and the model results should reflect these experimental observations.

The SN model calculated the overall deposition fraction for the entire heat exchanger without considering its spatial distribution. In the current model, deposition due to each different mechanism is calculated in the streamwise direction in a discretized manner. Thus, the heat exchanger is divided into distinct sections; each section is composed of a tube row and a finned surface whose length is equal to the longitudinal tube pitch and which covers the entire height of the heat exchanger. This allows the mechanisms to naturally determine the distribution of deposition as a function of streamwise location along the heat exchanger. Such discretization of the calculation of deposition fraction due to each fouling mechanism in the streamwise length of air flow may possibly lead to a more accurate model for the distribution of deposited particulate matter.

To implement this streamwise distribution calculation in the model, once particulate matter is predicted to deposit in a particular section of the heat exchanger, the dust composition (both particle size and number of particles) in the air incident on the downstream section of the heat exchanger is updated. Thus, this discretization scheme not only yields information about the

location of the deposition, but also affects the calculation of deposition fraction. Some mechanisms are governed by phenomena that behave nonuniformly over the cross section of the heat exchanger (e.g., deposition due to turbulence is determined by local turbulence parameters). While these local phenomena are considered in calculating the total deposition fraction, the non-uniformity of the deposited layer is neither tracked nor considered in subsequent calculations. Assessment of the bulk density of the deposited dust layer (compared to the particle material density) is critical for accurate alteration of the heat exchanger dimensions as a result of its fouling in the time-stepping model. The particle density of the dust is obtained from the manufacturer data (Powder Technology Inc., 2012). The bulk density of the deposited dust could, however, vary from the particle material density. The value currently used in the model is the bulk density of the test dust measured in the packaging as received from the manufacturer (550 kg/m^3).

4.2.3.7 Effect of Surface Orientation on Deposition Mechanisms

The orientations of the heat exchanger surface geometries (with respect to gravity and the flow direction) uniquely influence each of the deposition mechanisms, and are also accounted for in the current model. Calculation of the inertial impaction on tubes and fins only considers the front halves of the tubes, whereas gravitational deposition only considers the top halves of tubes. It can be safely assumed that the lower halves of tubes need not be considered for the remaining mechanisms as a consequence of universal assumption 7 (see Section 4.2.1). Thus, the region between the lowermost point of the tube and the trailing edge does not influence the calculation of any deposition mechanisms.

This approach is supported by prior experimental investigations. Abd-Elhady *et al.* (2009) observed the build-up of fouling layers on heat exchanger tubes as a function of the direction of airflow with respect to gravity. They observed that fouling layers were thicker at the bottom rows of heat exchangers than at the top rows for all cases (suggesting there is influence of gravity). Fouling layers began at different locations on the tubes of heat exchangers and grew in different directions along the tubes depending on the direction of air flow and gravity. For all cases, fouling deposits were most likely to begin to grow at the stagnation point of airflow and the point on the top of the tube exactly in line with gravity. These layers then grew towards each other and merged.

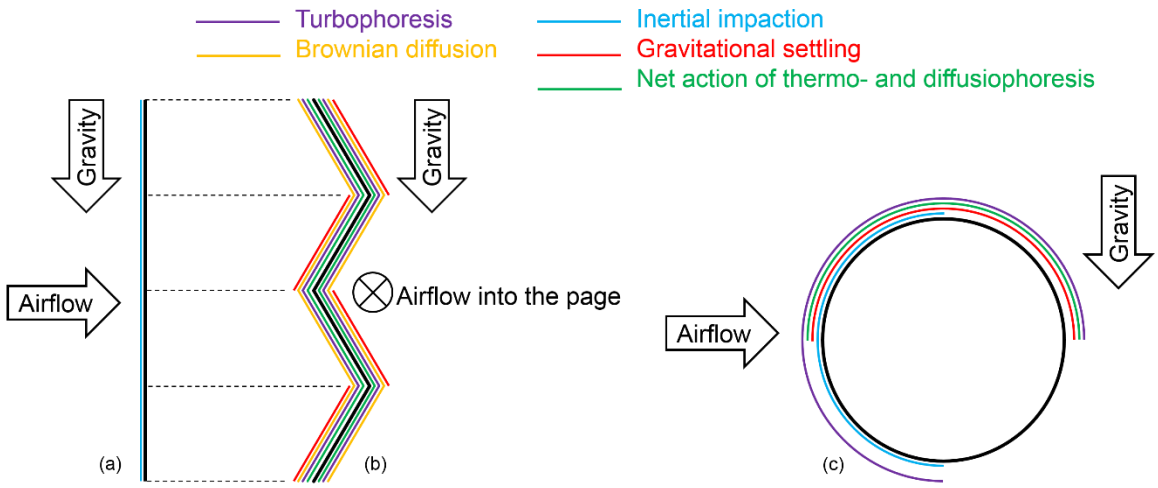

Figure 4.5. Assumed distribution of deposited dust, based on each deposition mechanism, on a wavy fin (as seen from its side (a) and from the front (b)) and on (c) a heat exchanger a tube as seen from the side.

Based on these experimental observations, the calculations of the deposition fractions on the other radial locations were subject to each different mechanism, taking into consideration the surface area on which fouling depositions were possible. Figure 4.5 shows the region of each fin and tube that was assumed to affect fouling by each individual deposition mechanism. The entire transverse surface areas of fins were assumed to be susceptible to fouling by all possible mechanisms. The front edges of fins were also assumed to be fouled as a result of inertial impaction of particles. While these surface-orientation-dependent regions of fouling are considered in calculation of the deposition fraction by each mechanism, the deposited dust is assumed to be uniform over the surface cross section for purposes of calculating the deposition layer thickness.

4.2.3.8 Streamwise Changes in Airflow Dust Composition

As a heat exchanger is fouled, the characteristics of suspended particulates in the airflow changes due to deposition. Not only does the total particulate concentration decrease due to fouling, but the particle sizes redistribute based on the size-dependent deposition mechanisms. This change would affect the local deposition fraction at each individual tube row, and thereby alter the total overall deposition fraction for the heat exchanger. Consideration of the spatial variation of suspended particulate composition in the air stream is a logical extension of modeling the streamwise distribution of deposited dust, which also requires modeling the deposition in a discretized manner. The current model removes particulate matter from the air stream that is

deposited on upstream heat exchanger sections and updates incident particulate dust composition for each discretized heat exchanger section.

4.3 Results and Discussion

4.3.1 Experimental Results Used for Model Comparison

The experimental results of Pak *et al.* (2005) and Yang *et al.* (2007) are used for validating the model predictions; inputs required for the model regarding the heat exchanger geometry, such as the tube pitches in transverse and streamwise directions of airflow, fin pitches, and fin thickness, are available from these studies. In both sets of experiments, the heat exchangers to be tested were installed inside a wind tunnel and connected to hot water loops for measuring the heat transfer performance. The inlet air temperature and inlet water temperature to the coils were fixed and maintained constant for all tests. A commercially available dust injector (LMS Technologies, Inc.) was used to introduce dust into the wind tunnel at a constant rate. The injector aspirated the dust into a nozzle and sprayed it into the air stream by passing it through a perforated disc. The disk ensured that the dust was well mixed and sprayed uniformly over the entire cross-section of the duct. The dust used for was ASHRAE Standard Test Dust (ASHRAE, 2012). Each coil was loaded with dust for a pre-determined number of hours at 100 grams per hour. Additional details about each test are provided in Table 4.3. All heat exchangers with more than one tube row had a staggered arrangement of tubes.

In the experiments, filters placed downstream of the heat exchangers were used to catch dust particles that passed through the heat exchanger. The filter was weighed before and after each test to determine the amount of dust caught trapped. The mass of dust injected into the air stream is known. Thus, the deposition fraction on the heat exchanger for the test can be experimentally determined as follows:

$$deposition\ fraction = \frac{mass\ of\ dust\ injected\ into\ the\ airstream - mass\ of\ dust\ caught\ in\ the\ downstream\ filter}{mass\ of\ dust\ injected\ into\ the\ airstream} \tag{4.18}$$

The experiments reported overall deposition fractions calculated over the entire duration of each test; the model updates the heat exchanger geometry on an hourly basis using on an hourly basis and then calculates a cumulative deposition fraction for the entire test period for comparison.

Table 4.3. Summary of operating parameters of experiments used for comparison against model predictions.

Study	Test Identifier	Tube Parameters [mm]	Number of Rows	Fin Type	Fin Density [fins per inch, FPI]	Dust Type	Duration of Test [hr]
Pak *et al.* (2005)	1A	D = 9.52 P_t = 30.5 P_l = 30.5	1	Plain plate	22	ASHRAE Standard Test Dust	3
	1B	D = 9.52 P_t = 30.5 P_l = 30.5	1	Louvered wavy plate	22		3
	1C	D = 9.52 P_t = 30.5 P_l = 30.5	2	Louvered wavy plate	22		3
	1D	D = 9.52 P_t = 30.5 P_l = 30.5	2	Louvered wavy plate	22		3
Yang *et al.* (2007)	2A	D = 9.52 P_t = 30.5 P_l = 30.5	2	Lanced plate	14		6
	2B	D = 9.52 P_t = 30.5 P_l = 30.5	4	Lanced plate	12		6
	2C	D = 9.52 P_t = 30.5 P_l = 30.5	8	Wavy plate	8		6
	2D	D = 9.52 P_t = 30.5 P_l = 30.5	8	Lanced plate	8		6

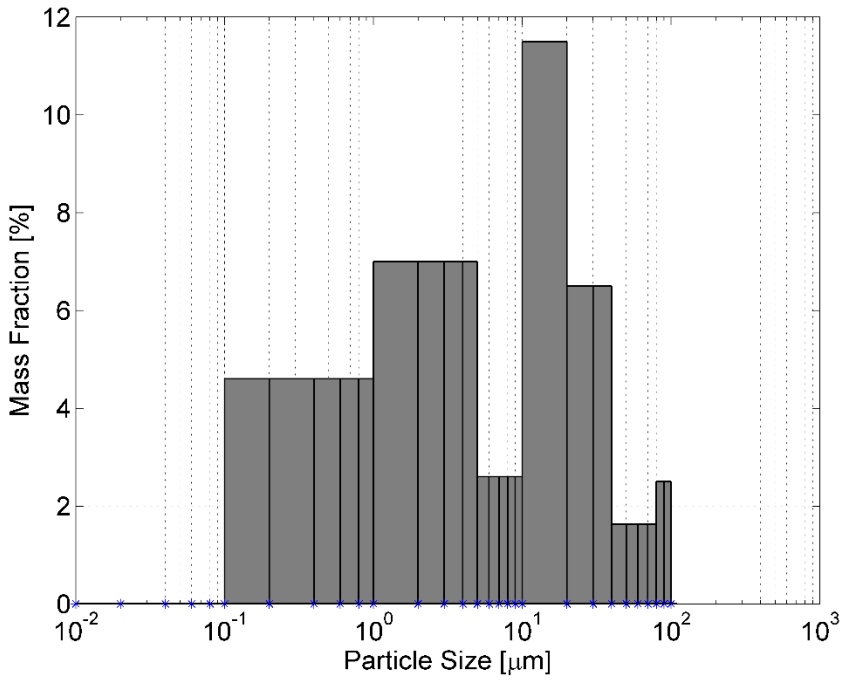

Figure 4.6. Mass-based particle size distribution of ASHRAE Standard Test Dust used in the fouling model.

Figure 4.6 is adapted from data published by Flanders Corporation (2003). It shows the mass-based particle size distribution of ASHRAE Standard Test Dust. The particle size distribution that was originally published used broader particle diameter bins; for the current model input, these bins were uniformly subdivided to increase the resolution of particle sizes on the deposition. These more finely resolved particle size bins are indicated by the vertical lines subdividng the bars in Figure 4.6. The particle size bins with finer resolution are used because the deposition fraction is a strong function of particle size; this approach yields a refined (and potentially more accurate) description of the particle sizes in the foulant buildup on the heat exchanger. ASHRAE test dust is a mixture of 72% by mass of ISO12103-1 A2 fine test dust, 23% powdered carbon, and 5% by mass of milled cotton linters. The particle density of the dust mixture was assumed to be a mass-fraction-weighted mean of the component particles. The calculated value of 550 kg/m^3 is given here for reference and was used to perform the analysis reported in this work.

4.3.2 Model Predictions

To evaluate the contribution of each individual change in the model structure to a change in the predicted overall deposition fraction, a test case (2C, Table 4.3) was evaluated using the model at different intermediate stages of model development. The changes made were not reverted between different stages; therefore, each predicted deposition fraction reflects the cumulative impact of all prior changes. Figure 4.7 presents the deposition fraction predicted by different versions of the model; Table 4.4 lists short descriptions of the model stages referred to in Figure 4.7. The SN model described in Siegel (2002) is considered as the baseline. The changes listed in Table 4.4 are described in greater detail in Section 4.2.3.

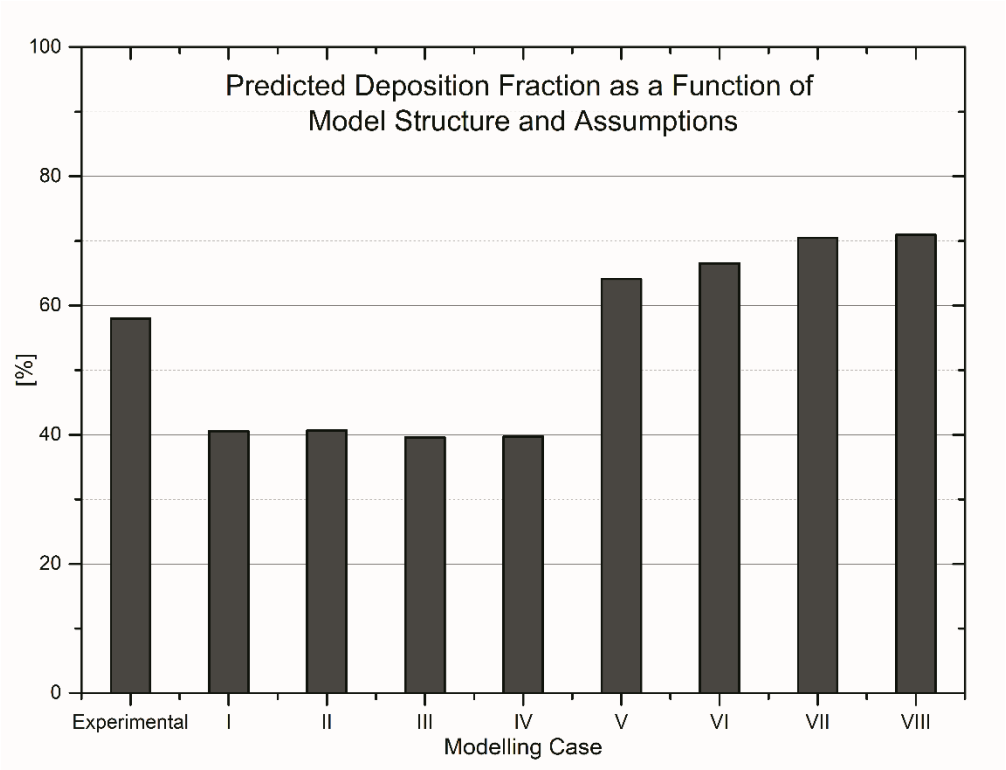

Figure 4.7. Change in predicted deposition fraction due to changes made in the model structure and assumptions as listed in Table 4.4.

Table 4.4 Description of modeling cases considered to evaluate impact of changes made from the baseline model.

Modeling Case	Description
I	Baseline: original model replicated
II	Thermophoretic and diffusiophoretic forces superimposed
III	Zone-based analysis of gravitational settling implemented
IV	Correlation used to calculate drag coefficient changed
V	Source for DNS data of turbulent flow through ducts changed
VI	Deposition due to turbulence calculated along all directions
VII	Heat exchanger discretized spatially
VIII	Process of fouling discretized temporally

The experimentally measured overall deposition fraction was about 58%. The baseline model (40.6%) underpredicted the experimental measurement. A superimposition of thermophoresis and diffusiophoresis resulted in no significant change in the model prediction. A zone-based modeling of gravitational settling resulted in a minor decrease in the predicted overall deposition fraction (39.6%). A change in the correlation used to calculate drag force acting on a dust particle resulted in no significant change in the model prediction. It should be noted that this change could potentially affect analysis of inertial impaction, gravitational settling, combined thermo- and diffusiophoresis, and deposition due to turbulence. However, the correlation is applicable only in the Newtonian regime and not in the Stokes regime. Thus, if particle motion did not fall within the Newtonian regime, a change in the correlation used to calculate drag force had no impact on the model prediction. For the current conditions investigated, the new drag force correlation was not anticipated to have a large impact; the new correlation was implemented because it includes the effects of particle shape and therefore can help in predicting the deposition of non-spherical particulates.

The largest change in the predicted deposition fraction occurred when the source of DNS data for turbulent flow through a duct was changed. The increase in predicted overall deposition fraction to 64.1% can be explained by one important factor. The DNS data used to assess deposition due to turbulence included information about secondary flows that exist in the duct.

These secondary flows, when added to the random velocity bursts, resulted in much higher calculated values for particle velocity towards the heat exchanger surface compared to the time required for a particle to pass through the heat exchanger core without collision. The extension of turbulent deposition to all directions resulted in a small increase in the predicted overall deposition fraction to 66.5%. The relatively small change from the previous case is expected can be explained by the fact that the calculation method accounted for scenarios that would erroneous double-counting depositioned of particles. Namely, if a particle was predicted to deposit on fins due to a random velocity burst in the horizontal spanwise direction, deposition on a tube by turbophoresis in the streamwise direction was not recounted as an additional deposition scenario in the Monte Carlo simulation. The sample size for the simulation was maintained at 10^7 cases to match the sample size of the simulation conducted by Siegel and Nazaroff (2003).

Spatial discretization of the fouling model increased the predicted deposition fraction to 70.5%, again an increase from the previous case. This could be attributed to some additional deposition calculated on downstream tube banks, which are not explicitly accounted for in the SN model. Temporal discretization of the fouling model resulted in a predicted overall deposition fraction of 71%, a small increase. This lower-than-expected contribution of accumulated deposition on fouling can be attributed to the fact that while the fouling agent used contained 5% by mass of cotton fibers, the propensity of dust particles to be caught in these fibers was not accounted for in the model. In addition, the distribution of deposition was assumed to be completely uniform over the entire discretized section of the heat exchanger. However, this assumption is difficult to verify experimentally, and may not be true. It is possible that some regions in the heat exchanger were fouled to a greater degree than other regions in the experiment. Thus, a severely blocked airflow passage might aggressively agglomerate dust particles, which the model is not capable to predict.

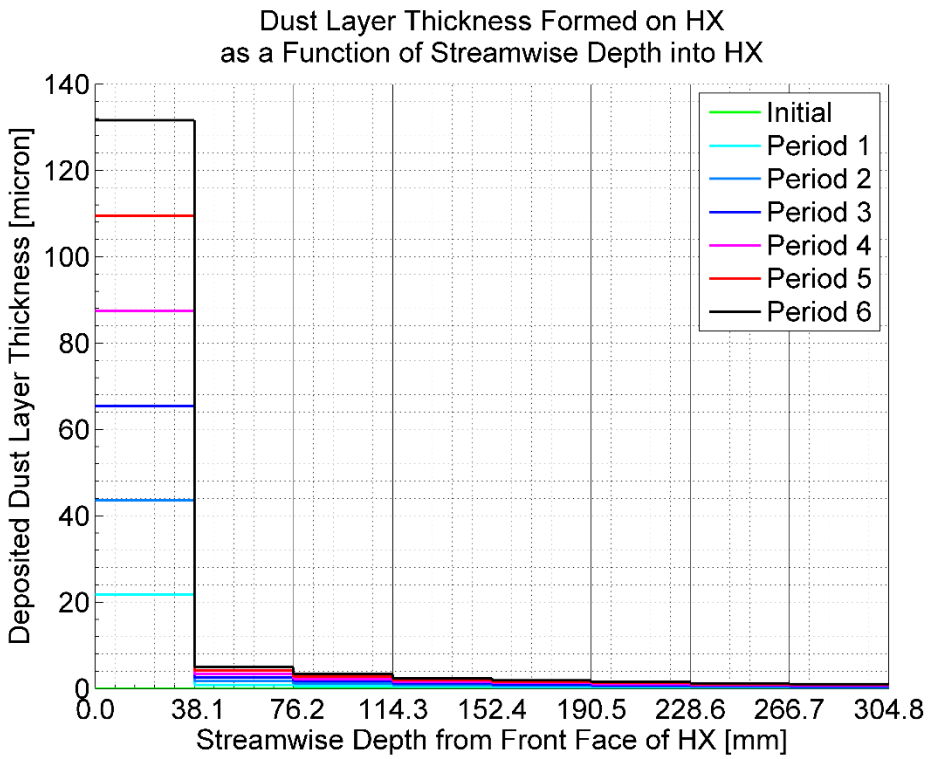

Figure 4.8. Thickness of deposition layer formed on the heat exchanger surface as a function of the streamwise depoth from front face and time (Test 2C).

The progressive growth of deposition layers on the heat exchanger surface is shown in Figure 4.8 for a selected test case (2C, Table 4.3). The deposition layer for a tube row accounts for the deposition on the section of the heat exchanger corresponding to that row of tubes, *i.e.*, the surface area of the tube row and the finned area corresponding to the tube row. The model predicts that the front section of the heat exchanger will see the majority of the deposition, while the heat exchanger surface further downstream will remain relatively clean. This agrees with experimental observations reported in literature (Pak *et al.*, 2005, Yang *et al.*, 2007, Bell and Groll, 2011, Ahn and Lee, 2005).

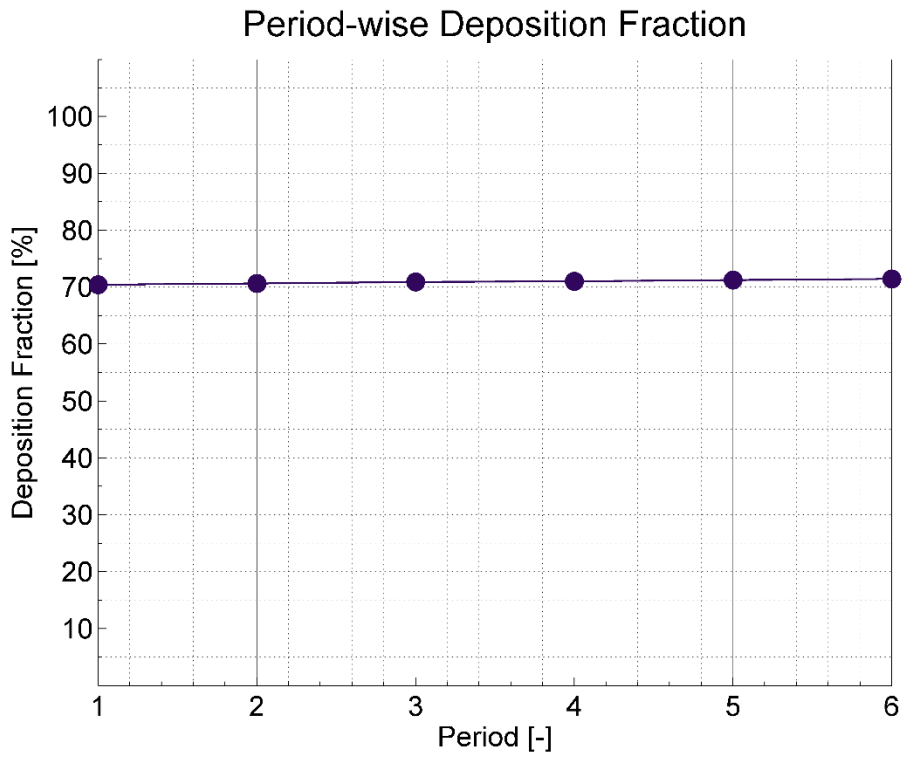

Figure 4.9. Total hourly deposition fraction for the entire heat exchanger (Test 2C).

The predicted temporally discretized deposition fraction is shown in Figure 4.9 as a function of time. There is a small increase in the deposition fraction each hour as the heat exchanger is progressively fouled, from 70.4% during the first fouling period to 71.4% for the last period. This also qualitatively agrees with experimentally observations, although the absolute increase in the deposition fraction with each hour is smaller than typically observed.

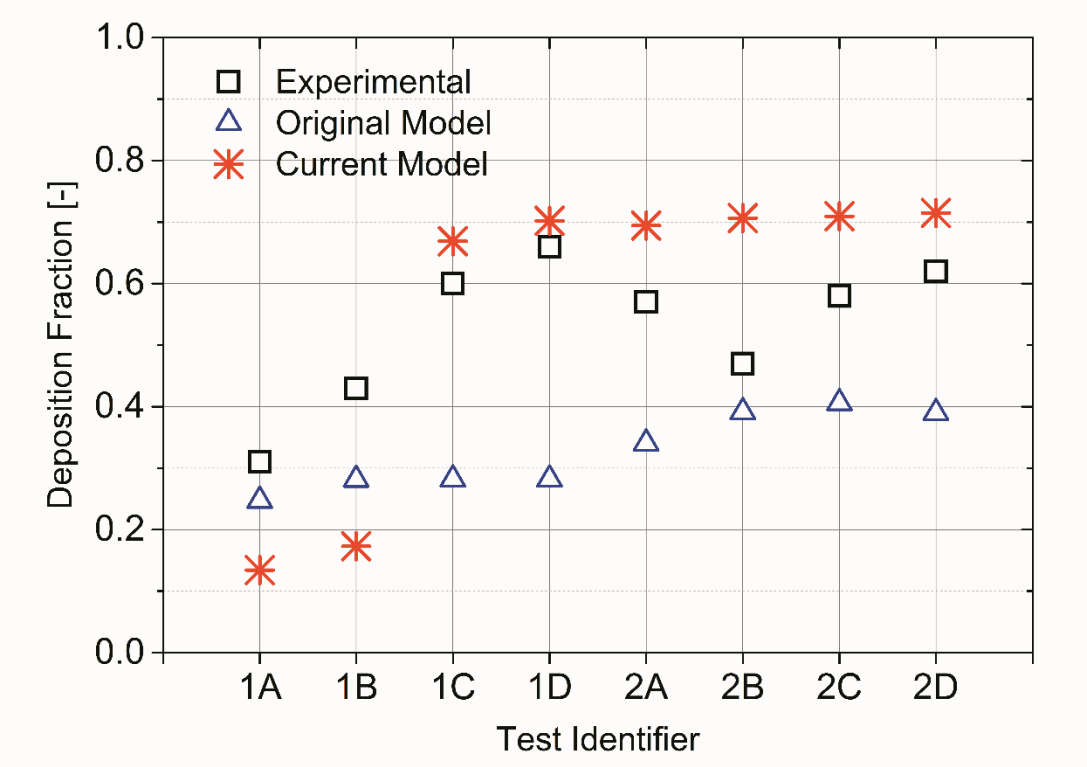

Figure 4.10. Comparison of experimental and calculated deposition fractions from both models.

A comparison between experimental and calculated deposition fractions for the different cases considered in Table 4.3 is presented in Figure 4.10. The calculated deposition fractions include predictions using the SN model and the model in its current form. The mean absolute error in the predicted deposition fraction decreases from 36.1% to 30.7% when prediction accuracy of the current model is compared to that of the SN model. In the first two cases, deposition due to turbulence was ignored by the model because the hydrodynamic entrance length for airflow between the fins was an order of magnitude smaller than the heat exchanger depth. Therefore, deposition due to turbulence was not calculated (in contrast to the SN model where turbulence was assumed to be independent of entrance length). Enhancements to the analysis of deposition from turbulence could improve prediction accuracy.

With inclusion of time-stepping in the calculated deposition fraction, in addition to other improvements made to the methods that estimate deposition due to each individual mechanism and their interactions, the overall deposition fraction predictions from the current model are closer (MAE of 29.9% compared to 36.4% for the SN model) to the experimental observations than the predictions from the SN model.

4.3.3 Possible Source of Error in the Model

4.3.3.1 Uncertainty in Estimating Experimental Parameters

A primary potential source of error in the results is that some geometric parameters of the modeled heat exchangers have not been specified in the literature (Pak *et al.*, 2005, Yang *et al.*, 2007). Critical parameters including the fin thickness and dimensions of the louvers, lances, and wavy structures of the fins were estimated from published photographs or practical experience. The fin thickness for all cases was assumed to be 130 microns using measurements made on an outdoor unit for a commercial air conditioning system available in the laboratory of the author of this work. To account for the louvers, the flow area blocked by the front edges of the louvers was added to the fin thickness; however, this addition does not accurately account for the increased deposition fraction observed experimentally on such surface enhancements. The effect of louvers is apparent in experimental results but accounting for the flows developed due to such surface enhancements is beyond the scope of this model.

4.3.3.2 Complicated Geometries of Heat Exchangers

The various nonuniformly shaped structures that are used to increase turbulence inside the heat exchanger, such as louvers, are complicated to account for in the current model. For example, some of the louvers are cut out of the fin surface leaving open slits in the fin surface transverse to the airflow. These slits provide edges for deposition of dust, however, this deposition is not captured by the mechanisms included in the current model; there exists no experimental data which has independently investigated the fouling of such slits. This is further complicated for experimental cases had fins which had both wavy structures as well as louvers, such as experimental cases 2B and 2D, or for case 1C that had a fin structure that was not continuous through the entire depth of the heat exchanger.

4.3.3.3 Particulate Collisions and Re-entrainment

The assumption that every collision of a dust particle with the surface results in deposition, as well as absence of re-entrainment of dust particles into the air stream, , would induce some error in the model. To theoretically model these phenomena requires information about the intermolecular and electrostatic forces of attraction between dust particles and the metallic surfaces for all of the different constituents of the dust. Quantification of these forces would require

extensive single-phenomenon data collection/validation for a variety of materials, and is outside the scope of the current work.

4.3.3.4 Bulk Density of Dust

The dust is a heterogeneous mixture of different components, and its bulk density will be a function of the densities of its components weighted by their concentration, in addition to the porosity of the layer, which can easily change due to the deposition mixing process or moisture content. Thus, while the bulk density can be measured experimentally under controlled conditions, it cannot be deterministically calculated when modeling heat exchangers operated in the field, and serves as a potential source of uncertainty in modeling efforts. The bulk density of dust used to calculate the thickness of dust layers on the heat exchangers attempts to account for the agglomeration of dust particles that may occur due to humidity in the air and the actual physical process of impaction on the heat exchanger surface.

4.3.3.5 Distribution of Prior Fouling on Surfaces

While the orientation of the surfaces is considered when calculating deposition by each mechanism, the distribution pattern of deposited particles is not tracked and its effects on subsequent fouling is not considered. Little experimental data exists which gives quantitative information about the distribution patterns, which prevents validation of any modeling exercise. Such data could be obtained by collecting and weighing fouling on adjacent rows separately.

4.3.3.6 Turbulence Inside the Heat Exchanger

Geometric enhancements on heat exchanger surfaces are meant to induce turbulence in the airflow. The internal geometry of heat exchangers where airflow patterns are repeatedly broken by tubes would also cause turbulence inside the heat exchanger. This turbulence could then cause deposition inside the heat exchanger. However, this information is not easily available in published literature. It is difficult to predict particle deposition due to complex turbulence patterns in a fouling model written in MATLAB that primarily uses deterministic, physics-based calculation. A numerical-simulation-based model would be more suited for that purpose. In this model, it is assumed that turbulence from flow inside a duct persists only a certain streamwise length into the heat exchanger. Thus, the contribution of this internally induced turbulence to deposition is neglected.

4.4 Conclusions

The model developed in this work is able to predict experimentally measured deposition fractions with improved accuracy relative to existing models, and could be used to evaluate fouling of HVAC&R heat exchangers having similar geometries to the test cases considered. The modified functionality of the model also enables approximation of the streamwise distribution of the deposited dust within the heat exchanger, and the effect that prior particle deposits have on later fouling (*i.e.*, temporal deposition characteristics). Due to the cumulative and combinatory nature of the approximations and assumptions made by the model, and on account of limited experimental data that only provides quantitative bulk deposition and qualitative descriptions of the dust distribution, more precise validation is difficult. Greater agreement with experimental data is difficult to obtain. Moreover, the nature of inherently uncertain nature of fouling means that a model tuned to a particular set of experimental data may not reliably predict other sets of measured data. In its current form, this model can be used to obtain reliable trends for the effects of different geometric and operating parameters on the fouling of heat exchangers. Rough estimates of the deposition fractions as a function of the heat exchanger geometry, thermophysical properties of air, and characteristics of the suspended particulate matter could then be used to avoid excessive fouling of fielded heat exchangers.

CHAPTER 5. PREDICTIVE MODEL FOR FINNED MICROCHANNEL HEAT EXCHANGERS

5.1 Literature Review

Tube-side fouling of heat exchangers has historically received more attention than air-side fouling. Studies that considered air-side fouling were summarized in a review by Marner (1990); while early research was focused on fouling of heat exchangers in energy recovery applications from combustion exhaust, heat exchanger fouling in heating, ventilation, and air-conditioning (HVAC) applications was investigated by Siegel and Carey (2001).

Fouling has been studied both through experiments and with modeling efforts. Ahn *et al.* (2003) measured the variation in pressure drop and cooling capacity of fin and tube heat exchangers due to fouling. The concentration and size of indoor pollutants, the characteristics of the fin surfaces, and the geometry of the heat exchangers were inferred to influence the fouling process. Fouling of finned microchannel heat exchangers was experimentally investigated by Bell and Groll (2011). They were observed to be more prone to fouling, and their performance was more sensitive to fouling as compared to finned tube heat exchangers. Haghighi-Khoshkhoo and McCluskey (2007) studied fouling of a finned microchannel heat exchanger with particulates in discrete particle size ranges, and observed the existence of a critical size range for which deposition of particles onto the surface in the heat exchanger core was a maximum.

A brief review of analytical models of heat exchanger fouling was given by Epstein (1977). These models were developed to predict tube-side fouling of heat exchangers. Epstein (1988) later deterministically calculated deposition velocities for particulate fouling of heat transfer surfaces via mechanisms including diffusion, inertia, gravitational settling, and thermophoresis. An analysis of adhesion to the deposition surfaces and models for particle re-entrainment due to turbulence were also presented.

A similar methodology was implemented by Bott (1988) to analyze gas-side particulate fouling of heat exchangers. The phenomenon of fouling was broken down into three regimes: transport of particulates to the deposition surface, adhesion to the surface, and removal from the surface. The transport of particles towards the deposition surface was further subdivided into two regimes: transport from the bulk flow to the boundary layer, and then across the boundary layer to the surface. Individual mechanisms such as Brownian motion, eddy diffusion, and thermal

diffusion were analyzed for transport across the bulk flow; mass diffusion, inertia, and thermal diffusion were analyzed for transport within the boundary layer. Deposition was then analyzed by comparing the time needed for the particle to travel from the free stream to the deposition surface against the relaxation time of the particle. This method of analyzing the complex phenomenon of fouling as a combination of multiple simpler mechanisms is retained in many later modeling efforts.

Siegel (2002) developed a detailed model to analyze the air-side particulate fouling of plain and wavy plate-finned tube heat exchangers as a function of their geometry, characteristics of the suspended particulate matter in the air stream, airflow conditions, and thermophysical properties of air. Previous researchers had focused on fewer deposition mechanisms. The model presented by Siegel (2002) appears to be the most comprehensive to date.

To the knowledge of the author of this work, models that predict particulate fouling of a finned microchannel heat exchanger have not been published to date. Also, while it is generally known and has been experimentally observed (for instance, by Moore, 2009) that the airflow passages become constricted as a heat exchanger is fouled, thus affecting the subsequent deposition (Bott and Bemrose, 1983, Ahn and Lee, 2005), existing models do not account for this phenomenon. The present work develops a model for the fouling of finned microchannel heat exchangers that relates the predicted accumulation of deposited dust to its effect on subsequent fouling.

5.2 Model Description

The model developed in the current work includes all of the conventional deposition mechanisms considered by Siegel (2002), but adapted for finned microchannel heat exchangers. Figure 5.1 presents a flow chart of the modeling procedure. Unlike previous modeling approaches, the analysis of fouling is discretized spatially and in time. Discretization in time allows assessment of the impact of prior fouling deposits on subsequent fouling. The analysis of deposition by each individual mechanism is performed as a function of particle size. The deposition of particulate matter in one discrete period is the aggregate of depositions in all streamwise sections for all particle sizes. The total deposition is the aggregate over all periods. In the following discussion, the terms suspended dust particulates and aerosol particles are used interchangeably.

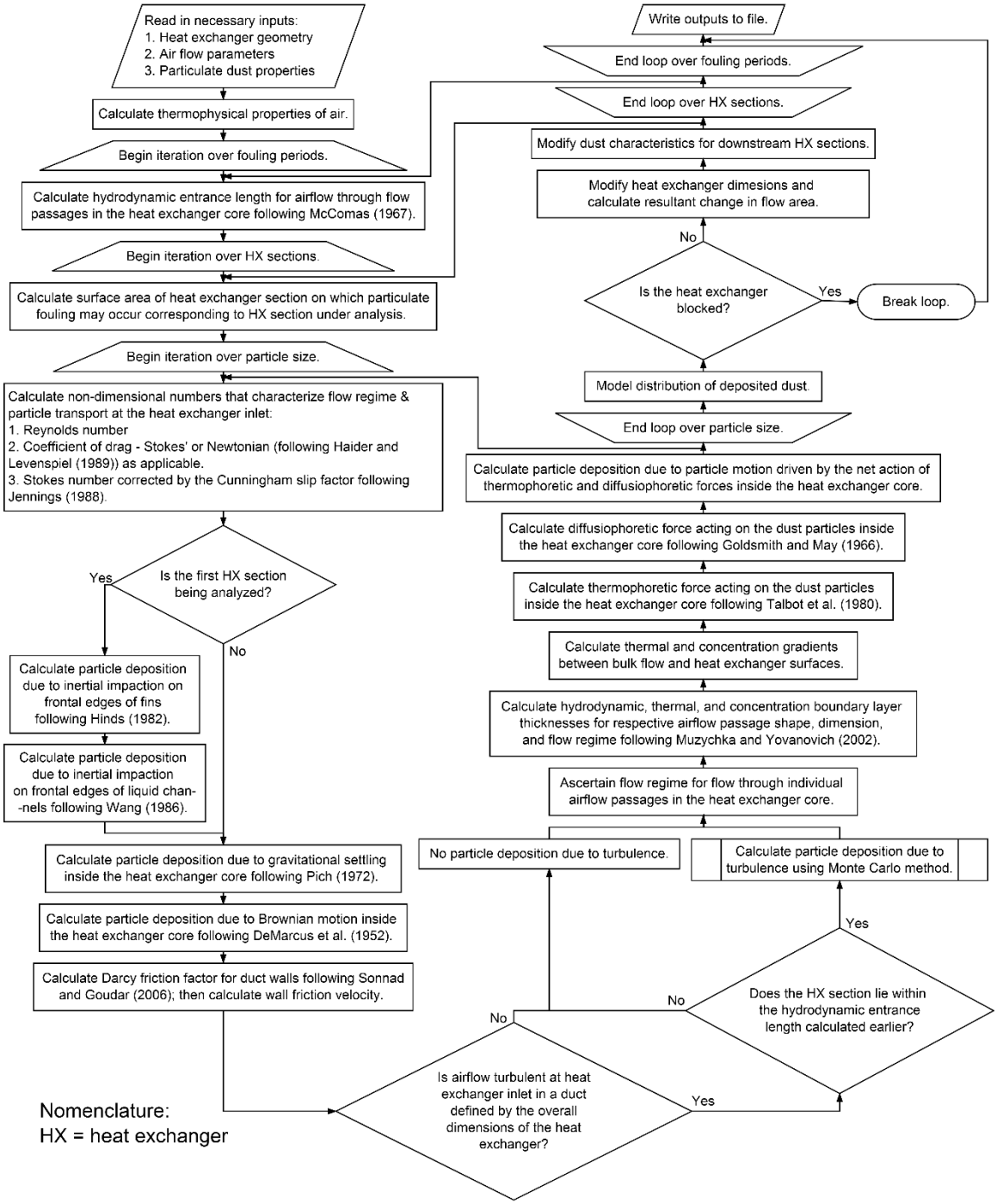

Figure 5.1. Flow chart of analytical model developed to predict fouling of finned microchannel heat exchangers.

5.3 Modeling Assumptions

Several assumptions were made in the development of the model which are applicable to all deposition mechanisms:

1. Suspended particulates in air are approximated as perfectly spherical particles of dust.
2. Suspended particulates in air are characterized by a known, mass-based distribution of the constituents.
3. The bulk density of the deposited dust aggregate is uniform over the entire surface of the heat exchanger.
4. The effective particle density of the suspended particulate matter in air is a weighted mean of the component densities.
5. All particles that collide with the heat exchanger surface deposit on the surface, i.e., there is no model for adhesion of particles.
6. Re-entrainment of particles after deposition is neglected.
7. Deposition occurs on front edges of fins, the lateral surface of liquid channels, all lateral fin surfaces, and on top of the liquid flow channels inside the heat exchanger core along the streamwise length.
8. The suspended particulates in air are always well-mixed, and are distribu3ed uniformly across the airflow cross-section.

5.4 Deposition Fraction

A non-dimensional physical quantity termed the deposition fraction is defined to quantify the extent of heat exchanger fouling:

$$D = \frac{m_{dep}}{m_{inc}} \tag{5.1}$$

where m_{dep} is the mass of dust deposited on the heat exchanger and m_{inc} is the total mass of dust that enters the front face of the heat exchanger. The complement of the deposition fraction is the penetration fraction. It quantifies the fractional mass of dust that passes through the heat exchanger without getting deposited, and is calculated as

$$P = 1 - D \tag{5.2}$$

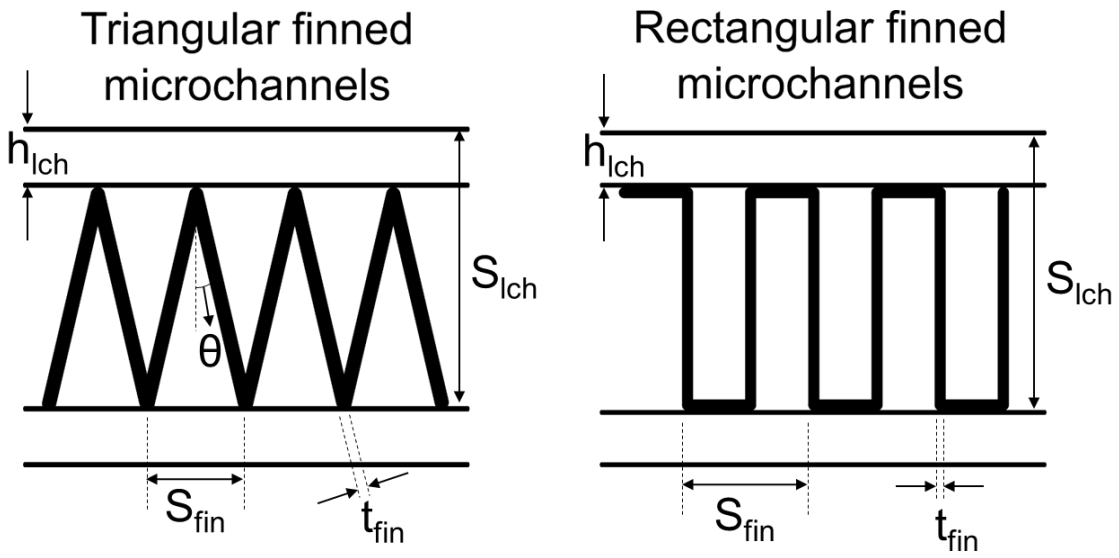

Figure 5.2. Finned microchannel geometries.

Existing fouling models that were developed for finned tube heat exchangers cannot be directly used to model the fouling of finned microchannel heat exchangers. The significant geometric differences between the two affect the airflow pattern, surfaces on which deposition is possible, and consequently the manner in which deposition due to each individual mechanism is calculated. Therefore, a revised implementation of the deposition modeling framework is necessary. Figure 5.2 presents schematic illustrations of the considered geometries of the finned microchannel heat exchange surfaces.

5.4.1 Inertial Impaction

Suspended particulate matter impacts the front edges of the microchannel fins and liquid channels. In addition, the air may flow around obstacles such as louvers, with multiple changes in direction once inside the heat exchanger. Suspended particles may not always perfectly track fluid flow. The inertia of individual particles dictates the degree of deviation of particle trajectories from fluid pathlines. Hinds (1982) defined a Stokes number as the ratio of a particle's 'persistence' to the size of the obstacle.

$$\mathrm{Stk} = \frac{\tau_p U_p}{l_c} \tag{5.3}$$

The particle relaxation time characterizes the time taken for a particle to adjust or relax its velocity to a new condition of external forces (Hinds, 1982). Here, the dominant external force field is gravity, and therefore the relaxation time is calculated as:

$$\tau_p = \sqrt{\frac{4C_C\left(\rho_p - \rho_a\right)d_p}{3C_D\rho_a g}} \tag{5.4}$$

The Cunningham slip correction factor, C_C, is calculated according to Jennings (1988), while the coefficient of drag, C_D, is calculated from the correlation developed by Haider and Levenspiel (1989). The particle Reynolds number for the drag coefficient is defined as:

$$\mathrm{Re}_p = \frac{\rho_a U_a d_p}{\mu_a} \tag{5.5}$$

where the particle velocity in air is approximated by the airflow velocity. Particles with low Stokes numbers track fluid pathlines; as the Stokes number increases, particles resist changes in their flow direction. Therefore, the Stokes number has been used to characterize particle deposition due to inertial impaction. Hinds (1982) proposed that the fraction of particles deposited on an obstacle in the flow field by impaction could be calculated using:

$$D_{imp} = \frac{\pi}{2}\left(\mathrm{Stk}\right) \tag{5.6}$$

In the current study, Stokes numbers were calculated for flow around the fin edges and the liquid flow channels to arrive at the deposition fraction. The associated characteristic length scale, l_c, used in equation (5.3) is t_{fin} for fins, h_{lch} for liquid channels when the fins are triangular, and (h_{lch} + t_{fin}) for liquid channels when fins are rectangular.

The deposition fraction must be corrected to account for the actual airflow area occupied by the fins or the liquid channels. A correction factor, ϕ, is implemented by considering the total available surface area on which deposition is possible, which is a function of the type and geometry of the fin structure. For inertial impaction on fins, the correction factor is defined as

$$\phi_{fin} = \left(\frac{2t_{fin}}{S_{fin}\cos\theta}\right)\left(\frac{S_{lch} - h_{lch}}{S_{lch}}\right) \text{ for triangular fins} \tag{5.7}$$

$$\phi_{fin} = \left(\frac{2t_{fin}}{S_{fin}}\right)\left(\frac{S_{lch} - h_{lch} - t_{fin}}{S_{lch}}\right) \text{ for rectangular fins} \tag{5.8}$$

For fouling by impaction on the liquid channels, the correction factor is defined as

$$\phi_t = \frac{h_{lch}}{S_{lch}} \text{ for triangular fins} \tag{5.9}$$

$$\phi_{lch} = \frac{h_{lch} + t_{fin}}{S_{lch}} \text{ for rectangular fins} \tag{5.10}$$

5.4.2 Gravitational Settling

Aerosol particles lose altitude under the action of gravity and settle on the floor of the airflow channel. For finned microchannel heat exchangers, the maximum distance that a dust particle will travel due to gravity before it settles on the floor of the channel is the transverse liquid channel pitch, S_{lch}. Pich (1972) calculated the deposition fraction of aerosol particles for laminar flow in rectangular channels. The deposition fraction for triangular microchannel structures was obtained in the current study by calculating deposition fractions using the expression developed for rectangular channels and numerically integrating over the triangular cross-section. The Reynolds number in the air-side channels is calculated based on the hydraulic diameter of a channel to ensure that the flow is in the laminar regime. The deposition fraction due to settling in laminar flow for the current model is calculated as

$$D_{gra} = \frac{2U_s L_l}{U_{hx}\left(S_{lch} - h_{lch} - t_{fin}/\sin\theta\right)} \text{ for triangular fins} \tag{5.11}$$

$$D_{gra} = \frac{U_s L_l}{U_{hx}\left(S_{lch} - h_{lch} - t_{fin}\right)} \text{ for rectangular fins} \tag{5.12}$$

5.4.3 Brownian Motion

Brownian motion is the irregular, random motion of an aerosol particle in air. This random motion may cause collisions between dust particles and the heat exchanger surface. It is assumed that the displacement of particles in the vertical plane due to Brownian motion is negligible compared to gravitational settling, and hence deposition by this mechanism is only considered for the vertically oriented surfaces of the heat exchanger. DeMarcus and Thomas (1952) developed an expression for fractional penetration of aerosol through narrow rectangular channels for laminar flow. Adapting this expression for the current study, the deposition fraction of particles due to Brownian motion is calculated as

$$D_{bro} = 0.9149e^{-2.8278\psi} + 0.05925e^{-33.5\psi} + 0.02587e^{-227.67\psi} \tag{5.13}$$

where the factor ψ is a constant depending on the geometry of the fin structure.

$$\psi = \frac{8D_{pa}\left(channel\ depth\right)\left(channel\ height\right)}{3U_{hx}\left(channel\ width\right)^2} \tag{5.14}$$

The diffusion coefficient, D_{pa}, is calculated as given by Hinds (1982).

5.4.4 Turbulence

Turbulence may cause deposition of particles due to turbophoresis, random bursts of velocity, and eddy/turbulent diffusion. These processes differ from one another in their time scale, in the nature of particle motion they cause, and in the phenomenon that drives them.

The transmission of an aerosol particle under forces caused by inhomogeneous turbulence in the fluid medium is termed turbophoresis. Inhomogeneous turbulence in air causes an imbalance in the momentum transferred to a particle suspended in air from air molecules on either side of the particle. This results in motion of particles from regions of high turbulence to regions of low turbulence. When particles have a non-zero value of momentum due to turbophoresis in a direction toward heat exchanger surfaces, there is a possibility they may collide with and deposit on the surface. Davies (1966) modeled the motion of particles in turbulence by modifying the diffusion coefficient by the eddy diffusivity of the fluid, and obtained an expression for the deposition velocity. Sehmel (1970) proposed that the aerosol particle eddy diffusivity was not the same as the eddy diffusivity of air. Caporaloni *et al.* (1975) presented a model for isothermal deposition of aerosol particles from turbulent fluid flow. They proposed that for a large volume of fluid, the diffusion coefficient for particles could be assumed equal to that of the fluid. Turbophoretic velocity was calculated as

$$U_{tur} = -\tau_p \frac{d\left(u'^2_{rms}\right)}{dx} \tag{5.15}$$

where the spatial coordinate, x, the turbulent fluctuation velocity u'_{rms}, and the calculated turbophoretic velocity U_{tur} are normal to the deposition surface. The particle relaxation time in equation (5.15) is calculated using equation (5.4).

In the current model, the time taken by a particle to deposit due to turbophoresis, termed as the turbophoretic deposition time, is calculated as the distance of the particle from the surface

divided by the turbophoretic velocity. Particle escape time characterizes the time required for a particle to pass through the heat exchanger core without deposition. The particle escape time is calculated as

$$\tau_{esc} = \frac{4C_C \rho_p d_p}{3C_D \rho_a v^2}, \text{ where } v = \bar{v} + v' \tag{5.16}$$

If the turbophoretic deposition time is less than the particle escape time, then the particle is assumed to deposit due to turbophoresis. The expression used to calculate the deposition fraction due to turbophoresis is

$$D_{tur} = probability\left(\frac{\tau_{d,tur}}{\tau_{esc}} < 1\right);\ \tau_{d,tur} = \frac{\Delta x}{U_{tur}} \tag{5.17}$$

The time taken by a particle to deposit due to turbulent fluctuation velocity, termed as the fluctuation deposition time, is calculated as the distance of the particle from the surface divided by the turbulent fluctuation velocity. If the fluctuation deposition time is less than the particle relaxation time, the particle is assumed to deposit due to velocity fluctuations. The expression used to calculate the deposition fraction due to random bursts of velocity is

$$D_{flu} = probability\left(\frac{\tau_{d,flu}}{\tau_p} < 1\right);\ \tau_{d.flu} = \frac{\Delta x}{v'_p} \tag{5.18}$$

The particle relaxation time in equation (5.18) is the same as that defined in equation (5.4).

However, the turbulent fluctuation velocity is a function of time and spatial location; turbulence data is reported as root mean square (RMS) values for the fluctuation velocities along all directions. An RMS value for the turbulent fluctuation velocity of a dust particle is calculated as a function of the RMS value of turbulent fluctuation velocity of airflow as given in Caporaloni *et al.* (1975). Consequently, the analysis of deposition due to turbulence becomes a stochastic calculation. Although all other deposition mechanisms are analyzed deterministically, deposition due to turbulence is analyzed as a Monte Carlo simulation. A straight section of duct with cross sectional area equal to that of the heat exchanger is assumed to extend upstream of the heat exchanger for calculating turbulence parameters. Multiple locations along the axis of the duct are considered, and a turbulent fluctuation velocity for the fluid is computed at each location by assuming a Gaussian (normal) distribution for the fluctuation velocity and randomly sampling around the RMS value. The deposition fraction due to turbulence is the total probability of

deposition from a Monte Carlo sample size of 441,000 computations. A particle is assumed to deposit via either of the above two methods. Diffusion driven by concentration gradients is neglected because the dust particles are assumed to be uniformly distributed.

The turbulent fluctuation velocity and eddy diffusivity are calculated using direct numerical simulation (DNS) data for turbulent flow through a duct from Huser and Biringen (1993). The hydrodynamic entrance length for airflow through the channels between the fins is calculated. It is assumed that turbulence from airflow upstream of the heat exchanger persists inside these channels until the airflow becomes fully developed. Deposition due to turbulence is calculated only for those streamwise sections where airflow is not fully developed.

5.4.5 Thermophoresis

Thermophoresis is the motion of aerosol particles along a temperature gradient at constant velocity under steady-state conditions (Waldmann and Schmitt, 1966). Collisions between air molecules and aerosol particles result in momentum exchange. The imbalance in thermal energy of the air molecules results in a directional force exerted on the particles. This force may cause particle motion towards a heat exchanger surface and ultimately lead to deposition. An expression for the net force acting on a particle due to a thermal gradient was developed by Derjaguin and Bakanov (1962) and Waldmann and Schmitt (1966).

Talbot *et al.* (1980) followed a regime-based analysis to calculate the thermophoretic force acting on particles in a temperature gradient, and calculated constants to fit the formulation over the entire Knudsen number regime. The current model employs their expression as

$$F_{the} = -\frac{6\pi\mu_a \nu_a d_p C_s \left(\frac{k_a}{k_p} + C_t \times \mathrm{Kn} \right) \frac{(\nabla T)_x}{T_\infty}}{(1 + 3C_m \times \mathrm{Kn}) \left(1 + 2\frac{k_a}{k_p} + 2C_t \times \mathrm{Kn} \right)} \tag{5.19}$$

where C_s = 1.17, C_t = 2.18, and C_m = 1.14. The temperature gradient is calculated between the heat exchanger surface temperature and the free stream temperature over a distance equal to the thermal boundary layer thickness. The thermal boundary layer thickness is calculated by assuming thermally developing or fully developed flow through the microchannels for laminar or turbulent flow as applicable.

Leong (1984) reported that for large aerosol particles thermophoresis was dependent on the shape and orientation of the particle in the temperature gradient. Since the current model approximates all dust particles as perfect spheres, this detail is not captured.

5.4.6 Diffusiophoresis

Diffusiophoresis is the motion of aerosol particles due to concentration gradients existing in air (Waldmann and Schmitt, 1966). Condensation of water vapor on the heat exchanger surface causes such gradients to exist. If humid air is modeled as a binary gas mixture, water molecules tend to diffuse towards regions of lower vapor concentration, while air molecules tend to move in the opposite direction. To conserve mass, airflow called Stefan flow occurs towards the surface (Hinds, 1982), exerting drag on the dust particles. Because air molecules are heavier than water molecules, aerosol particles tend to move in the direction of diffusion flux of air, possibly leading to deposition. An expression for the particle velocity resulting from the net effect of diffusion and Stefan flow was developed by Waldmann and Schmitt (1966). This formulation was divided into regimes as a function of the particle size. Bakanov and Derjaguin (1960) separately analyzed the diffusiophoresis of particles smaller than the mean free path of air, which was later extended to diffusiophoresis of larger particles in Derjaguin *et al.* (1966). The concentration of water vapor in air is calculated from the specific humidity of air. In air mixtures at near-atmospheric pressure, the concentration of water vapor in air can be approximated by the water vapor pressure in air. The concentration of water vapor in air is calculated as

$$c_v = \frac{\rho_{a,humid} - \rho_{a,dry}}{M_v} \tag{5.20}$$

The expressions used to calculate the diffusiophoretic velocity in air are

$$U_{dif} = -\frac{\sqrt{M_v} - \sqrt{M_a}}{\gamma_v\sqrt{M_v} + \gamma_a\sqrt{M_a}} \frac{D_{va}}{p_a} \frac{dp_v}{dx} \quad \text{for } Kn > 0.5 \tag{5.21}$$

$$U_{dif} = \frac{M_a - M_v}{\rho_{a,humid}} D_{va} \frac{dc_v}{dx} \quad \text{for } Kn < 0.5 \tag{5.22}$$

The mole fractions used in Eq. (18) are calculated as

$$\gamma_v = \frac{p_v}{p} \text{ and } \gamma_a = \frac{p_a}{p} \tag{5.23}$$

The diffusiophoretic velocity of a particle is calculated by assuming equilibrium between the diffusiophoretic force and the drag force acting on the particle. Diffusiophoretic velocities are

assumed to be in the Stokes regime, and therefore the Stokes drag formulation is used to calculate the the diffusiophoretic force acting on a particle as

$$F_D = 3\pi\mu_a d_p U_{the} \tag{5.24}$$

Leong (1984) reported that diffusiophoresis, in the case of large aerosol particles, was independent of particle shape. Therefore, for diffusiophoresis, the approximation of all dust particles as spheres is appropriate.

5.4.7 Thermodiffusiophoresis

Goldsmith and May (1966) proposed that aerosol particles, near a heat exchanger surface on which water vapor was condensing, were simultaneously subjected to thermophoretic and diffusiophoretic forces. Thermophoretic and diffusiophoretic velocities were calculated to be on the same order of magnitude. Experiments confirmed that superposition of the thermophoretic and diffusiophoretic forces yielded agreement with experimental measurements of deposition due to their combined effect. Therefore, in the current model, thermophoretic and diffusiophoretic forces are superposed and a deposition velocity is calculated for this net force. Since thermal and concentration gradients exist only in the boundary layer, the maximum distance a particle must travel before it collides with the heat exchanger surface is equal to the boundary layer thickness at that location. The ratio of time a particle would take to deposit on any surface due to the thermodiffusiophoretic velocity to the time needed for that particle to pass through the heat exchanger is equated to the deposition fraction as

$$D_{thedif} = \frac{\tau_{d,thedif}}{\tau_{esc}};\ \tau_{thedif} = \frac{\Delta x}{U_{thedif}} \tag{5.25}$$

5.5 Total Deposition Fraction

Aside from the superposition of thermophoretic and diffusiophoretic forces, the different deposition mechanisms are assumed to be mutually independent. The penetration fraction for each mechanism is calculated. These are then multiplied to obtain the net penetration fraction. The formulation used to calculate the net deposition fraction due to all mechanisms of deposition considered is given as

$$D_{net} = 1 - P_{imp,fin} P_{imp,lch} P_{gra} P_{bro} P_{tur} P_{thedif} \tag{5.26}$$

Inertial impaction on fins and liquid flow channels occurs at the front face of the heat exchanger, and only those dust particles which did not deposit due to inertial impaction enter the heat exchanger core. Gravitational settling is dominant for large particles and occurs only on the bottom surface of the airflow channels, whereas Brownian motion is dominant for small particles and occurs only on vertically oriented surfaces of the airflow channels. These two mechanisms can therefore be reasonably assumed as independent of each other. The correlation used to analyze deposition due to Brownian motion was developed neglecting the effect of gravity (DeMarcus and Thomas, 1952). Turbophoretic forces act on much smaller time scales than the other forces, because they are functions of instantaneous fluctuations in velocity, and thereby can be considered independent of the others based on the time scale. Multiple studies in the literature have chosen to couple two or more selected mechanisms on a case-by-case basis, such as turbophoresis, Brownian diffusion, molecular diffusion, and gravitational settling (Zhang and Ahmadi, 2000, Zhao and Wu, 2006). There is not a consensus in the literature regarding the independent or interdependent nature of all the deposition mechanisms, and this requires further experimental investigation to confirm the modeling assumptions employed.

5.6 Dust Accumulation

5.6.1 Streamwise Distribution and Thickness of Deposition Dust

Prediction of the spatial distribution of dust deposition is performed implicitly in the model. Since heat exchanger fouling is analyzed for discretized streamwise sections of the heat exchanger, deposition fractions are calculated for the each section independently. These are used to calculate the mass of dust deposited on the surface area of the heat exchanger contained in that section. Using the bulk density of deposited dust, the thickness of the dust layer deposited on that section is obtained. The layer thickness is used to modify the heat exchanger dimensions for each section to reflect the decrease in the cross-sectional area available for airflow as channels become blocked due to fouling. Consequently, the distance a particle needs to travel before it collides with the heat exchanger surface also decreases.

5.6.2 Streamwise Change in Suspended Dust Concentration and Composition

The spatial discretization of fouling allows determination of the change in concentration and composition of aerosol particles inside the heat exchanger along the streamwise flow path. Once the deposition for one section is analyzed, the mass of dust deposited in that section is removed from the airflow, and a new dust concentration and particle size distribution is defined that enters the downstream section. This reflects the actual physical process more closely, and is expected to yield better prediction accuracy.

5.7 Model Predictions

There is a limited amount of experimental data available in the literature regarding fouling of finned microchannel heat exchangers. The model requires detailed information about the geometry and operating conditions of the heat exchanger to make predictions. Of all previous experimental measurements, the necessary information is only reported by Bell and Groll (2011), as summarized in Table 5.1 and Table 5.2.

These heat exchangers were installed in a duct of cross-section 60 cm × 60 cm. A reducing section installed in the duct allowed for testing of the smaller heat exchangers without bypass airflow. ASHRAE Standard Test Dust and Arizona Road Test Dust were used as fouling agents. Dust was injected into the airflow upstream of the heat exchanger by aerosolizing these premixed, predefined compositions of particulates with compressed air, and forcing this airflow to pass through the heat exchanger to simulate fouling. At the inlet to the heat exchanger, air temperature was maintained at 25 °C with 40% relative humidity, whereas tube-side temperature was maintained at 42 °C. Air velocity was maintained at 1.5 m/s. These quantities were measured in the duct upstream of and not inside the heat exchanger. The Reynolds numbers for these operating conditions based on the hydraulic diameter of this duct are in the range of 38,800 to 78,500, rendering the flow inside the duct turbulent.

Table 5.1. Geometric information of finned microchannel heat exchangers from Bell and Groll (2011).

Identifier	Type of fin structure	Frontal area [cm]	Fin pitch [cm]
B	Louvered microchannels	40 × 50	1.3
C			1.1

To allow prediction of the fouling under the same conditions as Bell and Groll (2011), several geometric parameters were estimated based on published images and typical microchannel-finned heat exchangers. These are reported in Table 5.2. The modeling is conducted by discretizing the streamwise depth of the heat exchanger into three sections, and assumes a bulk density of the deposited dust as 375 kg/m^3 based on the measured density of the fouling agent used in the experiments.

Table 5.2. Estimated geometric parameters for the heat exchanger tested by Bell and Groll (2011).

Parameter	Value
Vertical fin pitch	10 mm
Fin thickness	110 μm
Liquid channel height	1.2 mm
Streamwise depth of heat exchanger	25.4 mm

Figure 5.3 shows the evolution of the spatially discretized dust deposition on the heat exchanger after equal periods of 40 minutes duration each. Heat exchanger sections are arbitrarily defined approximately 10 mm in length along the streamwise direction, so that there are three discretized sections that extend across the entire cross-sectional area. It can be seen that fouling is heaviest at the front of the heat exchanger, which matches the experimental observations of Bell and Groll (2011). Figure 5.4 shows the dust concentration as air passes through the heat exchanger for each discretized time period. The initial concentration of dust simulates the heterogeneous mixture tested. Both Figure 5.3 and Figure 5.4 are model predictions for heat exchanger C fouled with ASHRAE Standard Test Dust. There is preferential deposition of larger particles. Based on an analysis of each deposition mechanism, Brownian motion and thermodiffusiophoresis cause little to no deposition. Inertial impaction on fins is an important contributing factor for particles larger than 1 micron in diameter, while impaction on liquid channels contributes less, mainly for

particles larger than 5 microns in diameter. For particles larger than 50 microns, gravitational settling causes some deposition. Turbulence is a major contributor to deposition across all size ranges of particles.

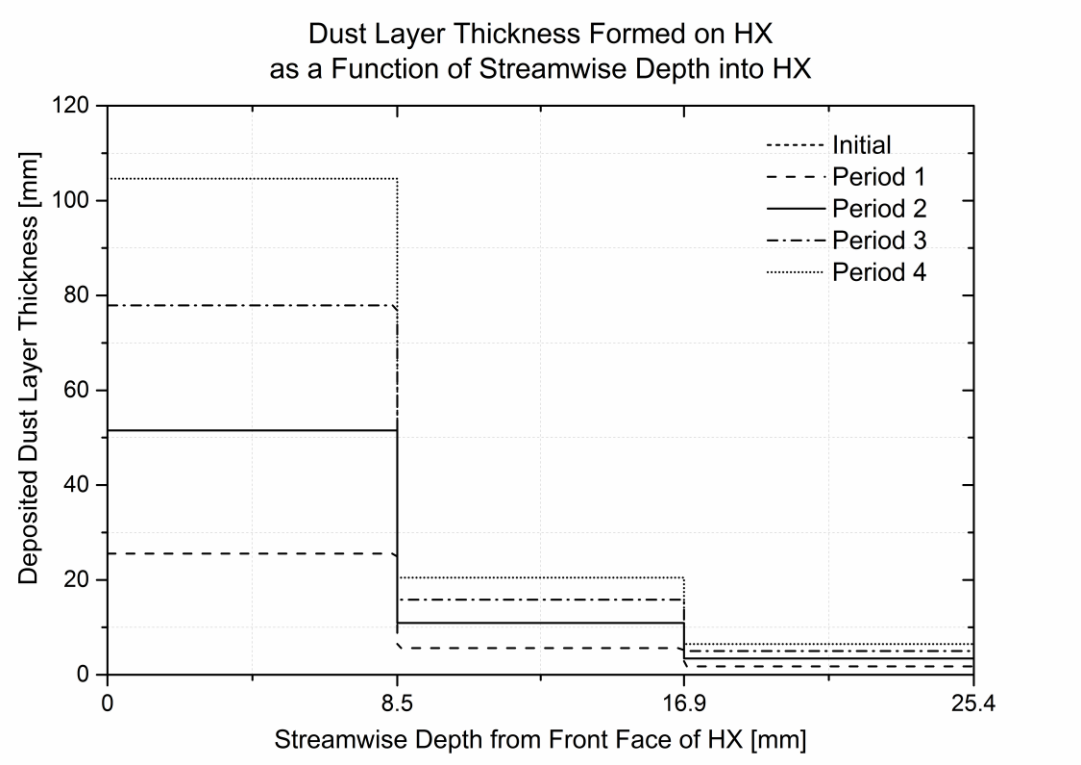

Figure 5.3. Predicted growth of deposition layer due to fouling.

The model predicts that heat exchanger B will have a deposition fraction of about 97% for both Arizona Road Test Dust and ASHRAE Standard Test Dust cases. This causes a respective reduction of 53% and 22% in the cross-sectional area available for airflow, which would lead to a significant increase in pressure drop through the heat exchanger. For heat exchanger C, ASHRAE Standard Test Dust will similarly have a deposition fraction in excess of 97%, and will cause a reduction in flow area of about 46%. While deposition fractions were not reported by Bell and Groll (2011), the experiment was conducted until the pressure drop across the heat exchanger doubled, which would be expected at approximately this amount of predicted flow area reduction. More detailed experimental data and more precisely defined heat exchanger geometries are required to confidently gauge the accuracy of the model.

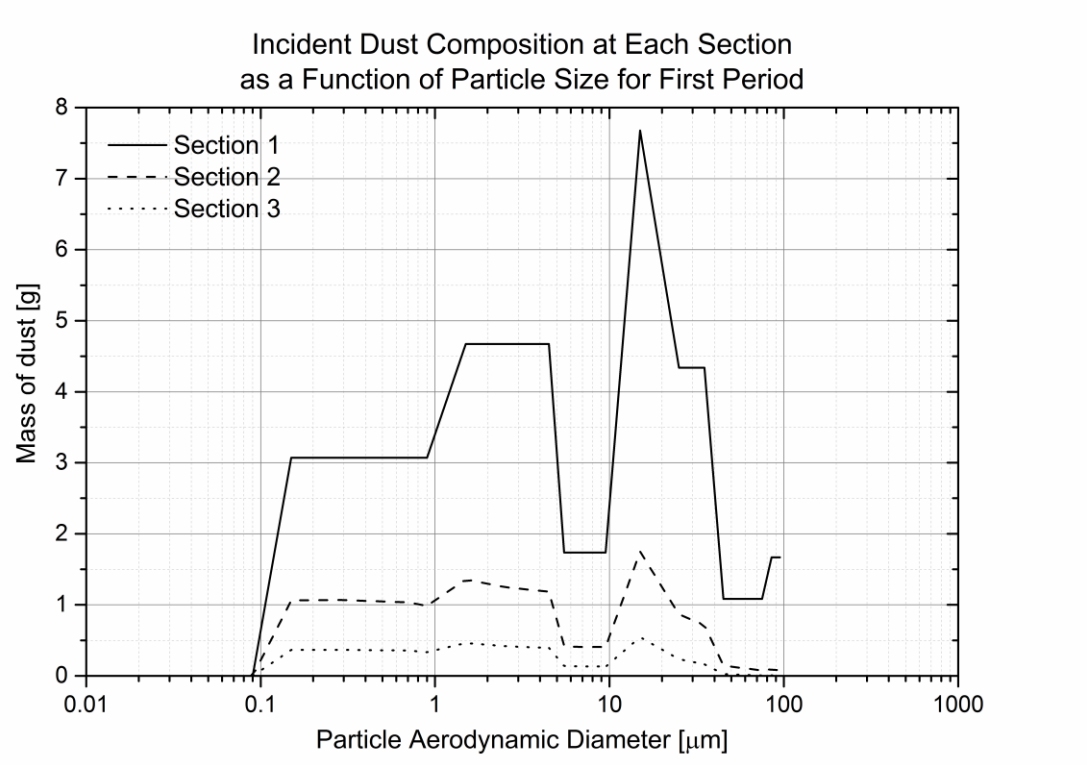

Figure 5.4. Size distribution of suspended particulate matter passing through the heat exchanger.

The model predicts an almost constant deposition fraction for consecutive periods of fouling without acceleration of the fouling rates due to partial closure of the channels. The neglected presence of fibers in the test dusts used in the experiments may lead to an under-prediction of reduction in cross-sectional flow area due to blockage. This is because fibers are large, cylinder shaped particles with low densities. The neglecting of fibers also may yield the near-constant deposition fractions in time, because fibers are the primary cause for accelerated fouling in heat exchanger regions that are already blocked.

5.8 Conclusions

A novel model for prediction of the fouling of microchannel heat exchangers is presented which includes all pertinent deposition mechanisms and implicitly predicts the streamwise distribution and thickness of deposited dust, as well as the streamwise change in suspended dust concentration and composition. The results of this study point to the need for further refinement and improvement in the mathematical models used to represent the physical phenomena that occur when particulate matter in the air stream fouls a heat exchanger.

CHAPTER 6. SUMMARY, RESEARCH CONTRIBUTION, AND FUTURE WORK

6.1 Initial Research Goals

Goals for this research effort were proposed as follows:

1. To conduct fouling experiments on a finned microchannel heat exchanger as per the designed test matrix from Section 3.2.5.
2. To tune the fouling model so that it reflects experimental trends better.
3. To expand the fouling model to predict performance of finned tube and finned microchannel heat exchangers after fouling.
4. To expand the fouling model to predict system performance when a component heat exchanger is fouled.
5. To conduct a literature review of ambient dust characteristics and concentrations; to explicitly specify the relationship between ambient dust and the fouling agent used in this work.
6. To investigate the relationship between fouling experiments and real applications to develop a correlation between the two.

6.2 Methodology

The bullet points in this section correspond to the specific goals mentioned in Section 6.1.

1. Fouling experiments are to be conducted as per the test protocol described in Section 2.3.3 on the experimental setup located in Ray W. Herrick Laboratories, Purdue University. Efforts should be taken to ensure that experiments are conducted with a high degree of consistency and results can be equitably compared with each other. Measurements from an individual test run should be analyzed to understand the transient phenomenon of fouling. Collated results from a parametric runs of experiments should be compared to understand the effect of change in said parameters on the experiment. Summary data should be published and detailed measurements be made available to researchers upon request.
2. Structural changes in the fouling model are to be made to ensure that the phenomenon of fouling is faithfully represented by the model. The deterministic, mathematical nature of

the model should be preserved. Necessary changes should be made to the subroutines to improve the prediction accuracy. Two parameters should be used to evaluate the performance of the model. Firstly, the difference between the model predictions and the experimental measurements are to be driven to the smallest possible value. Secondly, the model should reflect the trends observed in the set of parametric test runs with a high degree of accuracy.

3. A literature review is to be performed to identify reliable, accurate, commonly used correlations to predict performance of heat exchangers based on their geometry and operating conditions. The pressure drop across and heat transfer through the heat exchanger should be among the modelled parameters. The dust distribution predicted by the fouling model should be used to reduce the flow area available for airflow through the heat exchanger core, and to add a layer of thermally insulating dust on the air-side surface of the heat exchanger. A change in the airflow area is anticipated to affect the Reynolds number of flow through the heat exchanger core, which in turn is anticipated to affect the calculated pressure drop and heat transfer. The thermally insulating dust layer is anticipated to impact the calculated heat transfer. Experimental measurements made as part of this work, and those obtained from the literature could be used to validate the heat exchanger performance model.
4. The change in heat exchanger performance is to be propagated through a system performance model to predict effect of heat exchanger fouling on residential air-conditioning systems. Published models in the literature could be used *as is* to model performance of other components in a conventional residential air-conditioning system such as compressors and expansion devices.
5. An average particle size distribution of ambient dust in outdoor environments is to be obtained from published data. An average composition profile for ambient dust in outdoor environment is to be obtained from published data. These should be compared against ASHRAE Standard Test Dust, the fouling agent used in the fouling experiments in this work. The suitability of the fouling agent used in this work to simulate outdoor environments should be ascertained. Based on the outcome of this judgement, the use of ASHRAE Standard Test Dust as a fouling agent may be established; otherwise a better fouling agent could be suggested.

6. Experimental results obtained from parametric tests runs performed as part of this work will inform this analysis. Figure 6.1 proposes a procedure to convert laboratory experimental results to meaningful predictions about operation of heat exchangers in the field. There exist some inherent uncertainties with any such extrapolation; laboratory experiments must necessarily be run at strictly controlled operating conditions using a fouling agent that remain consistent and constant for the duration of the experiment. The actual operating conditions and ambient dust may change over the operation of a heat exchanger in the field. The fouling agent used in experiments may not represent the actual ambient suspended particulate matter with the desired degree of accuracy. Thus, a straightforward extrapolation as described in Figure 6.1 may not be realistic. Further research is required to accomplish this goal.

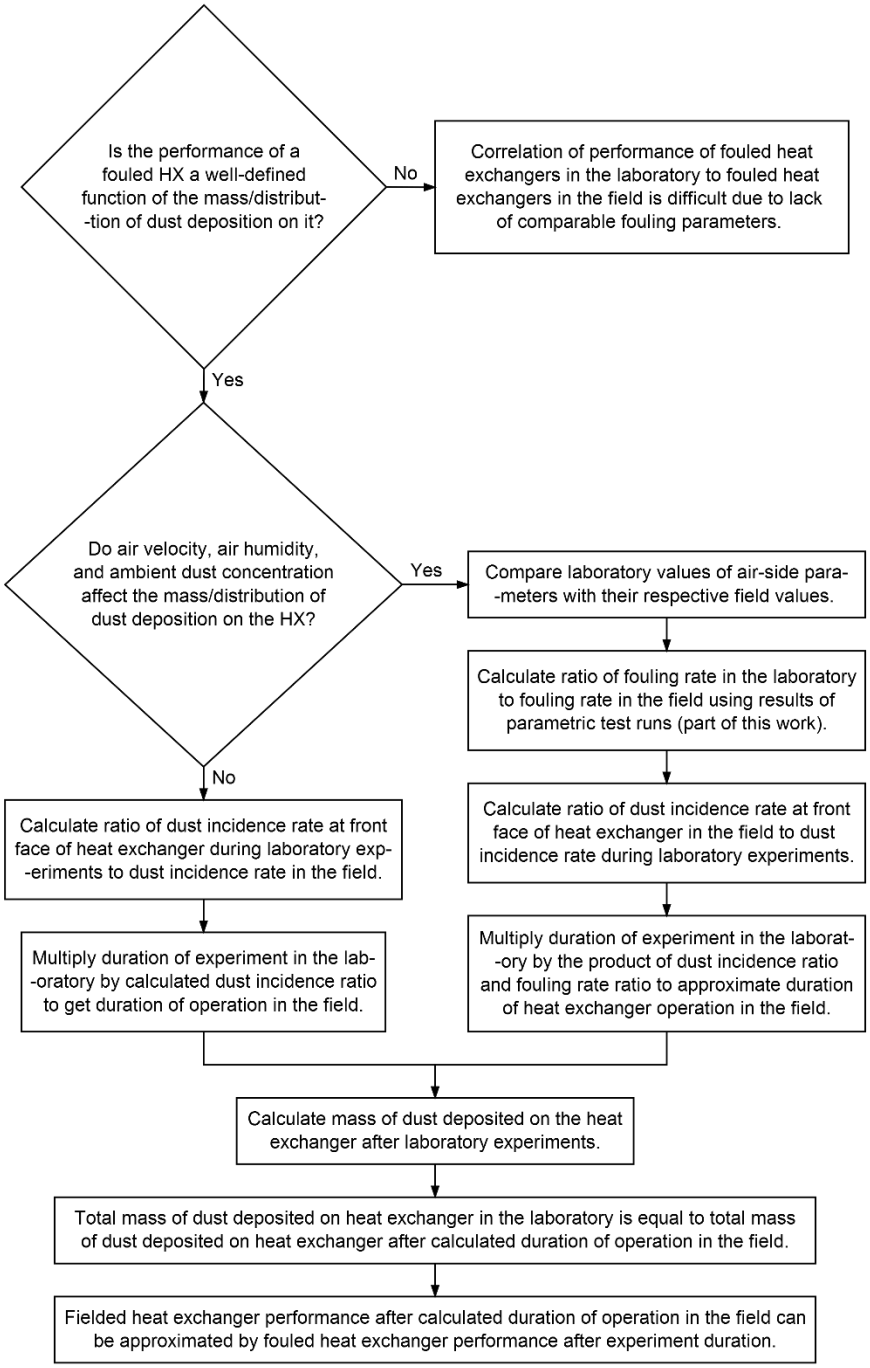

Figure 6.1. Application of results from laboratory experiments to make predictions about fielded heat exchangers.

6.3 Outcomes

The bullet points in this section correspond to the specific goals mentioned in Section 6.1.

1. Experimental results covering a broader range of operating conditions are in themselves a useful addition to the literature on heat exchanger fouling.
2. The validated heat exchanger fouling model would be made publicly available.
3. The heat exchanger performance model would help predict degradation in heat exchanger performance due to fouling.
4. The system performance model would be a tool in the assessment of the real impact of fouling on installed systems.
5. The current fouling agent used for fouling tests is the ASHRAE Standard Test Dust; a standard test dust defined to test filter efficiency. This study may result in the definition of a standard test dust aimed specifically at heat exchanger fouling.
6. A standard method would enable better conversion of results of laboratory fouling tests to real world applications.

6.4 Completion Assessment

The bullet points in this section correspond to the specific goals mentioned in Section 6.1.

1. All experiments defined in the test matrix are conducted as per the experimental method proposed.
2. The assumption that every particle–surface collision results in a particle to surface adhesion is under re-examination. Chapter 5 of this document is under revision, and it will be rewritten. The deviation of predicted fouling rates from measured fouling rates will be presented. Some deficiencies are still expected to remain in the model when attempting to match experimentally observed trends due to computational complexity or a lack of fundamental information—obtainable from chemical analyses, information that engineering experiments cannot provide.
3. The fouling model, originally written for plate finned tube heat exchangers has been extended to predict fouling of finned microchannel heat exchangers.

4. A system model to predict impact of heat exchanger fouling on system performance has not been developed. Its development is still intended, but its development will not be described in this dissertation.
5. A brief review of ambient dust characteristics and a comparison to those of the fouling agent is provided. The suitability of the fouling agent to simulate ambient dust is discussed.
6. A methodology to correlate test duration in a laboratory under accelerated fouling and operating duration in the field is proposed, but not further explored. This direction of enquiry is left as future work as an extension of the current research effort.

6.5 Benefits

The bullet points in this section correspond to the specific goals mentioned in Section 6.1.

1. The experimental data set could be used by other researchers to compare against their own measurements or to validate their modeling efforts.
2. The heat exchanger fouling model developed as part of this research could be used by researchers to further develop an even more generalized and accurate heat exchanger fouling model to assist in the design of heat exchangers resistant to air-side particulate fouling.
3. The heat exchanger performance model could be used as a tool in the design of cleaning schedules for heat exchangers to reduce fouling related inefficiencies and losses.
4. The system performance model would inform industry opinion on the importance of a more scientific approach towards heat exchanger fouling.
5. A standardized fouling agent would make fouling tests conducted in different laboratories comparable to each other and make the fouling experimental database more uniform.
6. A well-defined and justified way to apply information gained in the laboratory to the field would make this research more relevant to industry.

6.6 Future Work

It has been stated before in this document that the current investigation is the next step in a series of heat exchanger fouling studies conducted in Ray W. Herrick Laboratories, Purdue

University. It is believed by this student that this evolving research effort is at an inflection point. The phenomenon of fouling is characterized by certain time and length scales; and so are the experimental setup and its operation. To observe and measure the characteristics of the phenomenon under investigation requires a test setup and measurement and control equipment characterized by time and length scales an order of magnitude smaller than those characterizing the phenomenon. The current test setup would need to be modified to be able to control test conditions within smaller tolerances, and the measurement equipment would need to be upgraded to resolve smaller changes in measured quantities. The sensitivity of the phenomenon of fouling to a change in the heat exchanger design such as finned tube to finned microchannel, or a change in the fouling agent such as from ASHRAE Standard Dust to Arizona Road Test Dust may affect the phenomenon of fouling to a degree greater than that affected by a change in operating conditions. A solution would be to build smaller prototypes of heat exchanger designs and then conduct fouling tests on these scaled-down heat exchangers. This may make the experimentation more amenable to fine control.

The interaction between the heat exchanger surface and fouling agent particulates is a parameter that has not been independently investigated for the current combination of surface and particle. Quantitative information about this interaction is necessary to enhance the fidelity of the model to the experiment and significantly refine prediction accuracy. This information, however, cannot be gained from engineering experiments. These fundamental measurements would have to be made in a chemistry laboratory in an independent investigation.

The current model is computationally expensive. Modeling heat exchanger fouling for many designs under different operating conditions would be time consuming and unrealistic. A method to either supplement the solution speed, or to reduce the need to model all possible combinations of heat exchanger design and operating conditions is necessary to enable broad application of the model.

BIBLIOGRAPHY

Abd-Elhady, M. S., Rindt, C. C., & van Steenhoven, A. A. (2009). Optimization of flow direction to minimize particulate fouling of heat exchangers. *Heat Transfer Engineering, 30*(10)-(11), 895-902.

Abd-Elhady, M. S., Rindt, C. C. M., Wijers J. G., van Steenhoven, A. A., Bramer, E. A., & van der Meer, Th. H. (2004). Minimum gas speed in heat exchangers to avoid particulate fouling. *International Journal of Heat and Mass Transfer, 47*(17), 3943-3955.

Ahn, Y. C., Cho, J. M., Shin, H. S., Hwang, Y. J., Lee, C. G., Lee, J. K., Lee, H. U., & Kang, T. W. (2003). An experimental study of the air-side particulate fouling in fin-and-tube heat exchangers of air conditioners. *Korean J. of Chemical Engineering, 20*(5), 873-877. ISSN:1975-7220

Ahn, Y-C. & Lee, J-K. (2005). Characteristics of air-side particulate fouling materials in finned-tube heat exchangers of air conditioners. *Particulate Science and Technology, 23*(3), 297–308. doi:10.1080/02726350590955930

Air cleaner test code, SAE Standard J726-1993. Warrendale, PA: Society of Automotive Engineers International.

Ali, A. H., & Ismail, I. M. (2008). Evaporator air-side fouling: Effect on performance of room air conditioners and impact on indoor air quality. *HVAC&R Research 14*(2), 209–219. doi: 10.1080/10789669.2008.10391004

American Society of Heating, Refrigerating Air-Conditioning Engineers. (2013). Chapter 1: Psychrometrics. In *2013 ASHRAE Handbook: Fundamentals SI Edition* (1.1–1.16). Atlanta, GA: ASHRAE. ISBN:9781628705355

Annis, B. K., Malinauskas, A. P., & Mason, E. A. (1973). Theory of diffusiophoresis of spherical aerosol particles and of drag in a gas mixture. *Journal of Aerosol Science, 4*(4), 271-281. Bakanov, S. P., & Derjaguin, B. V. (1960). The motion of a small particle in a non-uniform gas mixture. *Discussions of the Faraday Society, 30*, 130-138.

ASHRAE 52.1 and 52.2 Test Dust Product MSDS Information. (2012, November 2). Retrieved February 2, 2015 from Powder Technology Inc.: http://www.powdertechnologyinc.com/product-msds-information/

Baghdar Hosseini, S., Haghighi Khoshkhoo, R., & Javadi Malabad, S. M. Experimental and numerical investigation on particle deposition in a compact heat exchanger. *Applied Thermal Engineering, 115*, 406–417. doi:10.1016/j.applthermaleng.2016.12.110

Bean, V., E. & Hall, J., M. (1999). New primary standards for air speed measurement at NIST. In *Proceedings of the 1999 NCSL Workshop & Symposium, Charlotte, NC* (pp. 413–421, Session 4E). Boulder, CO: National Conference of Standards Laboratories.

Bell, I. H., & Groll, E. A. (2011). Air-side particulate fouling of microchannel heat exchangers: Experimental comparison of air-side pressure drop and heat transfer with plate-fin heat exchanger. *Applied Thermal Engineering, 31*(5), 742–749. doi:10.1016/j.applthermaleng.2010.10.019

Bell, I. H., Groll, E. A., & König, H. (2011). Experimental analysis of the effects of particulate fouling on heat exchanger heat transfer and air-side pressure drop for a hybrid dry cooler. *Heat Transfer Engineering, 32*(3/4), 264–271. doi:10.1080/01457632.2010.495618

Bell, I., H., Wronski, J., Quoilin, S., & Lemort, V. (2014). Pure and pseudo-pure fluid thermophysical property evaluation and the open-source thermophysical property library CoolProp. *Industrial & Engineering Chemistry Research, 53*(6), 2498–2508. doi:10.1021/ie4033999

Boll, R. H., & Patel, H. C. (1961). The role of chemical thermodynamics in analyzing gas-side problems in boilers. *Journal of Engineering for Power, 83*(4), 451–467. doi:10.1115/1.3673236

Bott, T. R. (1971). *Gas side fouling in heat exchange systems*. (Atomic Energy Research Establishment Report No. R-6453). Harwell, U.K.: U.K. Atomic Energy Authority.

Bott, T. R. (1988). Gas side fouling. In L. F. Melo, T. R. Bott, & C. A. Bernardo (Eds.), *Fouling Science and Technology* (pp. 191-206). Dordrecht, Netherlands: Kluwer Academic Publishers. doi:10.1007/978-94-009-2813-8_13

Bott, T. R. (1988). General fouling problems. In L. F. Melo, T. R. Bott, & C. A. Bernardo (Eds.), *Fouling Science and Technology* (pp. 3-14). Dordrecht, Netherlands: Kluwer Academic Publishers. doi:10.1007/978-94-009-2813-8_1

Bott, T. R. (1995). *Fouling of heat exchangers*. doi:10.1016/b978-0-444-82186-7.x5000-3

Bott, T. R. & Bemrose, C. R. (1983). Particulate fouling on the gas-side of finned tube heat exchangers. *Journal of Heat Transfer-Transactions of the ASME, 105*(1), 178-183. doi:10.1115/1.3245538

Butte, W., & Heinzow, B. (2002). Pollutants in house dust as indicators of indoor contamination. *Reviews of Environmental Contamination and Toxicology, 175*, 1-46.

Caporaloni, M., Tampieri, F., Trombetti, F., & Vittori, O. (1975). Transfer of particles in nonisotropic air turbulence. *Journal of the Atmospheric Sciences, 32*(3), 565-568.

Cleaver, J. W., & Yates, B. (1976). The effect of re-entrainment on particle deposition. *Chemical Engineering Science, 31*(2), 147-151.

Cowell, T., & Cross, D. (1980). *Airside fouling of internal combustion engine radiators*. (SAE Technical Paper 801012). Warrendale, PA: SAE International. doi:10.4271/801012

Davies, C. N. (1966). Deposition of aerosols from turbulent flow through pipes. *Proceedings of the Royal Society of London, Series A, Mathematical and Physical Sciences*, *289*(1417), 235-246.

Davies, C. N. (1966). Deposition from moving aerosols. In C. N. Davies (Ed.), *Aerosol Science*, (pp. 393-446). London, Great Britain: Academic Press.

DeMarcus W., & Thomas, J. W. (1952). *Theory of a diffusion battery*. (Oak Ridge National Laboratory Publication No. ORNL-1413). Oak Ridge National Laboratory, Oak Ridge, TN: U.S. Atomic Energy Commission.

Derjaguin, B. V., & Bakanov, S. P. (1962). Thermophoresis of aerosol particles. *Nature*, *196*(4855), 669-670.

Derjaguin, B. V., Yalamov, Y. I., & Storozhilova, A. I. (1966). Diffusiophoresis of large aerosol particles. *Journal of Colloid and Interface Science, 22*(2), 117-125.

Environmental engineering considerations and laboratory tests. (U.S. Military Standard 810G W/CHANGE 1:2014). Washington, DC: Department of Defense.

Epstein, N. (1978). Fouling in heat exchangers. In National Research Council of Canada, Canadian Society for Chemical Engineering, & Canadian Society for Mechanical Engineering (Eds.), *Proceedings of the International Heat Transfer Conference 6, Toronto, ON* (pp. 235-253). Danbury, CT: Begell House Publishers.

Epstein, N. (1988).Particulate fouling of heat transfer surfaces: Mechanisms and models. In L. F. Melo, T. R. Bott, & C. A. Bernardo (Eds.), *Fouling Science and Technology* (143–164), Dordrecht: Kluwer Academic Publishers. doi:10.1007/978-94-009-2813-8

Evaluation of measurement data—Guide to the expression of uncertainty in measurement (JCGM 100:2008). Sèvres, France: Joint Committee for Guides in Metrology, Bureau international des poids et mesures

Garrett-Price, B. A., Smith, S. A., & Watts, R. L. (1984). *Industrial fouling: problem characterization, economic assessment, and review of prevention, mitigation, and accommodation techniques*. (Pacific Northwest National Laboratory Technical Report No. PNL-4883). Richmond, WA: U.S. Department of Energy.

Gavrilakis, S. (1992). Numerical simulation of low-Reynolds-number turbulent flow through a straight square duct. *Journal of Fluid Mechanics, 244,* 101-129.

Goldsmith, P., & May, F. G. (1966). Diffusiophoresis and thermophoresis in water vapor systems. In C. N. Davies (Eds.), *Aerosol Science* (pp. 163-194). London, Great Britain: Academic Press.

Haghighi-Khoshkhoo, R., & McCluskey, F. M. J. (2007). Air-side fouling of compact heat exchangers for discrete particle size ranges. *Heat Transfer Engineering, 28*(1), 58–64. doi:10.1080/01457630600985675

Haider, A., & Levenspiel, O. (1989). Drag coefficient and terminal velocity of spherical and nonspherical particles. *Powder Technology, 58*(1), 63-70.

Hinds, W. (1982). *Aerosol Technology: Properties, Behavior, and Measurement of Airborne Particles*. New York, NY: John Wiley & Sons.

Huser, A., & Biringen, S. (1993). Direct numerical simulation of turbulent flow in a square duct. *Journal of Fluid Mechanics, 257,* 65-95.

Inlet air cleaning equipment for internal combustion engines and compressors—Performance testing. (ISO Standard 5011:2014). Geneva, Switzerland: International Organization for Standardization.

Jennings, S. G. (1988). The mean free path in air. *Journal of Aerosol Science, 19*(2), 159-166.

Kallio, G. A., & Reeks, M. W. (1989) A numerical simulation of particle deposition in turbulent boundary layers. *International Journal of Multiphase Flow, 15*(3), 433-46.

Lankinen, R., Suihkonen, J., & Sarkomaa, P. (2003). The effect of air side fouling on thermal-hydraulic characteristics of a compact heat exchanger. *International Journal of Energy Research, 27*(4), 349–361. doi:10.1002/er.880

Leong, K. H. (1984). Thermophoresis and diffusiophoresis of large aerosol particles of different shapes. *Journal of Aerosol Science, 15*(4), 511-517.

Malayeri, M. R., Zornek, T., Balestrino, S., Warey, A., & Szymkowicz, P. G. (2011). In M. R. Malayeri, H. Müller-Steinhagen, A. P. Watkinson (Eds.), Proceedings of *International Conference on Heat Exchanger Fouling and Cleaning–2011, Crete, Greece* (pp. 74–81). Published online on www.heatexchanger-fouling.com

Malvern Instruments Ltd. (2015, October 20). Morphologi G3 particle size and particle shape image analyzer. Retrieved May 16, 2017, from http://www.malvern.com/en/products/product-range/morphologi-range/morphologi-g3/#

Marner, W. J. (1990). Progress in gas-side fouling of heat-transfer surfaces. *Applied Mechanics Reviews, 43*(1), 35-66.

Marner, W. J. & Henslee, S. P. (1984). *A survey of gas-side fouling measuring devices*. (Jet Propulsion Laboratory Publication No. 84-11). California Institute of Technology, Pasadena, CA: U.S. Department of Energy.

Marner, W. J. & Suitor, J. W. (1983) *Survey of gas-side fouling in industrial heat-transfer equipment*. (Jet Propulsion Laboratory Report No. JPL-PUB-83-74). California Institute of Technology, Pasadena, CA: U.S. Department of Energy.

Mason, D. J., Douch, N., & Heikal, M. R. (2002). Air side fouling of compact heat exchangers. In R. K. Stobart, P. R. N. Childs (Eds.), *Proceedings of the 2nd Conference on Total Vehicle Technology, Brighton, England* (pp. 131-142). London, England: IMechE (Published as *Total Vehicle Technology: How Do We Get the Innovation Back Into Vehicle Design?*)

McComas, S. T. (1967). Hydrodynamic entrance lengths for ducts of arbitrary cross section. *Journal of Fluids Engineering, 89*(4), 847-850.

Method of testing general ventilation air-cleaning devices for removal efficiency by particle size, ANSI/ASHRAE Standard 52.2-2012. Atlanta, GA: American Society of Heating, Refrigerating, and Air-Conditioning Engineers, Inc.

Miller, J. A. (1967). Mechanisms of gas turbine regenerator fouling. In International Gas Turbine Institute (Eds.), *Proceedings of the ASME 1967 Gas Turbine Conference and Products Show, Houston, TX* (pp. N.A.). New York, NY: ASME. doi:10.1115/67-GT-26

Montgomery, D. C. (2013). *Design and analysis of experiments* (8th ed.). Retrieved from http://www.wiley.com/WileyCDA/WileyTitle/productCd-EHEP002024.html. ISBN: 978-1-118-32426-4

Moore, D. A. (2009). Characterization of fiber accumulation fouling in fine pitched heat sinks. *25th Semiconductor Thermal Measurement and Management Symposium, San Jose, CA* (pp. 279–284). Piscataway, NJ: IEEE. doi:10.1109/STHERM.2009.4810776

Moser, R. D., Kim, J., & Mansour, N. N. (1999). Direct numerical simulation of turbulent channel flow up to Re = 590. *Physics of Fluids, 11*(4), 943-945.

Müller-Steinhagen, H., Malayeri, M. R., & Watkinson, A. P. (2005). Fouling of heat exchangers-New approaches to solve an old problem. *Heat Transfer Engineering, 26*(1), 1-4.

Müller-Steinhagen, H., Reif, F., Epstein, M., & Watkinson, A., P. (1988). Influence of operating conditions on particulate fouling. *The Canadian Journal of Chemical Engineering, 66*(1), 42–50. doi:10.1002/cjce.5450660106

Muzychka, Y. S. & Yovanovich, M. M. (2002). Laminar flow friction and heat transfer in non-circular ducts and channels: Part I – Hydrodynamic problem. In G. P. Celata, B. Thonon, A. Bontemps, S. Kandlikar (Eds.), Proceedings of *International Symposium on Compact Heat Exchangers, Grenoble, France* (pp. 123–130). Pisa, Italy: Edizioni ETS. (Published as *Compact Heat Exchangers: A Festschrift on the 60th Birthday of Ramesh K. Shah*) ISBN: 9788846706195

National Institute of Standards and Technology (2010). REFPROP (Database 23, Version 9.0) [Computer software]. Gaithersburg, MD: U.S. Department of Commerce

National Instruments Corporation (2014). NI LabVIEW 2014 [Computer software]. Austin, TX: National Instruments Corporation

NuCalgon. (2013). *Cal-Green*. (Material Safety Data Sheet for Product No. 4190-08). St. Louis, MO: NuCalgon. Retrieved July 27, 2015 from: http://www.nucalgon.com/assets/SDS/English/4190_SDS_ENG.pdf

Obadina, S., Fody, J., Dessiatoun, S., Ohadi, M., & Shooshtari, A. (2014). Effect of sand fouling on compact fin heat exchangers. In N. Kasagi (Ed.), *Proceedings of the 15th International Heat Transfer Conference, IHTC-15, August 10–15, 2014*. Kyoto, Japan: The Assembly for International Heat Transfer Conferences.

Pak, B. C., Groll, E. A., & Braun, J. E. (2005). Impact of fouling and cleaning on plate fin and spine fin heat exchanger performance. *ASHRAE Transactions, 111*(1), 496–505. ISSN:0001-2505

Particle size distribution of ASHRAE test dust by mass. (2003). Retrieved February 2, 2015 from Flanders Corporation website: http://www.flanderscorp.com/files/Technical_Data/ASHRAE+DUST+SIZE+DISTRIBUTION.pdf

Particulate Matter (PM). (2013, March 18). Retrieved February 2, 2015 from United States Environment Protection Agency: http://www.epa.gov/airquality/particlepollution/

Petrov, V. A. (1968). Fouling of air heater tubes on air side. *Teploenergetika, 15*(3), 16–18.

Pich, J. (1972). Theory of gravitational deposition of particles from laminar flows in channel. *Journal of Aerosol Science, 3*(5), 351-361.

Pilat, M. J., & Prem, A. (1976). Calculated particle collection efficiencies of single droplets including inertial impaction, Brownian diffusion, diffusiophoresis and thermophoresis. *Atmospheric Environment, 10*(1), 13-19.

Pritchard, A. M. (1988). The economics of fouling. In L. F. Melo, T. R. Bott, & C. A. Bernardo (Eds.), *Fouling Science and Technology* (pp. 3-14). Dordrecht, Netherlands: Kluwer Academic Publishers.

Pu, H., Ding, G., Hu, H., & Gao, Y. (2011). Effect of salt spray corrosion on air-side performance of finned-tube heat exchanger with hydrophilic coating under dehumidfying conditions. *HVAC&R Research, 16*(3), 257-272.

Pu, H., Ding, G., Ma, X., Hu, H., & Gao, Y. (2010). Air-side heat transfer and friction characteristics of biofouled evaporator under wet conditions. *Frontiers of Energy Power Engineering in China, 4*(3), 306-312.

Robinson, R. A., Butterfield, D., Curtis, D., & Thompson, T. (2004). *Problems with Pitots: Issues with flow measurement in stacks*. Retrieved from Source Testing Association website: http://www.s-t-a.org/Files%20Public%20Area/News%20and%20articles/articlepitots.pdf. Retrieved on December 30, 2015.

Road vehicles—Test dust for filter evaluation. (ISO Standard 12103–1:1997 and 12103–2:1997). Geneva, Switzerland: International Organization for Standardization.

Seinfeld, J. H., & Pandis, S. N. (1998). *Atmospheric Chemistry and Physics: From Air Pollution to Climate Change*. New York, NY: John Wiley & Sons.

Sehmel, G. A. (1970). Particle deposition from turbulent air flow. *Journal of Geophysical Research, 75*(9), 1766-1781.

Sehmel, G. A. (1971). Particle diffusivities and deposition velocities over a horizontal smooth surface. *Journal of Colloid and Interface Science, 37*(4), 891-906.

Sehmel, G. A. (1973). Particle eddy diffusivities and deposition velocities for isothermal flow and smooth surfaces. *Journal of Aerosol Science, 4*(2), 125-138.

Shi, Y.-T., Gao, M., Tang, G.-H., Sun, F.-Z., & Tao, W.-Q. (2012). Experimental research of CFB ash deposition on helical finned tubes. *Applied Thermal Engineering, 37*, 420–429. doi:10.1016/j.applthermaleng.2011.11.064

Siegel, J. A. (2002). *Particulate fouling of HVAC heat exchangers* (Doctoral dissertation, University of California, Berkeley). Retrieved from ProQuest Dissertations and Theses A&I. (Order Number 3082406)

Siegel, J., A., & Carey, V., P. (2001). *Fouling of HVAC fin and tube heat exchangers*. (Lawrence Berkeley National Laboratory Publication No. LBNL-47668). Lawrence Berkeley National Laboratory, Berkeley, CA: U.S. Department of Energy.

Siegel, J. A., & Nazaroff, W. W. (2003). Predicting particle deposition on HVAC heat exchangers. *Atmospheric Environment, 37*(39), 5587-5596. doi:10.1016/j.atmosenv.2003.09.033

Smith, S. A. & Dirks, J. A. (1985). *Costs of heat exchanger fouling in the U.S. industrial sector*. (Pacific Northwest National Laboratory Technical Report No. PNL-SA-13264). Richmond, WA: U.S. Department of Energy.

Sonnad, J. R. & Goudar, C. T. (2007). Explicit reformulation of the Colebrook-White equation for turbulent flow friction factor calculation. *Industrial and Engineering Chemistry Research, 46*(8), 2593–2600. doi: 10.1021/ie0640241

Sun, Y., Zhang, Y., Barker, D., Ford, S., & Johnson, M. (2012). Experimental evaluation of air-side particulate fouling performance of heat exchangers. *ASHRAE Transactions, 118*(1), 1116–1130. ISSN:0001-2505

Talbot, L., Cheng, R. K., Schefer, R. W., & Willis, D. R. (1980). Thermophoresis of particles in a heated boundary layer. *Journal of Fluid Mechanics, 101*(4), 737-758.

Thackeray, P. A. (1979). The cost of fouling in heat exchange plant. In Institution of Corrosion Science and Technology (Great Britain) & Institution of Chemical Engineers (Great Britain) (Eds.), *Proceedings of the Conference on Fouling: Science or Art?* (pp. 1-9). Guildford, United Kingdom: University of Surrey.

The MathWorks, Inc. (2015). MATLAB 2015b [Computer software]. Natick, MA: The MathWorks, Inc.

Vinakos, M. (2015). *Particle size analysis: ASHRAE standard test dust #1*. Downers Grove, IL: Particle Technology Labs, Ltd.

Vinakos, M. (2016). *Particle size analysis: ASHRAE standard test dust #1*. Downers Grove, IL: Particle Technology Labs, Ltd.

Waldmann, L., & Schmitt, K. H. (1966). Thermophoresis and diffusiophoresis of aerosols. In C. N. Davies (Eds.), *Aerosol Science* (pp. 137-162). London, Great Britain: Academic Press.

Walmsley, T. G., Walmsley, M. R. W., Atkins, M. J., & Neale, J. R. (2013). Fouling and pressure drop analysis of milk powder deposition on the front of parallel fins. *Advanced Powder Technology, 24*(4), 780–785. doi:10.1016/j.apt.2013.04.004

Wang, H. (1986). Theoretical adhesion efficiency for particles impacting a cylinder at high Reynolds number. *Journal of Aerosol Science, 17*(5), 827–837. doi: 10.1016/0021-8502(86)90036-4

Xu, Z., Zhang, Z., & Yang, S. (2007). Costs due to utility fouling in China. In H. Müller-Steinhagen, M. R. Malayeri. A. P. Watkinson (Eds.), *Proceedings of 7th International Conference on Heat Exchanger Fouling and Cleaning, Tomar, Portugal* (pp. 113-118). New York, NY: ECI Digital Archives.

Yang, L., Braun, J. E., & Groll, E. A. (2007). The impact of fouling on the performance of filter–evaporator combinations. *International Journal of Refrigeration, 30*(3), 489–498. doi:10.1016/j.ijrefrig.2006.08.006

Zhan, F., Tang, J. Ding, G., & Zhuang, D. (2016). Experimental investigation on particle deposition characteristics of wavy fin–and–tube heat exchangers. *Applied Thermal Engineering, 99*, 1039–1047. doi:10.1016/j.applthermaleng.2016.01.136

Zhang, H., & Ahmadi, G. (2000). Aerosol particle transport and deposition in vertical and horizontal turbulent duct flows. *Journal of Fluid Mechanics, 406*, 55-80.

Zhang, G., Bott, T. R., & Bemrose, C. R. (1990). Finned tube heat exchanger fouling by particles. In G. Hetsroni (Ed.), *Proceedings of the International Heat Transfer Conference 9, Jerusalem, Israel* (pp. 115-120). Danbury, CT: Begell House Publishers. OCLC:439777445

Zhao, B., & Wu, J., (2006). Modeling particle deposition from fully developed turbulent flow in ventilation duct. *Atmospheric Environment, 40*(3), 457-466.

VITA

Harshad V Inamdar obtained his Bachelor's degree in Mechanical Engineering from the University of Pune, Pune, India, in 2011. He obtained his Master's degree in Mechanical Engineering from Purdue University, West Lafayette, USA in 2012.

Harshad conducted his doctoral research at Ray W. Herrick Laboratories, Purdue University, West Lafayette, USA. While a student at Purdue University, he received the Lambert Teaching Fellowship and taught the ME 200 Thermodynamics I class.

Harshad is currently employed with Rheem Manufacturing, Fort Smith, USA as a Research Engineer.